VOLCANIC FORCING OF CLIMATE OVER THE PAST 1500 YEARS: AN IMPROVED ICE-CORE-BASED INDEX FOR CLIMATE MODELS

by

CHAOCHAO GAO

A dissertation submitted to the

Graduate School – New Brunswick

Rutgers, the State University of New Jersey

In partial fulfillment of the requirements

For the degree of

Doctor of Philosophy

Graduate Program in Environmental Sciences

Written under the direction of

Alan Robock

And approved by

_____

_____

_____

_____

New Brunswick, New Jersey
October, 2008

Volcanic Forcing of Climate over the Past 1500 Years:

An Improved Ice-Core-Based Index for Climate Models

by

Chaochao Gao

Dissertation submitted to the Faculty of Rutgers, the State University of New Jersey

in partial fulfillment of the requirements for the degree of

Doctor of Philosophy in Environmental Sciences

October, 2008

Advisory Committee:

Prof. Alan Robock, Chair/Advisor

Dr. Caspar Ammann

Prof. Anthony Broccoli

Prof. Georgiy Stenchikov

ABSTRACT OF THE DISSERTATION

Volcanic Forcing of Climate over the Past 1500 Years:

An Improved Ice-Core-Based Index for Climate Models

By

CHAOCHAO GAO

Dissertation Director:

Alan Robock

This dissertation has investigated one of the most important natural causes of climate change, volcanic eruptions, by developing an ice core-based volcanic forcing index, using 54 ice core records from both the Arctic and Antarctica. The extensive collection of ice core data reduces errors inherent in reconstructions based on a single or small number of cores. This enables us to obtain much higher accuracy in both detection of events and quantification of the radiative effects. We extracted volcanic deposition signals from each ice core record by applying a high-pass loess filter to the time series and examining peaks that exceed twice the 31-yr running median absolute deviation. We then studied the spatial pattern of volcanic sulfate deposition on Greenland and Antarctica, and combined this knowledge with a new understanding of stratospheric transport of volcanic aerosols to produce a forcing index that is a function of month from 501 to 2000 CE, latitude in 10° bands, and height from 9 to 30 km at 0.5 km resolution. This index is the longest and

most advanced volcanic forcing index of the type. It eliminates or minimizes many aspects of problems previous reconstruction had with the ice core records. The estimated uncertainty is a significant reduction from the factor of two uncertainty reported in previously constructed volcanic forcing indices.

We forced an energy balance climate model with this new volcanic forcing index, together with solar and anthropogenic forcing, to simulate the large scale temperature response. The results agree well with instrumental observations for the past 150 years and the proxy records for the last millennium. Through better characterization of the natural causes of climate change, this new index will lead to improved prediction of anthropogenic impacts on climate.

Using 33 ice core records we investigated the 15th century Kuwae eruption. We found it was indeed a single-phase eruption occurred during late 1452 to early 1453 CE and it emitted about 140 Tg of sulfate aerosols into the stratosphere with 2(SH):1(NH) hemispheric partitioning. This finding provides an important reference to evaluate and improve the dating of ice core records.

My Contribution to the Work

This dissertation work utilized ice core records from both Greenland and Antarctica to reconstruct a monthly and spatially dependent volcanic forcing index that is applicable to general circulation models. Dr. Alan Robock and Dr. Melissa Free developed the first ice-core-based volcanic forcing index (IVI) using multiple ice core records [*Robock and Free*, 1995]. With the recovery of large number of new ice cores, Dr. Robock and Dr. Caspar Ammann proposed to develop a new index utilizing all of the available ice cores. My primary contribution to the work was to collect and process the ice core records, identify the steps to reconstruct the index, search and decide the methodology involved in each steps through numerous communications with Dr. Robock and other scientists, write programs to reconstruct the index and report the scientific results.

We wrote three journal papers based on this dissertation work. The first paper was inspired by the discussion Dr. Steve Self, Dr. Robock and I had at the IAVCEI (International Association of Volcanology and Chemistry of the Earth Interior) General Assembly Meeting at 2004. Dr. Self suspected the 15th century Kuwae eruption was a double-phase eruption based on the petrology evidence and the spread of Kuwae signal in time among different Greenland ice cores. I analyzed the Kuwae signal from 13 Arctic and 20 Antarctic ice cores and found that it was indeed a single-phase eruption. We took a step further by analyzing the dating uncertainties associated with each ice core records and concluded that the Kuwae eruption actually took place in either later 1452 CE or early 1453 CE. The paper based on this work was published by *Journal of Geophysical Research* and was also figured as a Research Highlight in *Nature*, July 6, 2006. Our co-

authors from the Niels Bohr Institute at University of Copenhagen provided us 11 new Greenland ice core records that were unavailable to the scientific community previous. They and Dr. Paul A. Mayewski also gave us much useful information on the dating uncertainties in the ice core records.

The idea of writing the second paper came upon Dr. Robock and me when we collected a large number of ice core records and realized that number of ice cores changes from time to time and decreases dramatically before the 16th century. I also found that there was no study on the spatial distribution pattern of volcanic deposition for the entire Greenland and Antarctic ice sheets and thought the large ice core dataset we have offered a great opportunity to do such study. Dr. Robock recommended I to include the six PARCA ice cores [*Mosley-Thompson et al*., 2003] and 12 Greenland ice core records from *Clausen and Hammer* [1988] to obtain a more comprehensive understanding of the spatial pattern of the volcanic sulfate deposition in the ice sheets. During the time this study was conducted, Dr. Luke Oman was performing simulations of volcanic sulfate transport and deposition using GISS modelE. So we compared our ice core observations with model simulation and found good agreement between the two at large scale. The next step to calculate the stratospheric came naturally. I made the decision to use the three independent methods to derive the calibration factors after many useful discussions with Dr. Robock and Dr. Georgiy Stenchikov. They also ensured me that this was the best way to solve the problem based the best knowledge available at the time. Again, Dr. Oman conducted the model simulation of the 1783 Laki, 1815 Tambora, 1912 Katmai, and 1991 Pinatubo eruptions. The paper based on this work was also published by *Journal of Geophysical Research*.

After obtaining the stratospheric volcanic sulfate aerosol loading history for the past 1500 years, Dr. Robock and I were searching for ways to transform this mass loading into the monthly and spatially dependent forcing index, which is the ultimate goal of this dissertation work. Dr. Ammann recommended the transport and deposition parameterization by *Grieser and Schönwiese* [1999]. I obtained the original program code in FORTRAN from Dr. Grieser and rewrote it in MATLAB with some modification, especially some of the exchange coefficients. To interpolate the vertical distribution of the volcanic aerosols, Dr. Robock suggested that I use lidar measurements of Pinatubo aerosols by *Antuña et al* [2002]. I collected the 11 lidar observations from Dr. Antuña and wrote the program to derive the vertical distribution accordingly. Before writing the paper, both Dr. Robock and I realized that we need an estimate of the uncertainty of our reconstruction so that the users of this index can have an idea of what range of uncertainty they should expect from the forcing itself. I identified the areas in our reconstruction that involve uncertainties and performed the analysis. Both Dr. Robock and Dr. Ammann made insightful suggestions on the procedure and results. Dr. Ammann also recommended on the general separation between the global and local uncertainties. The results of this part of my dissertation work were summarized in a journal article that was ready to be submitted to the *Journal of Geophysical Research*.

Acknowledgement

First and foremost I would like to express my gratitude to my advisor, Dr. Alan Robock, for essential guidance and insight throughout my graduate career. More than anyone else, his influence has contributed to my development as a scientist.

I wish to thank Dr. Caspar Ammann, Dr. Anthony Broccoli, Dr. Georgiy Stenchikov for taking time to serve on my thesis committee and also for many useful conversations. Sincere appreciation is due to Dr. Stephen Self and Dr. Philippe Naveau for their helpful advice, original ideas, and encyclopedic knowledge.

I also want to thank all the scientists who have supplied us with ice core records both for the difficult work of obtaining and analyzing the cores and for allowing us to use them. This work would not be possible without their hard work. I am especially grateful to Dr. Juergen Grieser for providing their diffusion sedimentation model and Dr. Tom Wigley for providing his climate model and both for help using the models, Dr. Ellen Mosley-Thompson for not only providing her ice core records but assistant me searching for additional ones, and Dr. Melissa Free for her original work on the subject.

In addition, I thank everyone at the Department of Environmental Sciences for the unique and stimulating environment they have provided. I thank Dr. Luke Oman and Dr. Haibin Li for insightful discussions throughout my graduate study.

This work was mainly supported by The National Oceanic and Atmospheric Administration (NOAA) grant NA03-OAR-4310155. Additional support was also provided by the Chaire du Développement Durable de l'École Polytechnique, Paris, France.

Needless to say, my family deserves a great deal of credit for my development. I thank my parents and sister for all their love and support; my beloved daughter Michelle for her cooperation while I am finishing this thesis. And finally, I offer my most genuine thanks to my husband Yanfeng, whose love and encouragement carries me through my life.

Table of Contents

List of tables

List of figures

Chapter 1: Introduction

Over the course of last one to two millennia, a period often referred to as "late Holocene," the global average temperature has seen moderate fluctuations including the "Medieval Warm Period" (MWP, ~1000-1300 CE), a transition period (1300-1450 CE), and the "Little Ice Age" (LIA, 1450-1850 CE) [*Bradley et al., 2003; Jones and Mann, 2004*]. Figure 1-1 shows the latest temperature reconstruction for the Northern Hemisphere (NH), the Southern Hemisphere (SH) and the global average, respectively, based on multiple proxy data including instruments, documentary evidence, tree rings, and ice-core records for the past 1800 years [*Jones and Mann*, 2004]. In this figure one can clearly see the MWP, LIA episodes, as well as some cold periods during the 6^{th}, 15^{th}, 17^{th}, and 19^{th} centuries in NH. One also notices that the smoothed temperature fluctuates within ±0.4ºC for the whole period except for the rapid warming over the last century.

Fortunately, during the late Holocene the principal boundary conditions, such as Earth orbital geometry and global ice mass, have not changed appreciably [*Jones and Mann*, 2004]. Thus, the climate variations over this time frame are likely to represent the natural climate variability that may be expected over the 20^{th} century in the absence of any human influence. To evaluate the relative impact of modification of atmospheric greenhouse gas concentrations and land surface modifications on climate and further predict the likely effects of anthropogenic activities on future climate system, we must have a sound and quantitative understanding of the natural causes of climate change for the same period. To this end, both the knowledge of the forcing indices for the past one to two millennia and model simulations of the corresponding climate responses should be applied to study this problem [*Hegerl et al.,* 1997; *Crowley,* 2000; *Hegerl et al.,* 2006;

Ammann, 2007; *IPCC AR4,* 2007]. Possible natural causes of climate variation over this time period include external forcings induced by volcanic activity and solar irradiance variations, and internal variability of the coupled atmosphere and ocean system [*Robock and Free,* 1995]. Among these natural forcings, volcanism has been found to be the primary cause of pre-industrial temperature variability by various studies [*Free and Robock*, 1999; *Crowley* 2000; *Hegerl et al.,* 2004, 2006, 2007]. However, these studies also estimated different contributions of past volcanism as compared to solar forcing, largely due to the large uncertainties present in the different volcanic forcing reconstuctions. In the work I am presenting here, I have investigated one of the most important natural causes of climate change, volcanic eruptions, for the past 1500 years by developing a volcanic forcing index based on 54 ice core records from both the Arctic and Antarctica.

1.1 The Climatic Impact of Volcanism

Explosive volcanic eruptions have long been recognized as a possible natural cause of past climate variations. Large explosive volcanic eruptions emit sulfur, in the form of H_2S and/or SO_2, into the stratosphere. This sulfur was turned into the sulfate aerosols which cool the surface by reflecting the solar radiation and warm the stratosphere by absorbing both the shortwave and longwave radiations [*Self et al.,* 1981; *Rampino and Self,* 1982]. For example, the 1815 Tambora eruption has produced such a significant cooling effect that the following year has been often referred to as “the Year Without a Summer”.

There were a number of observational and theoretical studies on the climatic effect of volcanism since last century, as nicely summarized in *Robock* [2000]. The

climatic impact of volcanic eruptions was first proposed by Benjamin Franklin [*Franklin*, 1784] who associated the abnormally cold summer of 1783 CE in Europe and the cold winter of 1783-1784 CE with the Laki eruption in Iceland in 1783 CE. After more than a century, *Humphreys* [1913, 1940] compared time series of volcanic eruptions with climate data and suggested that there was some relation between volcanic events and temperature records. Other studies [*Miles and Gildersleeves*, 1978; *Bryson and Goodman*, 1980] also showed this relationship but its significance varies with the specific data and method used. *Mitchell* [1961], on the other hand, conducted a "superposed epoch" analysis that averages the data from several eruptions to isolate the volcanic signal from other presumably random fluctuations. *Lamb* [1970] published his Dust Veil Index (DVI), which has an extremely important influence on the modern study of the climatic impact of volcanic eruptions. Since then, improved data and more consistent reconstruction methods were developed to study the effects of volcanoes on climate [*Lamb*, 1977; *Robock*, 1978; *Bryson and Goodman*, 1980; *Toon and Pollack*, 1980; *Lamb*, 1983; *Angell and Korshover*, 1985; *Robock*, 1989, 1991;]. The two big eruptions at the end of last century, i.e., the 1982 El Chichón eruption and the 1991 Pinatubo eruption, provide great opportunities to further broaden and deepen our understanding of this issue. Observations and modeling studies [*Hansen et al.*, 1992; *Robock and Mao*, 1992, 1995; *Solomon et al.*, 1996; *Mao and Robock*, 1998; *Stenchikov et al.*, 1998; *Solomon*, 1999; *Stenchikov et al.*, 2002; *Briffa et al.*, 2004] have shown that large tropical volcanic eruptions such as these two recent events produced general cooling effect especially in NH summers, whereas dynamically induced warming over NH continents for the next couple winters following the eruptions. The cooling is the direct result of the

stratospheric volcanic aerosols scattering some solar radiation back to space. The warming, on the other hand, is caused by the atmospheric dynamical response to the enhanced temperature gradients that is produced by the radiative effects of the stratospheric aerosols together with the ozone depletion these aerosols caused via heterogeneous reaction. On one hand, the difference in the stratospheric heating strengthened the westerlies in sub-polar and mid-latitude regions in winter, which prevent planetary wave from penetrating in to higher stratosphere but reflected back to the troposphere, a circulation pattern contributing to the NH continental warming. One the other hand, the reduced temperature difference in the surface resulted in less vertical planetary wave energy flux. The above two effects reinforce each other, contributing to a strong and stable signal [*Stenchikov et al.*, 2002]. For eruptions at high latitude, like the 1783-1784 Laki eruption in Iceland and 1912 Katmai-Novarupta eruption, the radiative impact is much larger than the dynamical impact and most of the impact is confined poleward of 30 degree to high latitudes in the corresponding hemisphere [*Oman et al.*, 2005; *Oman et al.*, 2006].

Volcanic aerosols usually remain in the stratosphere for less than 2 to 3 years. Thus, their radiative effect is interannual rather than interdecadal in time scale. However, a series of eruptions could generate a decadal-scale cooling; plus, the feedbacks involving ice and ocean may also transform the short-term volcanic forcing into a longer-term effect. Therefore, the possible timescale of volcanic caused climate change can range from several years to decades [*Robock*, 2000].

1.2 Cause of Climate Change on Decadal to Century Scales

Causes of climate change on decadal to century scales include external forcings such as volcanic eruptions, solar irradiance variation, anthropogenic greenhouse gases and aerosols, land surface modification, and internal variability of the coupled atmosphere and ocean system. Great efforts have been devoted to estimating the portions different forcings have contributed in causing the climate change over the past one to two millennia, especially in distinguishing between the roles past volcanism plus solar irradiance have played and that of the anthropogenic impacts. *Robock* [1978, 1979] applied both DVI and solar forcing, which is proportional to the envelope of the sunspot number, to an energy balance model (EBM) with simple mixed-layer ocean and found that the volcanic forcing explained a much larger share of the temperature variability since 1620 than the solar series. *Gilliland and Schneider* [1984] used an upwelling-diffusion energy balance model with the Crete and Dome C ice-core records and found that volcanic forcing could account for up to 44% of the temperature variability since 1850 versus 17% for solar forcing. *Lean et al* [1995] produced a solar index based on the records of sunspot darkening and facular brightening, and suggested that solar forcing may have contributed about half of the observed 0.55ºC surface warming since 1860 and one third of the warming since 1970. *Free and Robock* [1999] applied four solar reconstructions and three volcanic indices to an EBM [*Wigley and Raper*, 1987, 1992] and found that with a climate sensitivity of 3.0ºC for doubling CO_2, the volcanic forcings are large enough to produce the required temperature variability for the LIA period. They also found that the combination of volcanic and solar forcings accounts for 61% of the total variance from 1600 to 1800. *Crowley* [2000] estimated that 41-64% of the pre-

anthropogenic low frequency variance in temperature was caused by volcanism and solar variability using a 1D-EBM; he also found that 22-23% of the decadal-scale temperature variance is caused by volcanism averaged over the entire pre-industrial interval, whereas over the period of 1400-1850 CE, the volcanic contribution increased to 41-49%. *Bertrand et al* [2002] applied 2 volcanic time series – VOL-Z as derived by *Zielinski* [1995] from GISP2 and VOL-C as obtained by *Crowley* [2000] using GISP2 plus Crete ice core – to a 2D-General Circulation Model (GCM). They found that volcanism accounts for 20% of the Northern Hemisphere decadal temperature variance over the pre-industrial interval and up to 36-42% over 1400-1850 CE. *Ammann et al.* [2007] applied the extended volcanic forcing reconstruction of *Ammann et al*. [2003], a range of published solar irradiance estimates, together with anthropogenic forcing to an AOGCM to simulate the temperature response from 850 CE to present. They found that while volcanic activities contributed (several tenths of a degree Celsius) to the cooling over the 13th, mid-15th, 17th, and early 19th century, the change in solar irradiance dominated the overall climate variation on interdecadal to century scale. However, the natural contribution to 20th century warming was estimated to be less than 0.2°C

From the studies summarized above, it can be seen clearly that while all the studies indicate that both solar radiation and volcanism are the two dominant external forcings causing the preindustrial temperature variation, their estimations of individual forcing's effect vary widely with the time periods, the specific solar and volcanic reconstructions, the types of models, and to a less extent, the proxy or observational temperature series used for comparison. The large uncertainties introduced during the reconstructions of the volcanic and solar indices, as well as the disagreements between

the temperatures reconstructions may both serve as the main source of the discrepancies among the results described in the former paragraph. One the other hand, internal climate variations such as ENSO further complicate the quantification of relative climate impacts of these external natural forcings. As a result, it is still not clear whether the poor agreement between some results and temperatures in certain periods is due to the error in the data or a true lack of relationship between the forcings and climate change. Further detection and attribution studies require better reconstruction of volcanic, solar forcing indices and temperature time series.

Section 1.3 describes in detail the uncertainties and limitations of the currently available volcanic forcing indices. The same or even larger uncertainties were found in the reconstructions of solar forcing history as well. Based on space-based radiometric measurements, scientists have well observed that the solar irradiance varies on the order of 0.1% peak-to-peak in an 11-year cycle [*Fröhlich and Lean*, 2004]. But they do not know whether multiple decadal changes in solar activities produce longer – term variations that are larger than observed thus far in the contemporary epoch, due to the limitation of knowledge about the relationships between solar irradiance and solar activity. Cosmogenic radionuclide records (i.e., ^{14}C from trees and ^{10}Be from Greenland or Antarctic ice cores) were often used to reconstruct the solar forcing history before the period of direct solar observations. However, changes in cosmogenic radionuclide records are not the exclusive result of solar variation. The strength and direction of the geomagnetic field and changes in climate can also influences the production and transport of cosmogenic radionuclide, respectively [*Muscheler et al*, 2007]. As a result, *Bard et al*. [2000] found that solar activity at around 1200 CE was similar, if not higher, than the

present value; while *Usoskin et al*. [2003] suggested that solar activity reached a distinct maximum during the past 60 years, a value significantly higher than during the past 1000 years.

1.3 Indices of Past Volcanism

Despite its climatic importance, currently available volcanic forcing indices all have drawbacks, as nicely summarized in several studies [*Robock and Free*, 1995; *Robock* 2000; *Zielinski* 2000]. The first volcanic forcing index - Dust Veil Index - was reconstructed by *Lamb* [1970] based on historical reports of eruptions such as dry fogs and red sunsets, temperature anomaly records, estimates of the volume of eruptive products, and the solar radiation measurements since 1883. Much of this information is rather subjective and the use of climatic information results in circular reasoning if the DVI is used as an index to compare with temperature variation. The Mitchell index [*Mitchell*, 1970] is just a more detailed version of Lamb's DVI, for the period 1850-1968 CE. The Volcanic Explosivity Index (VEI), first reconstructed by *Newhall and Self* [1982] then continuous updated by *Simkin and Siebert* [1994 and forward], is a measure of the explosion magnitude associated with each eruption. Therefore it cannot directly reflect the stratospheric sulfate loading which is the key measurement of the climate consequences. The Sato Index [*Sato et al.*, 1993] uses estimates of ejecta volume from *Mitchell* [1970] during 1850 and 1882, optical extinction data after 1882, and satellite data for the period after 1979. The recent part of this index may be an improvement over the DVI or VEI as it includes actual observations of the latitudinal and temporal extent of the aerosol clouds. However, it lacks consistency of the source data and only goes back to the 1850s. A limitation of most of these indices arises from the fact that events were

often only registered when there was a direct eyewitness report of the eruption from the ground. Thus, the problem of missing volcanic eruptions is unavoidable and becomes increasingly severe as we go further back in time, especially in the SH. More objective and continuous time series of volcanic eruptions can be obtained from ice core records, since they are direct measures of volcanic sulfate [*Hammer*, 1977; *Hammer*, 1980]. After big volcanic eruptions, a portion of sulfate aerosols are preserved in the snow and ice by precipitation or dry deposition over certain glaciers and ice sheets, causing variations in the conductivity of ice there. Thus, measurement of the total acidity or the actual sulfate content in the ice cores from those areas allows direct and relatively precise computation of the volcano time series [*Hammer*, 1977; *Hammer*, 1980].

During the past two decades, several studies [*Robock and Free,* 1995; *Zielinski* 1995; *Crowley* 2000; *Robertson et al.,* 2001; and *Ammann et al.*, 2003, 2007] have attempted to reconstruct volcanic indices from single or a few ice cores. *Hammer et al* [1980] was the first study to utilize the ice core acidity records (Crête ice core from central Greenland for the period from 7th to 20th century, and Camp Century from northern Greenland for the period from 8000 BC to 0 BC) in producing the volcanic forcing time series. The authors also introduced the use of nuclear bomb test fallouts as a calibration for calculating the volcanic sulfate aerosol loading in the atmosphere. *Crowley et al*. [1993] then reconstructed a 1420-yr record using the Crête [*Hammer et al.*, 1980] record. A volcanic signal was defined in this study if the acidity exceeded certain threshold (75% of the 1883 CE Krakatau peak value) within one year and dropped back to the background within the next two years. *Zielinski* [1995] reconstructed a 2100 year atmospheric loading history using the GISP2 ice core sulfate record. The author used

spline to remove the background variation and estimated the uncertainty range for his reconstruction. *Robock and Free* [1995] pioneered the use of multiple ice core records from both Greenland and Antarctica and reconstructed an ice-core-based volcanic forcing index (IVI) back to the 15th century. The use of multiple ice core records minimize the missing of volcanic events inherited in the previous reconstructions based on single record. The evidence from both polar regions also helps to distinguish the tropical eruption from high-latitude ones. *Crowley* [2000, an update of *Crowley and Kim*, 1999] also developed a volcanic forcing index for the same period based essentially on Crête [*Hammer et al.*, 1980] and GISP2 [*Zielinski et al.*, 1995] with some additional information embedded using the Arctic-Antarctic comparisons by *Langway et al.* [1995]. *Robertson et al.* [2001] combined five ice core sulfate records (GISP2, GR89, siteA from Greenland and Siple, Dyer Plateau from Antarctica) and reconstructed an annually and zonally averaged volcanic forcing history for the past 500 years. *Ammann et al*. [2003, 2007] applied a compilation based on up to 14 high latitude ice core records, among which five came from Antarctica, and developed a seasonal and latitudinally dependent volcanic time series for the past 12 centuries.

To combine the individual series into hemispheric composites, both *Crowley* [2000] and *Ammann et al.* [2003, 2007] reconstructions applied a suite of somewhat subjective, albeit in principle justifiable, corrections. One necessary correction involved adjustments in the time scales of the series to optimize the joint chronology across cores, and in order to combine the different types of data (i.e., electric conductivity measures, dielectric properties of the ice, and direct sulfate flux measurements) all reconstructions involve multiple ice core records applied an empirical scaling of the series to selected

reference events (Krakatau or Tambora). *Crowley* [2000] additionally applied a dampening factor for very large events (a factor of X to the power of 2/3 for events larger than 15 Mt) based on the apparent lack of proportional climate impacts in some reconstructions. Such a correction can be justified by the idea that aerosol growth in very large sulfate clouds might be more efficient [*Pinto et al.*, 1989]. These reconstructions also used the assumption that if anomalous sulfate was found in both hemispheres within a couple of years that a common tropical source was likely [see also *Palais et al.*, 1992; *Langway et al.*, 1995]. *Crowley and Kim* [1999] had tested the climatic impact of this assumption for unknown events by comparing a tropical source with two independent high-latitude events. They found that the effect of such a mis-identification was relatively small. Comparing all available ice-core based series shows general agreement in the depiction of periods of more intense volcanism. The individual peak forcing estimates however differ due to different, and often limited, data sources, particularly with regard to the important direct sulfate measurements [*Robock and Free*, 1996]. Due to the large spatial variability of volcanic deposition on ice sheets, there is the danger that reconstructions based on single or a few ice cores may omit certain events [*Zielinski et al.*, 1995], or they may bias the estimates of the magnitudes for individual eruptions [*Mosley-Thompson et al*., 2003; *Traufetter et al.*, 2004; *Gao et al*., 2007]. This points to the importance of using the largest ice core dataset possible to produce a more reliable volcanic index.

During the past 10 years a large number of new ice cores have been recovered, and most of these were analyzed using continuous sulfate measurements [*Cole-Dai et al.* 1997, 2000; *Sommer et al.* 2000; *Bigler et al.* 2002; *Palmer et al.* 2002; *Stenni et al.* 2002;

Budner and Cole-Dai, 2003; *Dixon et al.* 2004; *Traufetter et al.*, 2004; *Castellano et al.*, 2005; *Kurbatov et al.*, 2006]. This offers the potential for a dramatic improvement to reconstruct the volcanic forcing index over the past centuries and millennia. We have worked with the international ice core community and collected with their generous contributions a total of 53 ice core series with the goal to develop a comprehensive volcanic forcing time series targeted at applications for state-of-the-art climate model simulations. To generate such a series, a few steps have to be performed:

1. Ice core volcanic signal extraction
2. Dating correction for individual eruptions
3. Calculation of Arctic or Antarctic mean volcanic sulfate deposition, taking into account the spatial variation
4. Conversion from ice-core deposition to stratospheric sulfate loading
5. Transform the mass loading history into a spatio-temporal-evolving volcanic mass and forcing dataset

After briefly introducing the ice core time series in Chapter 2, I describe my work in developing each step of the above protocol toward reconstructing the comprehensive volcanic forcing index in Chapter 3-6. In Chapter 7 of this work I apply this new volcanic forcing dataset to an upwelling-diffusion energy-balance model (UDEBM) to simulate the temperature response, and discuss how the result compares to proxy reconstructions for the past millennia and the instrumental observations for the recent 150 years. I then conclude in Chapter 8 with summaries of this dissertation work and possible future research on this topic. Despite the significantly enlarged dataset (based on more

than double the number of records previously used), the remaining uncertainties are discussed in Chapter 6 and again in Chapter 8.

Chapter 2: Ice Core Records and Volcanic Signal Extraction Methods

With Dr. Alan Robock, I have been collecting and examining the ice-core data since August, 2003 and so far we have 53 ice-core records globally (Fig. 2.1 & 2.2, 20 in Northern Hemisphere, 32 in Southern Hemisphere, and one from the Tropical). More particularly, I have included in our reconstruction 11 new Greenland ice-core records that were unavailable to the scientific community previously. These 11 records were provided by a group at the Niels Bohr Institute at University of Copenhagen headed by Dr. Sigfus Johnsen. Figure 2.3 shows the electrical conductivity measurement time series from these 11 Greenland Ice-core sites, which clearly demonstrates the signals of 935, 1259 Unknown and 1783 Laki eruption.

I chose 36 ice core time series from the total 53 series we have collected to be used in this study, excluding the time series that were too short or that have large date gaps. Table 2.1 lists the general information and references of these 36 ice core time series. As can be seen from the table, different time series have different resolutions and data types and the challenge was to build an event chronology and quantify the corresponding magnitude for each event combining the various ice core time series. Here I adapted a two-step procedure to achieve this goal, that is, I used all of the 36 ice core records to determine the timing of each eruption but only the actual sulfate records to calculate the magnitude of ice core volcanic sulfate deposition. The reason I choose not to use other records, such as electrical conductivity measurement (ECM) records in calculating the volcanic deposition, is that ECM measures the acidity caused not only by sulfuric acid (H_2SO_4), but also by nitric (HNO_3), hydrochloric (HCl), and hydrofluoric (HF) acids. Besides, the acidity can be reduced by deposition of basic (as contrasted with

acidic) aerosol particles; and the values depend on the temperature at the time when the measurement was taken and the electrical current strength. Nevertheless, strong ECM peaks do qualitatively corroborate the timing of the arrival of volcanic sulfate to the ice.

For each sulfate record, I converted all of the actual sulfate records into one flux unit (kg H_2SO_4 km^{-2} yr^{-1}) following the steps described below and in detail in the Appendix. In addition, *Mosley-Thompson et al.* [2003] calculated the sulfate deposition of the Laki, 1809 Unknown, and Tambora eruptions for six Program for Arctic Regional Climate Assessment (PARCA) ice cores; *Clausen and Hammer* [1988, CH88 hereafter] also computed the deposition for the Laki and Tambora eruptions for 12 Greenland ice cores. The results from these two studies are listed in Table 2-2 & 2-3. I combined results from these 18 cores with our 36 ice core records to obtain a more comprehensive understanding of the spatial distribution pattern, as well as a more precise estimate of Greenland ice core sulfate deposition. This gives a total of 54 ice core records to be used in this study.

For each of the 36 ice core time series original to this study, I first calculated the annual mean values for each of the time series. Then we extracted the volcanic signals by applying the following procedure: (1) convert the sulfate concentration time series into fluxes (see Appendix); (2) remove the trend and the background variation with a high pass loess filter, a locally weighted least square quadratic estimate [*Cleveland* 1979; *Cleveland and Devlin*, 1988], to remove signals longer than 31 years; (3) calculate the 31-yr running median absolute deviation (MAD) of the residuals and select the potential volcanic peaks if they exceed the baseline plus 2 running MAD; (4) replace the selected

peak values with the median of the original time series, (5) repeat step 2 using the time series with the peaks removed, and (6) repeat step 3 to extract the volcanic peaks.

Figure 2.4 shows an example of how this method works. The original time series shown in Fig. 2-4 demonstrate a typical type of the ice core records - large volcanic peaks superposed on a slow changing baseline. A standard running average and standard deviation would not work for this type of time series because both quantities would be biased by the large peaks values. Instead I used the loess filter and MAD because they provide robust estimates for a wide range of population distributions, and do not require a normal distribution, which is the underlying assumption for the automatic extraction method [*Naveau et al.*, 2003] and other methods [e.g., *Robock and Free*, 1995, 1996] that extract peaks above a certain standard deviation limit. I chose an appropriate window length and extraction threshold by examining the properties of the detrended, peak-removed residuals such as normality, constant variance, and minimum autocorrelation. Based on spectral analysis of several of the time series, the 31-year filter falls at a spectral gap, which removes long-term variations while allowing for the full strength of volcanic peaks.

After extracting the potential volcanic signals I selected the years that have signals show in at least half of the available ice core records and assumed that these are the volcanic events recorded in the ice cores. Then I adjusted the timing of the signals so that the peak deposition lies in the same year in all cores. The dating adjustment was done by the following procedure: first I compared the extracted volcanic signals with other historical records, especially the IVI [*Simkin and Siebert*, 1994 and the forward update on http://www.volcano.si.edu/world/largeeruptions.cfm] to determine the year of

the eruption; then I assumed the peak ice core volcanic deposition to be the year following the eruption for tropical eruptions and the year of the eruptions for middle or high latitude ones, and then adjust the extracted signals up or down accordingly. The dating adjustments for each eruption in individual ice core time series were recorded and were available upon request. Ideally, one would expect the dating adjustments to be close or of the same sign for individual ice core time series. We did find adjustments of the same or similar value for events occurred closely such as within a couple of centuries. However, such similarity was lack from almost all of the ice core time series if the whole records were take into consideration. In some time series, such lack of similarity in dating error was probably caused by the use of age model and the assumption of same accumulation rate for different years. One advantage of using multiple ice core records is that for the old eruptions that we do not have the record, we can use volcanic signals from these ice cores to cross identify the year of the event and its magnitude. In the next chapter I will show you an example of using 33 ice core records to access the time and magnitude of the great 15th century Kuwae eruption – an important eruption in the time when some but not perfect data exists.

Chapter 3: The 15th Century Kuwae Eruption Signal

3.1. Introduction

The Kuwae volcano in Vanuatu (16.83°S, 168.54°E, Fig. 3-1) erupted in the middle of the 15th century [*Pang*, 1993], expelling 32-39 km^3 of dense rock equivalent [*Monzier et al.*, 1994]. This volume of expelled matter is more than six times larger that of the 1991 Pinatubo eruption and left "unmistakable marks in world climate records" [*Pang*, 1993]. While records of unusual weather and atmospheric optical phenomena and severe damage on agriculture [*Pang*, 1993], as well as the anomalously low tree ring densities [*Briffa et al.*, 1998], point to the year 1452 as the time of the eruption, dating of the Kuwae signal derived from individual ice core record ranges from 1450 to 1464. For example, *Cole-Dai et al.* [1997] found an acid "spike" that lasted for four years from 1454 to 1457 in the Siple Station ice-core. *Palmer et al.* [2002] reported deposition of a large volcanic eruption during 1459-1461 in the Law Dome record, which was also found to be the largest volcanic signal in the last seven centuries in this record. *Castellano et al.* [2005] assigned the Kuwae signal to the year 1460 in their EPICA Dome C core. Another Antarctic ice core, PS1 [*Delmas et al.*, 1992], displays a prominent acid peak which they determined to be about 1450. Similarly in the NH *Zielinski et al.* [1994] and *Zielinski* [1995] found a large volcanic signal at 1460-1461 in the GISP2 record. *Fisher and Koerner* [1994] discovered a volcanic deposition in 1455 in the A84 ice core. *Bigler et al.* [2002] found a large peak lasting several years in the early 1450s in the NGT-B20 ice core.

In several of these ice cores Kuwae appears as a major if not a dominant volcanic signal. For example, the sulfate flux of the Kuwae eruption derived from Plateau Remote

is five times that of the Tambora [*Cole-Dai et al.*, 2000], which raises the question about the relative magnitude of the Kuwae and other large volcanic eruptions during the past 2000 years. On the other hand, estimations of its atmospheric sulfate aerosol loading range from 150 Tg to 400 Tg based on individual ice core record [*Delmas, et al.*, 1992; *Zielinski*, 1995] and petrologic record [*Witter and Self*, 2006]. Due to different site characteristics, such as the relative contribution of different air-to-snow mass transfer mechanisms (wet and dry deposition, riming, and vapor transfer) of sulfate aerosols as well as the surface elevation and irregularities, temperatures, wind speed that affect the flux of sulfate aerosols [*Cole-Dai et al.*, 1997] and thus the magnitude of volcanic signals, studies based on multiple ice cores from both Antarctic and Greenland are required to better understand this problem, as suggested by previous studies [*Robock and Free*, 1995; *Free and Robock*, 1999; *Mosley-Thompson et al*., 2003].

In this study, I have incorporated the volcanic signals derived from 33 ice core records from both hemispheres to determine the timing and magnitude of the Kuwae eruption. Results obtained from these multiple ice cores reevaluate and complement the previous geological, historical and proxy data. The estimated timing of the eruption not only provides a tool to evaluate the dating of existing ice core records but serves as a volcanic reference horizon for future ice core dating and important case study for the effects of volcanic eruptions on climate change.

3.2. Ice Core Database

Among the 36 ice core records mentioned in Chapter 2 above 19 ice cores, 10 in the SH and nine in the NH, contain data beginning in or before the 15th century. From Table 2-1 one can see that there are 24 ice cores, 17 in the SH and seven in the NH, that

have sulfate records, among which only nine (7 SH, 2 NH) have records that go back to the 15th century. In this part of my study, I used all available ice cores (i.e., the 19 records with Kuwae signals) to determine the timing of the Kuwae eruption, but only the sulfate records (i.e., the nine cores with Kuwae sulfate records) to estimate the deposition of the eruption on the Antarctic and Greenland ice sheets. The estimated deposition was then evaluated and adjusted with the 24 total ice core sulfate records.

3.3. Timing of the Great Kuwae Eruption

For each ice core record, I extracted the potential volcanic signals following the procedure described in Chapter 2. Figure 3-2 shows the time series of the potential volcanic peaks extracted from the 10 SH ice core records for the period 1440-1465. Based on previous studies, one would expect the ice core signal of a tropical eruption to show up 1-2 yr after the eruption [*Cole-Dai and Mosley-Thompson,* 1999; *Legrand and Wagenbach*, 1999]. As the Kuwae caldera is located in the SH, one would expect to see the stratospheric aerosols confined mostly to the SH and to see its signature in SH ice much more strongly than in the NH.

One can see in Figure 3-2 that two records (Siple Station, DML_B31) show large peaks during the period 1454-1456; and three records (Talos Dome, DML_B32 and DML_B33) have peaks during 1453-1456. All of these five cores [*Cole-Dai et al.*, 1997; *Sommer et al.*, 2000b; *Stenni et al.*, 2002] were absolutely dated by counting seasonal cycles of non-sea-salt SO_4^{2-}, $\delta^{18}O$, sodium, calcium, and/or ammonium concentrations. The dating was then evaluated and refined by looking at radionuclide and volcanic markers, usually the 1955 and 1965 CE nuclear bomb test fallouts and the 1259 Unknown eruption, Tambora in 1815, and Agung in 1963. However, in the Talos Dome

the Kuwae Eruption was set to the year 1452 CE and used as a reference horizon [*Stenni et al.*, 2002]; in the DML_B31 and DML_B33 records the peak of Kuwae signals were turned out to be the year 1455 [*Sommer et al.*, 2000b]. Ice core records dated by multiple layer accounting are considerably more accurate, though accumulated dating errors up to 1-3 years do exist due to some ambiguous layers.

Among the rest of the ice core records, SP2001c1 [*Budner and Cole-Dai*, 2003] has a big signal during 1456-1458. Accounting for a possible dating error of up to ±4 years, the timing of the Kuwae deposition could lie somewhere between 1452 and 1462. The peak in Plateau Remote spans 1451-1455 in Fig. 3-2. This core was dated using an age model and the Kuwae peak was fixed to 1454 and served as a reference horizon [*Cole-Dai et al.*, 2000]. The Law Dome record [*Palmer et al.*, 2002] was composited from three ice-cores, DSS97 (1888-1995), DSS99 (1841-1888), and DSS (1301-1841), which may cause either missing or faulty annual layers at the conjunctions. Thus it is possible for the peak shown at 1460 in Fig. 3-2 to be off by a few years. The PS1 data I have only contain volcanic signals extracted by the authors [*Delmas et al.*, 1992], and it has a single value for each event though the authors stated that the Kuwae deposition lasted for 3 full years. The dating uncertainty is ±10 yrs during the period from 1259 to 1800 and the authors "re-date" the Kuwae event to the year 1452 according to tree ring evidence [*La Marche and Hirschboeck*, 1984]. G15 [*Moore et al.*, 1991] was dated by first using Agung, Tambora and the 1259 Unknown to fix the chronology and then interpolating between these events. Therefore, it is possible that the timing of Kuwae as interpreted from this core was off by several years. In general, the SH ice core records seem to suggest a 3-4 yr Kuwae deposition at about 1453-1456.

Evidence from NH ice core records is less clear. As shown in Fig. 3-3 several of the NH ice core records show double peaks during the period from 1450 to 1465, with one in the mid-1450s and the other at the beginning of 1460s. No signal was detected in the GRIPmain ice core records. Previous studies [*Fisher et al.*, 1985; *Langway et al.*, 1995] suggest that the Crête ice core has a high dating accuracy due to the low signal-to-noise variance ratios in terms of both accumulation rate and layer separation, plus there is virtually no melting in this site. I extracted a large acid spike during 1453-1454 in the Crête ECM record. Accounting for the ±1-2 yr dating error [*Hammer et al.*, 1980], this result suggests a Kuwae deposition during 1451-1456. Other NH ice core records that have a signal during this period are A84, Renland, and both of the NorthGRIP1 sulfate and ECM data. NGT_B20 [*Bigler et al.*, 2002] was dated based on identification of the well-known historical volcanic layers (Katmai 1912, Tambora 1815, Laki 1783, Huaynaputina 1600, unknown 1259, and Eldgjá 934) plus annual counting using the seasonal variation of calcium and sodium. The dating accuracy is ±5 yr, which places the Kuwae signal in the time interval 1446-1458. In the GISP2 record a larger signal was detected during 1458-1461. The volcanic signals in GISP2 are generally spread due to the biyearly sampling scheme used so the original signal is probably only in 1459-1460. *Zielinski et al.* [1994] assigned this signal to the Kuwae eruption. Here I suggest that this 1459-1460 peak is the deposition of a local eruption at the beginning of 1460s rather than Kuwae for the following two reasons. First, I found an almost constant dating error of –1-2 yr (i.e., 1 or 2 years earlier than the actual date) in GISP2 by comparing its volcanic signals with the other cores and the historical documents; therefore, it is unlikely that this signal represents the deposition of Kuwae eruption found to be in the middle

1450s, based on our SH ice cores results. Second, several other NH ice cores, such as the Crête, NorthGRIP1 sulfate, A77, A84, and Dye3 deep records (Fig. 3-3), also have separate peaks during the same period that are not due to the Kuwae aerosols. The missing of Kuwae signal in both the GISP2 and GRIPmain ice core record may be a result of the natural spatial variation of volcanic deposition; or it may be caused by the loss of snow and ice during the post-depositional redistribution or even the drilling and handing processes.

All of the ten SH ice core records in Figure 3-2 display only one dominant peak during the interval 1445-1465, suggesting that the Kuwae eruption was a single-phase volcanic event. The multiple peaks shown in some of the NH time series (Fig. 3-3) were probably caused by signals from other sources such as high latitude volcanic eruptions. Since the Kuwae eruption is at 17°S, it is reasonable to base our analysis on the SH ice core records and conclude that the eruption was indeed a single-phase event.

In summary, the ice core records support the previous discovery that there was a large volcanic eruption somewhere during the 1450s that emitted significant amounts of sulfate aerosols into both hemispheres. Although signals derived from individual ice cores indicate different timings of the Kuwae eruption, when accounting for the dating errors associated with each record, these signals seem to point to a volcanic deposition during the period 1453-1456, suggesting that the Kuwae eruption took place in either late 1452 or early 1453. This result is consistent with previous suggestions based on the geological record [*Simkin and Siebert*, 1994], historical records [*Pang*, 1993; *Simarski*, 1996], and proxy data [*La Marche and Hirschboeck*, 1984; *Pang*, 1993; *Briffa et al.*, 1998].

3.4. Magnitude of the Kuwae eruption.

Besides determine the time of the Kuwae eruption using these multiple ice core records, one can also estimate the magnitude of the eruption and thus its climate impact by calculating the amount of sulfate deposited in the polar regions. To do that, I first adjusted the timing of the Kuwae signals in each ice core record by lining them up during 1453-1456 and fixing the highest values at year 1454 in both hemispheres. I then calculated the hemispheric average sulfate deposition by simply averaging the depositions of the seven SH ice cores (SP2001c1, PS1, Plateau Remote, Talos Dome, Law Dome, Siple Station, and DML_B32) and two NH ice cores (NGT_B20 and NorthGRIP1) that have sulfate records. The resulting total sulfate deposition was 93.0 kg SO_4/km^2 and 24.8 kg SO_4/km^2 for SH and NH ice core records, respectively (Table 3-1). The difference between these two average values suggests an asymmetric distribution of the volcanic debris.

To evaluate how representative these seven SH and two NH ice core records are, I compared the average sulfate depositions derived from these records to those from a larger number of ice cores for several other well-known volcanic events when more ice core records were available. In the SH I calculated sulfate deposition averaged from the seven cores and those from 17 records for the 1809 Unknown, 1815 Tambora, and 1883 Krakatau eruptions. These results, together with those for the NH ice core comparisons, are shown in Table 3.1. I also plotted in Figure 3.4 the sulfate fluxes averaged over the seven vs.17 SH ice cores and two vs. seven NH ice cores, respectively, for the four years following the Tambora eruption. My results show that the sulfate fluxes based on these seven SH ice cores records are very close, within 5%, to those from 17 SH records for the

three events chosen. Therefore, it is reasonable to assume that my estimation of sulfate fluxes for the Kuwae eruption based on the seven SH cores is representative of what I would obtain from the 17 SH ice core records.

Similarly, I calculated the average sulfate deposition of the two Greenland cores and the total seven cores for the Laki, 1809 Unknown, 1815 Tambora, and 1883 Krakatau eruptions (Table 3-1). The results based on the two northern Greenland ice core records are smaller than those averaged over the seven Greenland cores. Also listed in Table 3-1 are the average sulfate depositions for the Laki, 1809 Unknown, and Tambora eruptions from six PARCA [*Mosley-Thompson et al*., 2003] ice cores, and 12 CH88 Greenland cores from *Clausen and Hammer* [1988]. For all of the three events, both the PARCA and CH1988 ice core records and the seven Arctic cores have systematically a larger sulfate flux than the two northern Greenland ice core records. Previous studies [e.g., *Zielinski et al*., 1997] found that there are large spatial variations in the volcanic depositions among different NH ice cores. I also found, for instance, that the Tambora deposition ranges from 25 kg/km^2 in B20 (79ºN) to 73 kg/km^2 in GISP2 (72.6ºN) and 85 kg/km^2 in 20D (65ºN). Since both NGT_B20 and NorthGRIP1 (75.1ºN) are located in northern Greenland with very low accumulation rates (10 and 15 cm water equivalent per year, respectively, comparing to 20-50 cm water equivalent per year for other Greenland ice cores) I speculate that this is the major reason why the average deposition from these two records is smaller than that derived from the seven records in our study and the two other groups of Greenland records. To make the estimation of Kuwae deposition representative of the entire Greenland, I first calculated the ratio of average deposition from the total seven NH cores to those from these two cores for the four later eruptions

and obtained the average ratio of 1.8. This value is close to the ratio obtained from the two other groups of Greenland records as mentioned above. Then, I adjust the estimation of Kuwae deposition by multiplying the Kuwae deposition obtained from the 2 NH ice cores by a factor of 1.8 and obtained a deposition of 44.6 kg SO_4/km^2. The adjusted result is listed in Table 3-1 and also plotted in Fig.3-4. If I apply the same procedure to the SH, I obtain the adjusted estimation of Kuwae deposition in the Antarctic of 97.7 kg SO_4/km^2, which is very close to our original estimation.

Comparing the sulfate deposition of Kuwae eruption to that for the Tambora eruption (Figure 3-4 and Table 3-1) I find that the magnitude of the Kuwae deposition is smaller than that for Tambora for the NH, but much larger for the SH. The greater hemispheric asymmetry of Kuwae as compared to Tambora is reasonable given that Kuwae (17ºS) is much farther from the Equator than Tambora (8ºS). On the other hand, besides the location of an eruption, the distribution of volcanic debris also depends heavily on the time of the year when the eruption took place, the location of the Intertropical Convergence Zone (ITCZ), the Quasi-Biennial Oscillation (QBO), and the stratospheric winds on the day of the eruption. These factors introduce an uncertainty when trying to estimate hemispheric loading from an eruption, but if one know the deposition, one can infer stratospheric loading for each hemisphere. This is illustrated by the 1963 Agung eruption, which occurred at 8ºS, the same latitude as Tambora, but also dispersed 2/3 of its volcanic aerosols into the SH, the same proportion as Kuwae, but different to that of Tambora's aerosols which were more evenly distributed.

Table 3-1 also shows the standard deviations of volcanic sulfate deposition for each eruption, from which one can see that there are large spatial variations in both

Antarctic and Greenland ice cores. Several factors can account for this variation, such as surface irregularity, elevation, temperature, wind redistribution, and relative contribution of wet-dry deposition. Fig. 3-5 shows the ratios between the net deposition of Kuwae and Tambora sulfate aerosols. The use of these ratios eliminates much of the inter-site variability described above [*Cole-Dai et al.,* 1997]. However, Plateau Remote still has an unusually large ratio (5.6) followed by Talos Dome (3.8), compared with the average ratio (1.1) of the other 6 ice cores. *Cole-Dai et al*. [2000] suggested that the high value in Plateau Remote was caused by the partial loss or gain of snow within annual layers, whose effects are more pronounced in the low-accumulation sites; whereas *Castellano et al.* [2005] speculated that the Kuwae distribution pattern can be a real spatial variation in its depositional fluxes. The high ratios in these two sites doubled the overall average ratio between Kuwae and Tambora, and our results may overestimate the mean Kuwae sulfate deposition in Antarctica if the high ratios in the above two sites are actually caused by net gain of snow. This once again addresses the importance of using multiple (as many as available) ice cores with full spatial coverage to obtain the forcing index of past volcanism.

3.5. Summary

I have used 33 ice cores, 13 from the Northern Hemisphere and 20 from the Southern Hemisphere, to examine the timing and magnitude of the Great Kuwae Eruption in the mid-15th century. My results suggest that the Kuwae eruption is a single-phase eruption which took place in late 1452 or early 1453, which may serve as a reference to evaluate and improve the dating of ice core records. The Kuwae eruption produced significant depositions that lasted up to four years in both Greenland and Antarctic ice

sheets, confirming the potential of this eruption for global climatic impacts. The large difference between the two hemispheric-average sulfate deposition densities (97.7 kg/km^2 in the SH vs. 44.6 kg/km^2 in the NH) indicates an asymmetric distribution of the volcanic debris between the two hemispheres. My results also suggest that the Kuwae eruption caused one of the largest aerosol events in the past 700 years, probably surpassing the magnitude of the aerosol cloud caused by Tambora eruption in 1815.

Witter and Self [2006] calculated the total atmospheric sulfate aerosol loading from the Kuwae eruption and found it to lie somewhere between 235 and 414 Tg. They used geological techniques to estimate the amount of sulfur the eruption actually injected into the stratosphere. By measuring the amount of sulfate that was deposited in ice cores, in principle one could do an inverse calculation to estimate the stratospheric loading, and then use this information to calculate the radiative forcing of the climate system [e.g., *Stenchikov et al.*, 1998], one of the ultimate goals of my research. In the following chapters I will illustrate the technique I have developed to estimate the stratospheric volcanic sulfate aerosols loading using these bipolar multiple ice core records.

Chapter 4: Spatial Variability of Volcanic Deposition

4.1. Introduction

Through the study of Kuwae eruption, I have shown that the acidity and actual sulfate records from polar firn and ice cores provided us unique details about the nature, timing, and magnitude of volcanic eruptions. Nevertheless, there are problems associated with ice core records, among which one big problem is the large spatial variation of volcanic sulfate deposition across the ice cores. As more ice cores have become available during the past two decades, many studies have pointed out that there was no spatially homogeneous deposition structure but rather strong differences among the Greenland and Antarctic ice cores. For example, the Tambora eruption in 1815 in Indonesia has sulfate fluxes estimated to be between 22.4 kg/km^2 at Plateau Remote [*Cole-Dai et al.*, 2000] and 133 kg/km^2 at Siple Station [*Cole-Dai et al.*, 1997]; the 1783-1784 Laki deposition ranges from 79.7 kg/km^2 at Humboldt (78.5°N) to 323 kg/km^2 at D3 (69.8°N) [*Mosley-Thompson et al.*, 2003], and from 100 kg/km^2 at North C (74.6°N) to 291 kg/km^2 at Milcent (70.3°N) [*Clausen and Hammer*, 1988]. This large spatial variability raises the question of the reliability of previous reconstructions of atmospheric volcanic sulfate loadings based on a single or only a few ice core records. It also causes problems when comparing the relative magnitudes among different eruptions as well as comparing the same volcanic signal seen in different ice sheets.

The spatial variation of volcanic sulfate deposition may be attributed to site characteristics such as surface irregularity, temperature, wind speed, and surface elevation that can modulate the local accumulation [*Cole-Dai and Mosley-Thompson*, 1999]. The variation may also be caused by local or regional circulation patterns before

and during the time of deposition as well as the different deposition mechanisms [*Robock and Free*, 1995]. Estimations based on the average of multiple ice core records can reduce some of the uncertainties [*Robock and Free*, 1995, 1996; *Free and Robock*, 1999; *Mosley-Thompson et al.*, 2003]. However, the number of ice core records decreases as one goes back in time and only a few ice cores are available before 1000 A.D. The uncertainty introduced by the change of ice core availability can be reduced with knowledge of the spatial distribution pattern of volcanic sulfate aerosols.

In this part of the study, I have incorporated the volcanic signals derived from 26 ice cores that have actual sulfate records, plus the estimates of Laki and Tambora sulfate deposition in six PARCA and 12 CH88 Greenland ice cores, to estimate the spatial distribution of volcanic sulfate aerosols in Greenland and Antarctic ice sheets. This is the first study to use ice core records to investigate the spatial distribution patterns of volcanic sulfate at regional to continental scales. My results not only provide a guideline to reconstruct a long-term volcanic forcing index with a reduced body of ice core records, but also serve as a reference to evaluate model simulations of volcanic deposition.

4. 2. Ice Core Database and Volcanic Deposition Calculation Methodology

I have selected seven major low-latitude eruptions during the last millennium, Unknown (1259), Kuwae (1452 or 1453), Unknown (1809), Tambora (1815), Krakatau (1883), Agung (1963), and Pinatubo (1991), to study the spatial pattern of the volcanic sulfate deposition in the ice cores. These events were chosen because all of them are large explosive volcanic eruptions (VEI $\geq$ 5 [*Newhall and Self*, 1982]) that have signals in almost every available ice core record. In Greenland, there are only six ice cores with original sulfate data and among the six cores only three (i.e., NGRIP1, GISP2, and B20)

go back before 1500 A.D. I thus decided to use the 1809 Unknown, Tambora, and Krakatau eruptions as examples for low-latitude eruptions and added Laki (1783) and Katmai (1912) to represent high-latitude eruptions. *Mosley-Thompson et al.* [2003] calculated the sulfate deposition of Laki, 1809 Unknown, and Tambora eruptions for six PARCA ice cores; *Clausen and Hammer* [1988, CH88 hereafter] also computed the deposition for the Laki and Tambora eruptions for 12 Greenland ice cores. I have 26 ice cores that have actual sulfate record. So here I combined these two analyses with my 26 ice core results to obtain a more comprehensive understanding of the spatial pattern in Greenland ice cores. The volcanic deposition signals were extracted the same way as described above for each record. Then I evaluated the sulfate fluxes for the above nine events from the 26 cores and adjusted the timing of the signals so that the peak deposition of each event corresponds to the same year. After that, I calculated the total deposition for each eruption in the individual ice core by summing the deposition in the years that follow the eruption. The resulting sulfate deposition, together with those from six PARCA and 12 CH88 records, were plotted for individual eruptions.

4.3. Spatial Distribution of Volcanic Sulfate Deposition

4.3.1. Greenland Ice Cores

Figure 4-1 shows the spatial distributions of the Laki, 1809 Unknown, Tambora and Krakatau volcanic sulfate deposition in the Greenland ice cores; Fig. 4-2 shows the spatial patterns of the deposition interpolated into 0.5°×0.5° grid points. The interpolation was done using a *Cressman* [1959] objective analysis on the station data to yield a gridded result representing the station data (done with GrADS). From the figures we see that despite some local variations among the ice cores there are some common

spatial patterns at regional scale, which generally follows the pattern of annual total precipitation (solid + liquid) [*Box et al.*, 2004]. For example, there is above average deposition along the intermediate elevations on the western slope with the maximum located near 70°N, below average deposition on the northeast side of the Greenland ice divide with minima found in the interior area of northern Greenland, and large deposition on the west coast of north Greenland above Melville Bay. We found a positive linear correlation between volcanic deposition and annual accumulation rate at the 95% confidence level for three (Laki, 1809 Unknown, and Tambora) of the four eruptions (Fig. 4.3). The smaller significance in the case of Krakatau eruption (89%) was due to the small samples of volcanic anomalies. This correlation between volcanic deposition and annual accumulation rate is in agreement with the results of *Legrand and Delmas* [1987] and [*Mosley-Thompson et al.*, 2003], which indicates that the sulfate aerosols are more or less homogeneous in the atmosphere and the deposition in the ice sheet depends on the accumulation rates. No significant difference at regional scale was found between the spatial distribution of the Laki and Tambora fallouts, which implies that the deposition mechanism is probably the same for the low-latitude and high-latitude eruptions in Greenland.

From Figs. 4-1 and 4-2 we can also see that ice cores in northern Greenland (> 72°N) usually have less than average volcanic deposition, except for the ones on the west coast. Thus, volcanic stratospheric loadings based only on northern Greenland ice core records (e.g., B20, Humboldt, NorthGRIP1, and North Central) may very likely have been underestimated. The ice cores located at elevation 2000-2500 m on the west slope of the ice sheet (e.g., NASA-U, D2, and D3) usually receive larger than average

deposition, probably caused by precipitation enhancement due to orographic lifting. Maximum deposition was found in the cores located between 40°W and 45°W near 70°N, such as Crête sites B and D. Stratospheric aerosol mass loadings derived only from these cores may thus have been overestimated.

Larger spatial variations exist in deposition in the ice cores across Greenland, and the amplitude of this variability varies among different eruptions. For example, the spatial variability (defined as the ratio between the spatial standard deviation of sulfate deposition and the mean deposition) changes from 34-46% for high-latitude eruptions such as Katmai and Laki, to 41-48% for big low-latitude eruptions such as 1809 Unknown and Tambora, and further to 61-129% for smaller equatorial eruptions such as Krakatau and Agung. We also found that increasing the number of ice cores did not necessarily reduce the spatial variability. For instance, the variation of Laki and Tambora was larger than that of Katmai and 1809 Unknown although the number of cores available for Laki and Tambora was four times and twice as large as Katmai and 1809 Unknown, respectively. Spatial variability of the same or larger magnitude also exists at local scale. In the summit region of central Greenland we found a decrease of 53% from Crête site D to Crête in the volcanic sulfate aerosol deposition for the Laki eruption and 55% for Tambora, and a further decrease of 60% across the ice divide from Crête to Crête site E for Laki and 75% for Tambora. *Clausen et al.* [1988] also found that site E is located in an accumulation "shadow" area compared to the corresponding region east of the ice divide.

4.3.2. Antarctic Ice Cores

Figure 4-4 shows the spatial distributions of sulfate deposition for the 1809 Unknown, Tambora, Krakatau, and Agung eruptions respectively in the Antarctic ice cores. From these figures we can see a distribution pattern that is similar in regional scale for all of the four events: large deposition over the Antarctic Peninsula, West Antarctica and along the coast of East Antarctica; and small values over the plateau of East Antarctic and around Dronning Maud Land and Victoria Land. This pattern is generally in agreement with the long-term accumulation distribution in Antarctica [*Bromwich et al.*, 2004]. In the case of individual ice cores, Siple Station always has the highest deposition, followed by Dyer and the ITASE cores, all located in West Antarctica. *Reusch et al.* [1999] and *Dixon et al.* [2004] found that West Antarctica is the most stormy area of the continent, affected by several large atmospheric low-pressure systems, the Amundsen Sea Low, the Weddell Sea Low and the Davis Sea Low, which serve as the primary transport mechanisms for moisture and aerosols to the West Antarctic ice sheet. This leads to more precipitation and therefore more sulfate deposition in West Antarctica. The deposition at the four South Pole cores is relatively stable and is close to the continental averages. Law Dome usually has higher than average deposition. Plateau Remote, Dome C, DML-B32, Talos Dome and Hercules Névé always have lower than average deposition. Among the five sites, Plateau Remote and Dome C are located in one of the lowest long-term accumulation zones, with annual precipitation accumulation less than 50 mm/yr and elevation above 3000 km. These two cores also have the lowest correlation coefficients with the other sites, which indicates that the volcanic deposition in these sites is not representative of other regions of Antarctica and vice versa. *Cole-Dai et al.* [1997] found

the important role of post-depositional redistribution in regulating the volcanic signals in Plateau Remote. On the other hand, Plateau Remote and DML_B32 are the only two among these 19 cores that have records during 0-1000 A.D. Proper adjustment is thus needed to account for the spatial difference when using these two records to construct volcanic forcing time series for the early periods.

Figure 4-5 shows the spatial distribution of sulfate deposition for the 1259 Unknown, Kuwae, and Pinatubo eruptions. Although the numbers of ice core records available for these events are smaller than those for the previous four events, the spatial patterns of volcanic sulfate deposition are generally in agreement. The only exceptions are the larger-than-average deposition in Plateau Remote and Talos Dome for the Kuwae eruption. The reasons for these departures of volcanic sulfate deposition from the general pattern are yet to be investigated. It might have been caused by post-redistribution of the volcanic deposition or by different weather conditions, such as the circulation pattern at the time when the volcanic debris was deposited on the Antarctic ice sheet. Similar to the variability among the Greenland ice cores, we found a spatial variability of 44% and 48% for the 1809 Unknown and Tambora eruption separately across the Antarctic ice cores. The variability increased to 49%, 54%, and 65 % for the moderate eruptions as Krakatau, Pinatubo, and Agung eruption respectively. The increase of variability for small eruptions may either due to a larger signal to noise ratio or a less uniformed stratospheric "volcanic cloud".

4.3.3. Comparison with GISS ModelE simulations

Oman et al. [2006] conducted a set of simulations of the volcanic aerosol transformation and distribution following the Pinatubo, Tambora, Katmai, and Laki

eruptions using the GISS ModelE general circulation model coupled to a sulfur chemistry module. I compared the model simulated volcanic deposition with our ice core observation and found that at regional and continental scales the model produced spatial patterns similar to those from ice core observations. Figure 4-6 shows the model-simulated volcanic sulfate deposition in both Greenland and Antarctica and their corresponding ice core observations for the Tambora eruption. Similar to ice core measurements, the model produced low deposition along the east side of the ice divide as well as for interior Northern Greenland, and high deposition in the West and Central Greenland and coastal regions. Besides, the model produced a similar deposition pattern in both Greenland and the overall Arctic region for all of the four eruptions (Fig. 4-7), just like what the ice core observation indicated. Over Antarctica it produces high deposition in West Antarctica and low deposition in the east Plateau region. Different from the ice core observations, the highest deposition in the model is found to be over the Transantarctic Mountains.

Due to the coarse horizontal resolution, 4°x5° horizontal resolution and 23 levels in vertical, the model cannot capture details of local, small-scale variations of sulfate deposition. The average deposition over the grid points where we have ice core measurements is as much as twice as large as that of ice core observations for Tambora (59 kg/km^2 vs. 78.4 kg/km^2 in Greenland, 51 kg/km^2 vs. 113.3 kg/km^2 in Antarctica). The difference in the magnitude of sulfate deposition between the model simulation and ice core observations could be caused by the SO_2 to SO_4 conversion efficiency (100%), the hemispheric partitioning of volcanic clouds, and the transport speed and pathways of the sulfate aerosols between the model realization and what actually happened during

each eruption. Furthermore, the model's coarse resolution and smooth topography may hinder its capability to accurately simulate the deposition; and its lack of a proper simulation of the QBO may cause a noticeable impact on the aerosol distribution for low latitude eruptions [*Hitchman et al.*, 1994; *Haynes and Shuckburgh*, 2000].

4.4 Calculation of the Greenland and Antarctic mean volcanic sulfate deposition

As shown in From Figs. 4-1 and 4-3 the ice core sites are not evenly distributed in either Greenland or Antarctica. We have the majority of ice cores that were drilled from the central Greenland and West Antarctica. To account for this spatial inhomogeneity in ice core distribution, I first calculated the local average deposition for each area where there are at least two ice cores drilled close by. For example, in calculating the Tambora deposition in the Arctic I first calculated the average deposition in central Greenland, southern Greenland, and the northwest coast (i.e., average of Camp Century and GITS) of Greenland. Then I combined these local averages with the deposition from other ice cores, including Mt. Logan, to calculate the Arctic-mean deposition for Tambora. Similarly for Antarctic ice cores, I first calculated the local average deposition for the SP2001c1, SP95, PS1, PS14 cores at the South Pole; Siple Station, ITASE015, ITASE013 in the central Antarctic Peninsula; and ITASE001, ITASE991, ITASE004, ITASE005 in the western Antarctic Peninsula; respectively; before calculating the Antarctic means. The resulting Arctic and Antarctic mean sulfate deposition for the above nine eruptions, together with the number of ice cores available, are listed in columns 3 and 4 of Table 4-1. The deposition for 1259 Unknown and Kuwae eruption is adjusted (see Table 4-1 footnotes) to account for the reduction of ice cores available during those periods.

4.5 Summary

In summary, despite some local variability in Greenland and a few discrepancies in Antarctica, the volcanic sulfate deposition obtained from these 24 Greenland (six in Table 2-1, six PARCA, and 12 CH88), one Mt. Logan, and 19 Antarctic ice cores displays consistent spatial distribution patterns that resemble the general pattern of annual precipitation accumulation rates in Greenland and Antarctica, respectively. GISS ModelE simulations of the aerosol distribution following the Pinatubo, Tambora, Katmai, and Laki eruption revealed similar pattern at regional to continental scale. This indicates that the volcanic debris is more or less evenly distributed in the atmosphere before it reaches the surface, and precipitation played an important role in removing the volcanic aerosols. I also found that deposition in most of the individual ice cores is consistent in its ratio to the Greenland or Antarctica mean deposition for all of the eruptions listed above, being consistently smaller or larger. This provides a valuable reference to evaluate the estimations of volcanic forcing that were based on one or several particular ice core records.

On the other hand, spatial variability of about 45% was found for sulfate deposition across both the Greenland and Antarctic ice cores for large eruptions such as Tambora and 1809 Unknown, and this variability increases substantially for moderate eruptions such as Pinatubo and Agung because of lower mean deposition. I also found site to site variations as large as a factor of four among nearby ice cores in Greenland. Therefore, it is important to obtain good spatial coverage of ice cores from different geographical areas to accurately estimate atmospheric volcanic sulfate loading. Most of the currently available ice core records are concentrated in the areas of central Greenland,

central South Greenland, West Antarctica, and the South Pole. Future studies using ice core records may benefit from new cores drilled in other regions. For the early periods, when there are only a few cores available from certain regions, the total volcanic deposition should be carefully adjusted according to their ratios to the Greenland or Antarctica mean [*Gao et al.*, 2006].

Finally, it is worth mention that the volcanic sulfate deposition presented here for Greenland is from three different studies that used three different methods to extract the volcanic peaks. Different from this work, the 1809 Unknown and 1815 Tambora volcanic signals in the six PARCA ice cores were obtained by subtracting the background excess sulfate (EXS) from the EXS associated with 1810, 1811, 1816, and 1817 CE, respectively. The background EXS was calculated as the average value of the decade around 1810s but exclude the 1810, 1811, 1816, and 1817 CE values [*Mosley-Thompson et al* 2003]. The Laki and Tambora sulfate deposition in the 12 Greenland ice core records [*Clausen and Hammer*, 1988] was obtained by first perform chemical ion-chromatographic analysis (IC) of SO_4^{2-} and pH measurements on selected sites - siteA, Dye3, 4B and 18C for Laki as well as siteA and 18C for Tambora. Then the pH measurements on these selected samples from Laki and Tambora layers were used to calibrate the ECM to sulfate records. Despite the difference in methodology, the results should be robust because for volcanic eruptions as large as Laki, 1809 Unknown, and Tambora, the background variation should not affect the extraction of peaks and calculation of volcanic deposition no matter what method was used.

Chapter 5: Estimation of Stratospheric Volcanic Sulfate Loading

5.1 Introduction

By measuring the amount of sulfate that was deposited in ice cores, in theory one could do an inverse calculation to estimate the stratospheric loading, and then use this information to calculate the radiative forcing of the climate system [e.g., *Stenchikov et al.*, 1998]. To do this inverse calculation one has to make simplifying assumptions about the area of deposition of the sulfate and the representativeness of deposition on ice for the total atmospheric loading. The simplest assumption would be that sulfate deposition was uniform worldwide, and one could just multiply the mass of sulfate per unit area measured in the ice by the surface area of the Earth (5.1×10^8 km^2). But our data from Kuwae [*Gao et al.*, 2006] show that the SH polar deposition was twice of that of the NH, suggesting more total deposition in the SH. One could also assume uniform deposition in each hemisphere and that the ice core deposition was representative of the hemispheric average. However, the GISS model simulations show that most deposition occurs at midlatitudes (30°-60°) in each hemisphere, in regions of tropopause folds and strong stratosphere-troposphere transport along the jet stream and storm tracks (Fig. 5-1).

An alternative is to make simplifying assumptions about the transport and deposition of the volcanic sulfate aerosols, and use some reference event to calibrate the stratospheric loading. Several previous studies [e.g., *Clausen and Hammer*, 1988; *Langway et al.*, 1988; *Zielinski*, 1995] used factors derived from observations of radioactivity from nuclear bomb tests to estimate stratospheric sulfate loading, assuming a similar global distribution pattern between the radioactivity from bomb tests and sulfate injected into the atmosphere by violent volcanic events. Other studies [e.g., *Cole-Dai*

and Mosley-Thompson, 1999] assumed a similar global transport pattern for all of the low-latitude eruptions and used the observed aerosol loading of the Pinatubo eruption and its deposition in six South Pole ice cores to calibrate atmospheric loadings of other low latitude eruptions. However, *Zielinski* [1995] found that the atmospheric loadings derived in the first group of studies were 2-5 times larger than those calculated from stratospheric observations for recent eruptions by *Sato et al.* [1993]. The radioactivity data used in these studies was based on the United Nations Scientific Committee on the Effects of Atomic Radiation (UNSCEAR) 1982 Report [*UNSCEAR*, 1982] which used the total atmospheric loading rather than the stratospheric portion. In the second group of studies the calibration was only done for the South Pole ice cores and the result may be very different for ice cores in other regions. In addition, the hemispheric partitioning of volcanic clouds could be quite different than that for the Pinatubo eruption, depending on the location of the eruption, height of the plume, location of the ITCZ, phase of the QBO, and stratospheric winds when the eruption took place.

In this chapter of my Ph.D. work, I re-examined the bomb-test calculations using the up-to-date UNSCEAR 2000 Report [*UNSCEAR*, 2000]. This new available report includes new information that was previously unavailable and it separates the stratosphere from the troposphere. Besides, I updated the Pinatubo-based calibration factor using our extended assembly of ice core observations. I also calculated another set of calibration factors using the *Oman et al.* [2006] coupled chemistry/climate model simulations and evaluated the sensitivity of these calibration factors among the different methods. Finally I calculated the stratospheric loadings of the large volcanic eruptions

during the past 1000 yr by applying these factors to the 44 ice core records (the 26 ice core sulfate records from this study plus the six PARCA and 12 CH1988 ice cores).

5.2 Calculation of the calibration factors for tropical eruptions

Clausen and Hammer [1988] used the total atmospheric fission injections from USA and USSR bomb tests taken from *UNSCEAR* [1982] and calculated the calibration factor (L_B = the total β activity injected into the atmosphere by the bomb tests / the total β activity measured in Greenland ice cores) to calculate the global volcanic aerosol loadings for seven individual Greenland ice cores. Their calculation was based on the assumption that the transport and deposition of bomb test debris resemble those of volcanic aerosols on a large scale. Table 5-1 lists the deposition rates of total β activity (from $^{90}Sr + ^{137}Cs$) from the 1952-54 low NH latitude (11°N, LNL) and 1961-62 high NH latitude (75°N, HNL) bomb tests in 13 Greenland ice core sites. Since the total β activity was measured at least 10 years after the bomb tests in the ice cores, the measured activity is mainly due to ^{90}Sr and ^{137}Cs. The values were originally measured from the 24 Greenland ice core records by *Clausen and Hammer* [1988]. Some of the records are from the same sites or sites that are next to each other and I averaged these records to give a total 13 total β activity measurements. Figure 5-2 shows the spatial distribution of these 13 total β activity measurements in the Greenland ice sheet. Comparing Fig. 5-2 with Figs. 4-1 and 4-2, one can see that the two data sets have similar spatial coverage, though they were collected from different ice cores. The pattern of total β activity in general resembles the distribution pattern of volcanic sulfate aerosols, with large deposition near 70°N and small deposition in northeast Greenland. This confirms the previous assumption made by *Clausen and Hammer* [1988]. It also verifies, to a certain

degree, the reliability of using bomb-test-derived factors to estimate stratospheric sulfate loadings. Here I re-calculate the factor by using the stratospheric-partitioned fission yields from the most up-to-date report [*UNSCEAR*, 2000]. I only use the stratospheric portion of the fission yields because we are interested in estimating the volcanic sulfate loading in the stratosphere. The procedures for calculating the factors include: (1) calculate the stratospheric partitioned total fission yields (*TFY*) for the 1952-54 LNL bomb tests and 1961-62 HNL tests separately based on Table 1 of *UNSCEAR* [2000] (2) calculate the corresponding total β activity (*TBA*) by multiplying *TFY* with sum of the production rates of ^{90}Sr (0.105 MCi of *TBA*/Mt of *TFY*) and ^{137}Cs (0.159 MCi of *TBA*/Mt of *TFY*), and (3) calculate *L* by dividing the *TBA* obtained in step 2 by the average *TBA* measured in ice cores in Table 2 of *Clausen and Hammer* [1988]. The value for each step is listed in Table 5-2. The resulting factor is 1.51×10^9 km^2 for the 1952-54 LNL bomb tests and 1.22×10^9 km^2 for the HNL ones. The value is much smaller than those derived by *Clausen and Hammer* [1988] for the LNL tests (i.e., 3.35×10^9 km^2), but almost the same for the HNL tests (i.e., 1.46×10^9 km^2). The reason is that only about 50% of the fission produced by the LNL tests was in the stratosphere whereas more than 90% of the fission produced by the HNL tests end up in the stratosphere at polar latitudes (Table 4 from [*UNSCEAR* 2000]).

In the SH the total β activity from only three ice cores was measured by *Clausen and Hammer* [1988], which is too few to give a reliable estimate of a calibration factor given the large spatial variation in the Antarctic ice cores. However, since we have nine Antarctic ice cores that have Pinatubo signals, Law Dome, DML-B32, ITASE015, ITASE005, ITASE004, ITASE013, ITASE001, ITASE991, and SP2001c1, we can use

these ice core records and satellite observations of Pinatubo sulfate aerosol loading to derive a calibration factor (L_P = the total sulfate aerosol injected into the atmosphere by Pinatubo / the average sulfate deposition measured in Antarctic ice cores) to calculate the global volcanic aerosol loadings for Antarctic ice cores. Previous studies [e.g., *Krueger et al*., 1995] found that Pinatubo injected 15-20 Mt of SO_2 gas into the low and middle stratosphere. Assuming 75% H_2SO_4:25% H_2O weight composition [*Toon and Pollack*, 1973] and a complete conversion of SO_2 to H_2SO_4 aerosols, this amount of SO_2 would produce 30-40 Mt of sulfate aerosol in the stratosphere. On the other hand, the average Pinatubo sulfate deposition derived from the above nine Antarctic ice cores is 14.8 kg/km^2, which gives L_P ranging from 2.0×10^9 km^2 to 2.7×10^9 km^2.

The above calibration factors were calculated based on information derived from a single to a few events occurring at one latitude and altitude band under certain weather conditions, whereas the distribution of volcanic debris may differ significantly depending on the timing, latitude and altitude of the volcanic injection, and the natural synoptic variability. For example, observations found that although the 1982 El Chichón (17°N) and 1991 Pinatubo (15°N) eruptions were only two degrees in latitude apart, the volcanic cloud was confined mostly to north of the Equator for the former while almost evenly distributed north and south of the Equator for the latter eruption [*Robock*, 2000]. For eruptions in the SH, the 1883 Krakatau eruption (6°S) had more or less symmetric deposition of sulfate aerosols and the 1963 Agung eruption (8°S) dispersed most of its aerosols in the SH. I have found in the previous chapter that the 1452 or 1453 Kuwae eruption **(**17°S) also deposited about twice as much aerosol in the SH as in the NH. Therefore I propose that the low-latitude eruptions tend to disperse half to two thirds of

the aerosols in the hemisphere where the eruptions take place depending on the particular distribution of the winds. With this assumption I can estimate a range of calibration factors based on Greenland and Antarctic ice core records, respectively, for low-latitude eruptions with different hemispheric partitioning. For Antarctic ice core records, since my calculations indicate that the average deposition of these nine ice core records with a Pinatubo signal is very close to that from the total 19 Antarctic cores for all of the four earlier tropical eruptions (i.e., the 1809 Unknown, Tambora, Krakatau, and Agung) , and satellite observations showed a relatively even distribution of the Pinatubo clouds between NH and SH, it is reasonable to assume that the Pinatubo-observation derived factor (L_P = 2.0-2.7×10^9 km^2) gives a fair representation of the calibration factor for tropical explosive eruptions with symmetric distribution. For eruptions that disperse 2/3 of the aerosols in the SH L_P becomes 1.5-2.0×10^9 km^2; and for eruptions that have 1/3 of the deposition in the SH L_P is 3.0-4.0×10^9 km^2. For Greenland ice core records, if we assume the bomb test debris had a symmetric distribution, L_B is 1.5×10^9 km^2 for eruptions with even hemispheric partitioning and 1.1 ×10^9 km^2 or 2.25 ×10^9 km^2 for eruptions that disperse 2/3 or 1/3 of the aerosols in the NH, respectively. On the other hand, if we assume the bomb test debris had a 2:1 NH:SH distribution, then L_B becomes 2.0×10^9 km^2 for eruptions with even hemispheric partitioning and either 1.5 ×10^9 km^2 or 3.0 ×10^9 km^2 for eruptions that disperse 2/3 or 1/3 of the aerosols in the NH correspondingly. Therefore, when using volcanic deposition calculated from Greenland ice core records we obtained L_B ranges of 1.1-1.5×10^9 km^2 for eruptions that disperse 2/3 of the aerosols in the NH, of 1.5-2.0×10^9 km^2 for eruptions with symmetric distribution, and of 2.0-3.0×10^9 km^2 for eruptions that disperse 1/3 of the aerosols in the NH. *Bennett*

[2002] found injection to equatorial stratosphere deposit 69-74% of it radionuclides in the same hemisphere. Since the LNL bomb tests took place at 11ºN and were more likely to disperse more debris into the NH, the calibration factor from the high end may give more accurate estimations of the actual loadings.

The above calculations point to a mean calibration factor ($\overline{L}$) of about 2.0×10^9 km^2 ± 1.0×10^9 km^2 to be applied to deposition in each ice sheet to estimate the global aerosol loading for tropical eruptions. The uncertainty is about 50% of the mean value, which accounts mostly for the different hemispheric portioning of the volcanic debris and in part for the uncertainty in the satellite measurement of Pinatubo atmospheric loading. If I apply half of the value (1.0×10^9 km^2) to the average sulfate deposition in Greenland and Antarctica separately to calculate the loading in each hemisphere and add the two hemispheric loadings to obtain the global atmospheric loading, it is not necessary to know a priori what the hemispheric partitioning was of the initial aerosol cloud, and the ice core data will reflect the actual atmospheric loading. In this way, the uncertainty may be reduced. This assumes that removal and transport processes are on average the same in each hemisphere, but this assumption requires further investigation with detailed validated models and observations.

The GISS ModelE simulation of the 1991 Pinatubo eruption produced an average sulfate deposition of 38.4 kg/km^2 over Antarctica and 42.6 kg/km^2 over Greenland. These two average values were calculated from an area-weighted average from 70°S to the South Pole and for 66°N-82°N, 50°W-35°W, respectively. The model simulation converted 20 Mt of SO_2 gas into a sulfate aerosol yield of 36 Mt by assuming a 75 wt% H_2SO_4 and 25 wt% H_2O composition. This gives a calibration factor (L_{GISS} = the global

sulfate aerosol yield in the model / the Greenland or Antarctic average sulfate deposition simulated in the model) of 0.94×10^9 km^2 and 0.85×10^9 km^2 for determining the sulfate aerosol yield from Antarctica and Greenland sulfate deposition for tropical eruptions, respectively. In the simulation of the 1815 Tambora eruption, 55 Mt of SO_2 gas was injected into the 24-32 km layer which was converted into 107 Mt of sulfate aerosols. The model produced average deposition of 113.3 kg/km^2 and 78.4 kg/km^2 over the same areas in Antarctica and Greenland as for the Pinatubo eruption. Therefore, L_{GISS} is 0.94×10^9 km^2 and 1.36×10^9 km^2 correspondingly. The hemispheric difference in the average deposition, and thus the calibration factors, is caused by the model's hemispheric partitioning of the aerosol (64% in NH and 36% in SH for Pinatubo and 35% in NH and 65% in SH for Tambora). Accounting for the effect of hemispheric partitioning, we obtained the global mean calibration factor ($\overline{L}_{GISS}$) as 0.91×10^9 km^2 and 1.09×10^9 km^2 for Pinatubo and Tambora, respectively.

5.3 Calculation of the calibration factors for high latitude eruptions

Two high-latitude simulations, for the 1912 Katmai and the 1783-1784 Laki eruptions, were conducted using the same model. For Katmai, 5 Mt of SO_2 gas was converted to 9.3 Mt of sulfate aerosol and the model produced an average sulfate deposition of 17 kg/km^2 over the same area of Greenland as described for Pinatubo. Therefore, L_{GISS} of 0.55×10^9 km^2 was derived for estimating the total Katmai atmospheric loading based on sulfate deposition in Greenland. A similar calibration factor was calculated for Laki. The Laki eruption was simulated using the SO_2 emission estimate from *Thordarson and Self* [2003], in which a total of 122 Mt of SO_2 gas was injected over an 8 month period with approximately 80% going into the upper troposphere/lower

stratosphere. Model simulations produce a total sulfate aerosol yield of 165 Mt over the entire eruption. The average sulfate deposition over Greenland was 284 kg/km^2, gives L_{GISS} as 0.58×10^9 km^2. This value is very close to what we derived from Katmai even though the two eruptions are very different in both the duration and height of gas injection and the relative distance from Greenland. *Stevenson et al.* [2003] also simulated the atmospheric loading and sulfate deposition of the Laki aerosols using specified modern atmospheric circulation coupled to a chemistry model, but their emission assumptions resulted in about 70% of the SO_2 being directly deposited to the surface before being oxidized to sulfate aerosol. As a consequence, both the lifetime and the total atmospheric loading of the sulfate aerosols were substantially smaller than those from our estimates [*Oman et al.*, 2006] and petrology estimates [*Thordarson and Self*, 2003]. Figure 4-7 shows that the model produced similar spatial deposition patterns for Laki and Katmai, as well as the two tropical eruptions. Thus, we conclude that most Laki sulfate aerosols circulated around the Arctic with the polar vortex before being deposited on the Greenland ice sheet. Since the Laki and Katmai eruptions represent the breadth of different types of NH high latitude eruptions it is reasonable to assume that the average calibration factor of the two events (0.57×10^9 km^2) is applicable to all NH high latitude eruptions.

5.4 Stratospheric volcanic aerosol loadings for the largest eruptions during past millennium

Table 5-3 summarizes the calibration factors calculated from the above three methods, from which I find that the model-derived factors are substantially smaller than those from the other two methods. For tropical eruptions, it is very likely that the model

underestimates the factors by up to 50% due to the faster than observed transport of volcanic aerosols from tropical eruptions which resulted in a greater sulfate deposition in high latitudes. The bomb-test calculation and Pinatubo observation derived factors may thus provide better estimates of the stratospheric mass loading of the tropical eruptions. No matter what method was used, the resulting calibration factor is significantly larger than the total area of the Earth (0.51×10^9 km^2). Model simulations (Fig. 5-1) suggest that this is because most of the deposition is in the mid to high-latitudes and also over the southern reaches of the polar ice sheets in each hemisphere, and less so in the most poleward areas.

For the NH high latitude eruptions, since there is no candidate eruption that has both satellite observations and an ice core sulfate record, I cannot derive a calibration factor as I did for Pinatubo. The bomb test calculation is also not a reliable method because most HNL bomb tests were conducted in Novaya Zemlya (75°N, 60°E), 11°-17° north of where the Laki (64°N) and Katmai (58°N) eruptions took place, as well as 8° north of the Arctic Circle. Therefore, the transport and deposition of the nuclear debris may not be a good model for that from lower latitude volcanic eruptions. In addition, the HNL bomb tests were characterized by near instantaneous release of volatiles to heights larger than 20 km, whereas Laki in particular featured an eight-month long eruption with 13-14 km high plumes and the atmospheric mass loading was confined to the low stratosphere and troposphere [*Thordarson et al.*, 1993; *Fiacco et al.*, 1994; *Thordarson et al.*, 2001]. Since both the atmospheric circulation and lifetime of aerosols are fundamentally different for the stratosphere and troposphere [*Holton et al.*, 1995], the HNL bomb tests likely misrepresent the transport and deposition of NH high latitude

volcanic aerosols. Model simulations of the Laki and Katmai eruption, on the other hand, were found to give reasonable estimates of the transport and dispersal of the aerosols [*Oman et al.*, 2006].

According to the previous discussion, I decided to combine the bomb test calculation and Pinatubo observation derived factors to calculate the stratospheric sulfate aerosol loadings for tropical eruptions, while using the model-derived calibration factors to calculate the stratospheric sulfate aerosol loadings for high-latitude eruptions. Specifically for the tropical eruptions I applied $\overline{L}_{1/2} = 1.0\times10^{9}$ km^2 to the Greenland and Antarctic average deposition separately to calibrate the loadings for the corresponding hemisphere, then added the loadings calculated from each hemisphere to give the final estimate of the global loadings; for NH high latitude eruptions I applied $\overline{L}_{GISS} = 0.57\times10^{9}$ km^2 to the average deposition in Greenland ice cores and obtained the NH aerosol loading which also stands for the global loading. The resulting atmospheric sulfate loadings of the largest eruptions during the past 1000 years were listed in column six and seven in Table 4-1.

Column 8 in Table 4-1 listed the estimation of atmospheric volcanic sulfate aerosol loading based on radiation, petrology, and satellite observations, where we can see that in most cases our estimation agrees well with the other estimates. I estimated the stratospheric loading of Tambora sulfate aerosols to be 110 Tg. This value agrees with the estimation of 93-118 Tg based on a petrology study [*Self et al.*, 2004] but substantially smaller than the estimation of ~200 Tg by *Stothers* [1984]. *Self et al.* [2004] speculated that the large value in *Stothers* [1984] could be caused by a locally denser section of the overall volcanic cloud. The stratospheric loading of Laki is 93 Tg of

sulfate aerosols, which is smaller than the estimates based on radiation [200 Mt, *Stothers*, 1996] and geology [200 Mt, *Thordarson and Self*, 2003], the second of which was used as input for the climate model simulation of *Oman et al*. [2006]. This is because I only estimated the stratosphere loading while the other two studies reported the total atmospheric loading instead of the stratospheric component. Observational studies [*Thordarson et al.*, 1993; *Fiacco et al.*, 1994] estimated that about one third to one half of the emissions from Laki were injected into the stratosphere. Thus if I multiply my estimates of Laki loading by a factor of two, this would give a total atmospheric loading of 186 Mt which is in line with other estimates. My estimates for the rest of the eruptions (e.g., the total stratospheric sulfate aerosol loading of 30 Tg from Pinatubo, 17 Tg from Agung, and 11 Tg from Katmai) agree well with other independent studies (30±10 Tg from Pinatubo [*McCormick and Veiga*, 1992; *Bluth et al.*, 1993; *McPeters*, 1995], 15±5 Tg from Agung [*Rampino and Self*, 1984; *Kent and McCormick*, 1988; *Self and King*, 1996], and 11 Tg from Katmai [*Stothers*, 1996], respectively). My estimate of stratospheric sulfate aerosol loading from Krakatau (22 Tg) is relatively smaller than that from the petrology (30-50 Tg by *Rampino and Self* [1982, 1984]) and radiation (44 Tg by *Stothers* [1996]) estimates; so does the Kuwae eruption (138 Tg in this study vs. 235-414 Tg in *Witter and Self* [2006]). The petrology calculation is larger than ice core result probably because the former estimates the amount of sulfur the eruption injected into the stratosphere and there is a question of what percentage of sulfur has been converted into sulfate acid.

5.5 Stratospheric volcanic aerosol loadings for the past 1500 years

In the previous section, I calculated the stratospheric sulfate aerosol loading for nine large explosive volcanic eruptions during the past millennium taking into account the spatial variation. These estimates agreed fairly well with those based on radiation, petrology and satellite observations. To develop a 1500-yr long stratospheric volcanic sulfate loading index I applied the same methods and procedure except that I added 10 ECM records to the 44 sulfate records used above. These ECM records were included to give a better indication of the time of the eruptions. They were proven to be especially helpful for smaller events where more detail is needed to get a good signal to noise separation. Another modification is in the way to calculate the area-mean volcanic sulfate deposition. Instead of calculating the local mean deposition of cores that lie close to each other for each eruption, I calculated a set of ratios between the individual core vs. Greenland or Antarctic mean volcanic deposition and applied these ratios globally to individual ice core before they were used to calculate the Arctic or Antarctic mean depositions. In particular, I selected five large low-latitude eruptions – 1809 Unknown, 1815 Tambora, 1883 Krakatau, 1963 Agung, and 1991 Pinatubo – during the past two centuries and calculated the ratios between the volcanic deposition in individual ice cores and that of the Greenland or Antarctic mean for each of the five events. I then calculated the mean ratio for each ice core time series by simply averaging the five ratios. These mean ratios were then applied to each ice core time series before attempting to calculate the Greenland or Antarctic mean deposition to ensure that, on average, the relative contributions from each core would remain the same. By doing so, we reduce the bias caused by having only a few ice core records available in the early period.

Fig 5-3 plots the total sulfate aerosol injection (Tg) in NH, SH, and Global respectively for the volcanic eruptions during the period 501-2000 CE. We see that the largest stratospheric sulfate aerosol injection events being the 1259 Unknown, 1453 Kuwae, 1815 Tambora eruptions in tropical regions, and the 1783 Laki eruption in NH high latitude. The Kuwae sulfate injection was one year later in NH than SH since the peak deposition showed up a year later in Arctic ice cores. We also found a series of moderate to large sulfate injections during the 13th century - AD1228, 1258, 1268, 1275 and 1285. With our estimation of the 1259 Unknown eruption, the cumulative volcanic sulfate flux in 13th century was 2 to 10 times larger than that in any other century within the last millennium.

Fig 5-4 and Fig 5-5 show the comparison of the annual stratospheric volcanic optical depth time series between this work and that of *Robertson et al*. [2001], as well as this work and four recent reconstructions, respectively. From the figures we can see that our volcanic forcing time series are generally in good agreement with the other recent reconstructions. We found very good agreement between this work and *Robertson et al*. [2001] reconstruction which was also based on multiple ice core records. The peak optical depth for most of the big eruptions were larger in this work (Fig 5-3), but the total global mean optical depth for the individual events were similar in the two reconstructions. Both of the ice-core-based volcanic forcing indices found a couple pf events that were missed among the other non-ice-core-based reconstructions, for example, the 1947 Hekla eruption in South Iceland.

5.6 Summary

In this part of the study I calculated a set of calibration factors to convert ice-core-deposition to global aerosol loading from three independent methods: the radioactive deposition from nuclear bomb tests, satellite observations of Pinatubo aerosol loading, and climate model simulations of volcanic sulfate transport and deposition following the 1783 Laki, 1815 Tambora, 1912 Katmai, and 1991 Pinatubo eruptions. The factors were then applied to the 54 ice core sulfate records to calculate the stratospheric aerosol loading for the volcanic eruptions during the past 1500 years. The results agree fairly well with the estimations based on radiation, petrology, and satellite observations.

Chapter 6: Monthly and Spatially Dependent Forcing Index

6.1. Introduction

The time series of stratospheric volcanic sulfate aerosol loading reconstructed in the previous chapters gives us a sense of relative magnitude of volcanic events during the past 1500 years. This series can be converted into an optical perturbations index and further into a radiative forcing series used in a simple EBM to simulate the temperature response. However, to properly represent the dynamical aspects of volcanic forcing a more detail dataset with latitudinal and vertical information of the evolution of the volcanic aerosol clouds is necessary. As recent studies [*Robock and Mao*, 1993; *Robock*, 2000; *Ammann et al.*, 2003; *Graf et al.*, 2007] have shown, the seasonal evolution of volcanic aerosols might also be important particularly because of its impact on winter hemisphere temperature gradients which in turn affects atmospheric circulation [*Stenchikov et al.*, 2002]. *Sato et al.* [1995, updated to present] provide a nice compilation of stratospheric volcanic optical depth with respect to the wavelength λ = 0.55 μm at 24-point latitude grid with monthly resolution for the satellite period. But no detail spatial observation exists prior to the 1960s. Measurements of atmospheric radiation extinction are available from sites in both hemispheres [*Dyer and Hicks*, 1968] only after 1961; the NIMBUS 7 satellite provides data from polar regions since 1979 (Stratospheric Aerosol Monitor, SAM II; *McCormick et al.* [1979], and *McCormick* [1994]); the Stratospheric Aerosol and Gas Experiment (SAGE II, *McCormick and Wang*, [1987]) provides data between about 70°N and 70°S since 1984. If one is interested in spatio-temporal dependent volcanic forcing index before 1961 one has to reconstruct this property from other information sources.

Because aerosol transport is largely driven by the seasonally changing wind patterns in the stratosphere, a simple transport scheme could be applied. *Grieser and Schoenwiese* [1999] and *Ammann et al*. [2003, 2007] applied very simple seasonal evolution of aerosol clouds that allows simulation of the spread after any eruption. Ignoring potential modifications due to the phase of the QBO, the resulting mean distribution from such a transport model nevertheless looks realistic. The seasonal and latitudinal dependence of these two volcanic indices provide a more realistic estimation of the impact volcanic aerosol had on global climate change prior to the satellite period, compared to earlier volcanic forcing indices. However, the *Grieser and Schonwiese* [1999] estimation was based on VEI thus not directly related to climatic perturbation potential and it only went back to 16th century. The *Ammann* [2003, 2007] reconstruction was compiled from 14 ice core series which also include ECM records. By applying the *Grieser and Schönwiese* [1999] parameterization to our ice core reconstructions I produced a volcanic forcing data set (IVI2) that is a function of month and latitude. I also interpolated the vertical distribution of volcanic aerosols based on information obtained from 11 lidar measurements of the backscattering coefficient after the 1991 Pinatubo eruption [*Antuña et al.*, 2002], assuming that the aerosols from every eruption have the same vertical distribution as Pinatubo.

6.2. Latitudinally and Monthly Dependent Index

The horizontal transport of aerosol in the stratosphere is achieved by applying a non-local diffusion formalism [*Grieser and Schönwiese*, 1999]. I divided each hemisphere into eight equal-area latitude belts (Table 6-1) and assumed an isotropic transport within the tropics, extratropics, as well as anisotropic exchange among tropics,

extratropics, and polar regions [*Grieser and Schönwiese*, 1999]. Therefore, at each given time n, we can define a transilient matrix *A* to describe the temporal evolution of a spatial pattern by

$$a(n+1) = A_s a(n) \qquad (1)$$

where $a(n) = \{a_1(n), a_2(n), ..., a_{16}(n),\}$, with $a_i^*(0) = a^*$ represents the initial aerosol loading in the latitude belt of eruption i at the time of eruption $n = 0$. The transilient matrix *A* is not constant in time but rather depends on the seasons. Therefore, the matrix has $16 \times 16 \times 4 = 1024$ coefficients. To reduce the very high degree of freedom the authors made the following assumptions:

- Assume symmetric seasons so that there are only two different ones: an extreme one (a winter- and a summer hemisphere) and a moderate one without hemispheric differences. This reduces the amount of coefficients in the transilient matrix to $16 \times 16 + 16 \times 8 = 384$.
- Consider very short time steps and apply a local (non-isotropic) exchange. This means that only the diagonal and the first subdiagonals of the matrix are filled with non-zero elements. Therefore we only need to know $2 \times 16 + 4 \times 15 = 92$ coefficients. Taking also into account the conservation of mass the sum over any column or row of the matrix has to be unity. This leads to 30 independent coefficients.
- Assume an isotropic transport within the tropics, anisotropic exchange between tropics and extratropics, isotropic transport within the extratropics (two seasons) and isotropic exchange between extratropics and polar regions in the summer- and winter hemisphere as well as during the moderate seasons. Together with the condition of conservation of mass this leads to only eight independent coefficients, which have to be taken from or estimated from literature.

Table 6-1listed the eight monthly transport coefficients among different latitude belts for different seasons used in this work. Also listed in Table 6-1 are the original exchange coefficients used in *Grieser and Schönwiese* [1999]. Compared to *Grieser and Schönwiese* [1999] I increased the diffusion rate from the tropics to the extratropics and from the extratropics to the polar region, as well as the exchange coefficient within the extratropics during summer and fall to allow more transport of aerosols from low latitudes to high latitudes. The exchange coefficients in *Grieser and Schönwiese* [1999] were obtained from recent studies of stratospheric mass transport and most of the estimates contain uncertainties. I modified a few of the exchange rates according to these uncertainty estimates in order to increase spread of aerosols from tropics to high-latitude. For example, in calculating the exchange rate (0.45) within extratropics during summer/full, *Grieser and Schönwiese* [1999] assumed a 50% reduction from its winter/spring value (0.9). However, Hitchmann *et al.* (1994) found this seasonal difference to range from 20% to 50%, which indicates that the summer/fall exchange rate can lies anywhere between 0.45 and 0.72. I used the same time step (2 days) as *Grieser and Schönwiese* [1999] to ensure the local exchange. Given that, the exchange coefficients between latitude belt i and k in percent per time step $a_{i,k}$ can be easily obtained as

$$a_{i,k} = 1 - (1 - m_{i,k})^{1/15} \qquad (2)$$

where $m_{i,k}$ is the monthly exchange coefficient listed in Table 6-1.

Another major difference is that for tropical eruptions I put initial sulfate aerosol in each hemisphere (according to ice core estimates) and only allow the transport within each hemisphere, i.e., there is no transport between the two lowest latitude belts in the

tropics. I adopted this approach because for the early eruptions we have no information about the location or season of the eruption and thus the hemispheric partitioning of the sulfate aerosols. Since the ice core estimates give us relatively accurate estimates of the hemispheric distribution of volcanic aerosols [*Gao et al.*, 2006], we can preserve this information by allowing transport only within the corresponding hemisphere. For eruptions without recorded month of eruption, I assumed that they occurred in April, as was done for the Volcanic Explosivity Index [*Simkin and Seibert*, 1994]. For eruptions without recorded location, I assumed a tropical eruption if there are signals in both Arctic and Antarctic ice cores, but a mid- to high-latitude eruption if signals were only found in one hemisphere. *Crowley and Kim* [1999] had tested the climatic impact of this assumption for unknown events by comparing a tropical source with two independent high-latitude events. They found that the effect of such a mis-identification was relatively small.

To generate the time dependent data, I assume a linear buildup of the total aerosol mass for four months after eruption, leading to a maximum mass loading according to the strength of the eruption. After that I assume an exponential decrease of the stratospheric aerosol mass with a global mean e-folding time of 12 months. Since the major sink mechanism for stratospheric aerosol is stratosphere-troposphere folding in midlatitudes and the Brewer-Dobson circulation related sink in high latitudes [*Holton et al.*, 1995], I assume little loss due to sedimentation in the tropical regions (e-folding time of 36 months) and keep the sedimentation to an average e-folding time of 12 months in the extratropics. In the polar region, I set the e-folding time to be three months during winter to account for the strong subsidence in the polar vortex and six months for the rest of the

year. By applying this latitude-season dependent function that describes the production and sedimentation of aerosols and the non-local diffusion formalism to simulate the transport of aerosols in the stratosphere, I obtained a distribution of volcanic aerosols in latitude and time. Figure 6-1 shows an example of the resulting spatial and temporal distribution of the stratospheric volcanic optical depth for three years after the Pinatubo eruption in 1991. The optical depth was calculated by dividing the aerosol loading (in units of gram) by per 1.5×10^{14} [*Stothers*, 1984]. In the figure we see a linear increase of aerosol loading for the first four months and the seasonal transport to the poles. The result agrees fairly well with the satellite measurement and GCM calculations of Pinatubo optical depth [*Stenchikov et al*., 1998]. Figure 6-2 shows the distribution for the 1809 Unknown and 1815 Tambora eruptions, where we can see not only the spread of volcanic aerosol in space and time but also the relative magnitude between the two eruptions. The total sulfate aerosol fluxes in the two polar regions after the Tambora (47 kg/km^2 and 49 kg/km^2 in the Arctic and Antarctic respectively) and Pinatubo (13 kg/km^2 and 15 kg/km^2 in the Arctic and Antarctic respectively) are also in general agreement with the ice core observations (59 kg/km^2 and 51 kg/km^2 in Arctic and Antarctic respectively for Tambora, and 15 kg/km^2 for Pinatubo in the Antarctic), which serves as an important confirmation of the reliability of our transport and deposition program, despite its simplicity.

In the next step, I interpolated the vertical distribution of volcanic aerosols using information obtained from 11 lidar measurements of the aerosol backscattering coefficients at 0.525 μm wavelength after the 1991 Pinatubo eruption [*Antuña et al.*, 2002]. *Ansmann et al.* [1997] and *Antuña et al.* [2003] found a general good agreement among lidar, SAGE2 and AVHRR measurements six months after the Pinatubo eruption.

The difference between SAGE2 and lidar derived extinction measurements was mainly caused by the large variability in the aerosol clouds. Due to the Earth Radiation Budget Satellite's orbital characteristics, the sample resolution of SAGE2 is 1/40 days. And in regions with high aerosol loading (optical depth $\tau > 0.15$) there are many gaps in the measurements [*Antuña et al.* 2003]. AVHRR does not have measurements for winters [*Ansmann et al.* 1997]. The lidar measurement, on the other hand, has greater vertical and temporal resolution, but limited spatial information. Therefore, I used lidar measurements from 11 sites to increase the spatial coverage. For each lidar dataset, I first calculated the total column backscattering coefficient for heights from 15 km to 30 km; then I calculated the ratios between backscattering coefficient for each 0.5 km depth and the total column value. This gives us the vertical distribution of Pinatubo aerosols in the stratosphere for the region. Then I divided Earth into tropics (0-30°), midlatitudes (30-60°), high latitudes (60-70°), and polar region (70-90°), and calculated the regional mean vertical distribution of Pinatubo aerosol by averaging the lidar measurements in the corresponding regions. Finally I applied these four sets of vertical distribution function to the monthly volcanic aerosol data I obtained above, assuming that each eruption has the same vertical distribution as Pinatubo in the corresponding regions. Figure 6-3 shows an example of the vertical distribution of volcanic aerosols six months after the Tambora eruption. We see that the center of sulfate aerosols loading shifted from 18 - 25 km in the tropics to 14 - 20 km in the midlatitudes. The aerosols were more concentrated in the NH because it was in October and the wind blows the volcanic cloud toward the winter hemisphere.

6.3. Advantage of IVI2 and estimate of its uncertainties

6.3.1 Improvement of IVI2 from previous reconstructions

Robock and Free [1995] identified eight problems in using ice core records as measures of volcanic aerosol loading: (1) other sources of acid and bases; (2) other sources of sulfate; (3) dating uncertainties; (4) local volcanoes; (5) limited knowledge of the aerosol's pathway from the stratosphere to the ice; (6) stochastic nature of snowfall and dry deposition; (7) mixing due to blowing snow; (8) temperature dependence of ECM measurements. In the present study I used only the sulfate records to calculate the stratospheric volcanic sulfate aerosol loadings, which eliminated the first and the last problems. The signal extraction and deposition calculation methodology minimized the errors associated with problems (2) and (3); and our extended body of ice cores from both Greenland and Antarctica helped to distinguish local volcanoes from tropical ones in conjunction with the recent VEI index [*Siebert and Simkin,* 2002]. The information of the spatial distribution pattern obtained in chapter 3 was used to estimate and reduce the uncertainties caused by problems (6) and (7).

The extensive number of ice core records reduces the errors inherent in previous studies that were based on single or a small number of ice cores, which enables us to obtain much higher accuracy in both detection of events and quantification of the radiative effects. Another improvement of this work from previous ones is that I adjusted the dating of each potential volcanic signal in the different cores, taking into account the information of dating uncertainty in individual ice core record, the geological and historical records.

6.3.2. Uncertainties in the reconstruction of IVI2

Despite the great improvement IVI2 has compared to other volcanic forcing indices, there are still remaining uncertainties. The biggest uncertainty comes from the calculation of calibration factors used to convert ice core sulfate deposition into atmospheric aerosol loadings. While the distribution of volcanic debris differs significantly depending on the latitude, altitude, timing of the eruption and the direction of the winds when the eruption took place, the calibration factors used in this study were derived from a single to a few events occurring at one latitude and altitude band under certain weather conditions. To account for this limitation, we calculated L_B and L_P under different assumptions of hemispheric partitioning and estimated the uncertainty range for the mean calibration factor $\overline{L}$ (25%). Simultaneous use of ice core records from both poles tells something about the hemispheric partitioning of volcanic clouds and thus would be an optimal way to estimate the global loadings. However, fewer ice core observations are available as one goes back in time to give a reliable indication of the hemispheric partitioning as well as the magnitude of the atmospheric mass loading. Therefore, proper adjustments are needed when using few ice cores to estimate strength of the earlier eruptions or the results should be interpreted with caution. Furthermore, the bomb-test-calculation and Pinatubo-observation derived factors are only for NH and SH respectively, due to the limited radioactivity and Pinatubo deposition measurements. The inconsistence of calibration methods may have introduced certain uncertainties in the estimation. Besides, calibration against a well-known eruption requires a linear relationship between the sulfate emitted into the stratosphere and the sulfate recovered from the ice core measurement. The linear relationship does not always hold, especially

for the large eruptions. *Pinto et al.* [1989] found that for eruptions that emitted sulfur larger than 15 Mt, their stratospheric sulfate aerosol loadings may not be proportional to the magnitudes of eruptions. That is because beyond this point, the increase of sulfur does not necessarily increase the number of aerosols but mainly working on increases the size of aerosol particles and these larger particles have shorter lifetimes in the atmosphere.

As described in Chapter 4, I found spatial variation of about 50% for the 1815 Tambora deposition among both Arctic and Antarctica ice cores, and this number could be substantially larger for less well known or less significant eruptions. Though our extensive body of ice core records significantly reduced the error associated with the estimations of the ice core volcanic sulfate deposition when compared to previous studies. The number of available ice cores constantly changes from one eruption to another and decreases dramatically for the early period. It is difficult to give a global quantitative estimate of the uncertainty related to the calculation of the ice core mean volcanic sulfate deposition. Further expansion of ice core availability in the future studies will help to reduce this uncertainty.

Besides the variation in the ice core depositions, there are uncertainties associated with the assumptions I made during the procedure to estimate the stratospheric aerosol loading, such as the choice of (1) twice the 31-yr running MAD as the threshold to extract the volcanic signals (called 31pts+2MAD hereafter) and (2) April as the month of eruption. To test the sensitivity to these assumptions in my reconstruction, I applied different choices of the above assumptions to the ice core records for the period from 1801 to 2000, keeping other procedures the same. The time frame was chosen because

this is the period where we have the most ice core records and also several moderate to large volcanic events.

(1) Uncertainty Associated with Different Signal Extraction Criteria

To estimate the sensitivity of the threshold and window length in the volcanic signal extraction procedure, I first changed the threshold to be 1.5MAD and 3MAD respectively while keeping the window length as 31-yr; then we changed the window length to be 11-yr, 51-yr, and 101-year, respectively while keeping the threshold as 2MAD. This gives us six different sets of criteria including the original set. Applying these six sets of criteria to the ice core records for the past 200 year, I found that the different criteria do not significantly change either the detection of signals or their magnitude for moderate to larger volcanic eruptions (Figure 6-4). The signals from small eruptions were not identified by the either the 51pts+2MAD or the 101pts+2MAD criterion or both. Therefore, given a certain threshold, the extraction method is less sensitive for longer the running means. This is because the larger the window lengths the more volcanic events in the targeted period, which tend to increase the background noise to signal ratio. The 31pts+1.5MAD criterion picked up some additional signals as compared to the other methods. Most of these additional signals are either false volcanic signals or too small to be climatically significant. The 11pts+2MAD criterion usually gave a lower estimate of sulfate loading for eruptions closely following another event, because it tends to filter out the decadal signal produced by consecutive eruptions as the background variation. Therefore, I disregard the 11pts+2MAD criterion from further calculation and discussion. The coefficient of variance among the five criteria is as small as 4% for large eruptions like Tambora in 1815, and it increases to about 10% for

moderate eruptions such as Krakatau in 1883 (Table 6-2). In chapter 2 I described why I chose 31pts+2MAD as our signal extraction criteria. Here I found that the estimated sulfate loading and the corresponding climate impacts are insensitive to the criteria chosen within a reasonable range, and the maximum uncertainty associated with the different choice of criteria is about 10%. The El Chichón signal appears to be sensitive to the choice of threshold (Fig. 6-4) because most of our Arctic ice core records end before or around 1980s and the signals becomes more difficult to be distinguished from the background toward the end. The El Chichón signal was missed from our Antarctic cores for almost all of 6 criterions probably due to its very asymmetric hemispheric distribution [*Robock*, 2000].

(2) Uncertainty Associated with Eruptions Occurring in Different Seasons

In the above ice-core-based volcanic forcing reconstruction I assumed the eruptions to occur in April if there is no record of the particular time of the eruption. This may introduce additional uncertainty because the seasonality of volcanic emission can affect its atmospheric transport and deposition in different latitudes. Since I was using a stratospheric transport parameterization to simulate the real world activity, I evaluated the uncertainty associated with this seasonality assumption in the transport parameterization program. In particular, I set the eruption time to be January, April, July and October representing winter, spring, summer, and fall (NH) eruptions, respectively and ran the program at different seasons. I assessed the difference in the high latitude volcanic sulfate deposition for each setting because this may reflects the uncertainty associated with our calculation of the total stratospheric aerosol loading using ice core records. Figure 6-5 plots the time series of sulfate deposition in the latitude band 60°-90°

for Tambora eruption in each hemisphere. The major difference is the lag of deposition in time and how the signal is spread over multiple years. In terms of the total deposition, the difference among the four seasons is about 10%. A spring eruption distributed the least loading in NH high latitudes and the most in SH high latitudes among the four seasons, with the opposite for a fall eruption.

Figures 6-6 and 6-7 show the time series of Tambora sulfate aerosol loading in the midlatitudes and low latitudes for the four seasons. I found no significant differences (about 3% and 1% in extratropics and tropics, respectively) in the total loading. The major difference is again the lag of loading in time. In tropical regions, since the solar radiation is relatively constant year around, this time lag in loading does not change the overall radiative affect; in mid-latitudes, however, this seasonal difference in peak loading may significantly change its overall radiative impact. For example, I found a large shift of sulfate aerosol loading from the first NH summer and fall to the following winter and spring in both hemispheres for a July and October eruption. As a result, we would expect the direct radiative (cooling) effect to be less in NH midlatitudes for a summer or fall eruption as compared to a spring eruption. In SH midlatitudes, the reduced cooling and increased warming later on balanced each other to some degree and we cannot predict the overall radiative effect based on our simple analysis. GCM simulations are necessary to test the detailed radiative, dynamic, and temperature responses associated with eruptions in different seasons, but it is beyond the scope of this work.

According to the above comparison, the seasonality of eruption introduced another 10% uncertainty into my calculation of volcanic forcing time series.

Nevertheless, the numerical distribution program is too simple to include some important climatic effects such as the QBO, and thus the seasonality difference may be larger than estimated here.

6.4 Summary

I have used 54 ice core records, 32 from the Arctic, including the 12 Clausen and Hammer ice core and six PARCA cores, and 22 from Antarctica to generate a new volcanic forcing index for the past 1500 years. The index is a function of month from 501 to 2000, latitude in 10° bands, and height from 9 to 30 km at 0.5 km resolution. It is the longest and the most advanced volcanic forcing time series of this type, because it was based on the most comprehensive set of ice core records, plus an updated signal extraction method, ice-core-deposition to global stratospheric aerosol loading conversion factors, and a more advanced spatial-temporal transport parameterization scheme.

By using an extensive number of ice core records and accounting for the spatial variation of volcanic deposition in Greenland and Antarctic ice sheets, I significantly reduced the uncertainty in the new volcanic forcing index when compared to early studies. However, there are still a 4-10% uncertainty caused by different volcanic signal extraction criteria, and 10% uncertainty in high-latitude sulfate deposition when assuming different eruption season in the transport program simulations. On top of that, the calibration factor ($2.0\pm0.5\times10^9$ km^2) we used to calculate the global total volcanic sulfate aerosol loading from Arctic and Antarctic mean sulfate deposition introduces an additional 25% of uncertainty [*Gao et al.*, 2007]. Accounting for these uncertainties we found a total uncertainty of around 40% in our reconstruction for large eruptions such as Tambora and 45% uncertainty for moderate eruptions like Krakatau and Pinatubo, regardless of the

uncertainty in calculating Arctic and Antarctic mean sulfate deposition using multiple ice core records. Nevertheless, these uncertainties are much smaller than the factor of two uncertainty estimated in the early studies [e.g., *Zielinski* 1995].

Chapter 7: Modeling the Climate Responses to the Large Explosive Volcanic Eruptions

7.1. Introduction

Once the monthly and spatially dependent volcanic forcing index is available, ideally one can apply the time series to a general circulation model (GCM) to simulate the temperature response of volcanic eruptions. So far, transient calculations have been carried out by *Hansen et al* [1997] and *Oman et al*. [2006] with Goddard Institute for Space Studies (GISS) model, and *Timmreck et al.* [1999] with the Hamburg climate model (ECHAM4), *Broccoli et al*. [2003] with the Geophysical Fluid Dynamic Laboratory (GFDL)-R30 model, *Wigley et al.* [2005] with the National Center for Atmospheric Research (NCAR)/U.S. Department of Energy (USDOE) parallel climate model (PCM), *Ammann et al.* [2007] with the NCAR Version 1.4, a global coupled atmosphere-ocean-sea ice-land surface model, respectively. However, due to its large numerical effort and computation time such GCM runs are beyond the time frame of this study. On time-scales of the past one to two millennia, it is likely that both the external forcings and the internal oscillations of the climate system have played the most important roles in causing the climate variation. Time-dependent GCM simulations of volcanic effects are likely to be obscured by the relatively large internal variability of the models. A simple upwelling-diffusion energy-balance model (UD EBM), on the other hand, can help us to reveal aspects of the climate response to volcanic forcing that are difficult to examine with other methods. *Stenchikov et al.* [1998] found from GCM calculations that the aerosol radiative forcing following the Pinatubo eruption is not sensitive to the dynamical atmospheric response to this forcing. This encourages

radiative forcing calculations without using GCMs. MAGICC, namely, the model for the assessment of greenhouse gas–induced climate change [*Wigley and Raper,* 1992, 2001] has been used in various Intergovernmental Panel on Climate Change (IPCC) reports to emulate the AOGCM results. *Wigley et al.* [2005] tested its ability to produce the volcanic caused climate response against the NCAR/USDOE Parallel Climate Model. The very close agreement they found justifies the use of MAGICC to obtain reliable estimates of how the climate responses to various volcanic eruptions with some confidence.

7.2. Model Configuration

The model I used in this study is an updated version of MAGICC that was designed specially for volcanic runs (Tom Wigley, personal communication). The model consists of an atmospheric energy balance model coupled to an upwelling-diffusion ocean model. The atmospheric EBM has land and ocean boxes in each hemisphere, and the UD ocean model in each hemisphere has 40 layers with inter-hemispheric heat exchange in the mixed layer (Fig 7.1). Some important model parameters were set as the following:

- Upwelling rate (W): 4m/yr
- Vertical diffusivity (K): 2.3 cm^2s^{-1}
- The depth of mixed layer (h): 60 m
- The ratio of the temperature of downwelling high-latitude water to that of the rest of the mixed-layer water (π): 0.2
- The climate sensitivity: 3.0ºC

The input forcing for MAGICC is the global mean monthly radiative forcing (in W m^{-2}) at the top of the atmosphere. Therefore, I converted the time series of global

stratospheric volcanic aerosol loading (in unit of Tg) obtained in Chapter 4 into radiative forcing (in unit of W m^{-2}) by first dividing the loading by 1.5×10^{14} [*Stothers*, 1984] to obtain the optical depth (τ); then multiplying the optical depth by 20 [*Wigley et al.*, 2005] to obtain the radiative forcing in W m^{-2}. The solar forcing over the past 1000 years was obtained by scaling the solar modulation estimates [*Muscheler et al.*, 2007] to a recent solar irradiance reconstruction [*Wang and Lean*, 2005]. For anthropogenic forcing we applied the IPCC SRES A1B forcing scenario with median anthropogenic aerosol forcing [Q(2000) = 1.4 W/m^2, Tom Wigley, personal communication]. The model was run from 850 CE to 2015 CE with climate sensitivity set to be 3.0 °C for doubling CO_2 concentration.

7.3. Model simulated temperature responses

Figure 7-2 shows the model simulated global annual average temperature response to the solar, volcanic, anthropogenic forcing alone in color and that to the total radiative forcing in black. From the model we can see that the model produced maximum cooling ranges from about 0.2°C for the moderate eruptions to 3°C for the 1259 Unknown eruption. We found that the series of eruptions during the 13th century played the dominant role in causing the temperature decrease for the century; while both solar and volcanic forcing contributed to the overall cooling during the period from 15th century to the early part of the 19th century. The warming in the 20th century was the combined effect of solar, volcanic, and GHG forcing, with the GHG played the dominant role.

Figure 7-3 shows the comparison between the model simulated global mean temperature and instrumental observation for the past 150 years. We found a good

agreement between the model results and observation. The model accurately simulated the cooling of about 0.2-0.3°C for the three tropical eruptions, i.e., 1883 Krakatau, 1963 Agung, and 1991 Pinatubo eruption during this period. One the other hand, the model did not produce cooling for the 1982 El Chichón eruption. The El Chichón signal was missed from our ice-core-based reconstruction because most of our Arctic ice cores end before or around 1980s, and due to its asymmetric distribution [*Robock*, 2000] no El Chichón signal was extracted from the Antarctic ice core records. Therefore, we conducted another MAGICC run where we replaced our ice-core-based reconstruction with Sato's [*Sato et al*, 1993 and updated to present] values after 1970 CE and compared the model response to NH temperature reconstructions [Fig. 6.10 in *Climate Change 2007*] for the past millennium (Fig. 4). The model simulation generally captured the temperature variation on the decadal to central scale: relatively warm period between the 9th and 12th century following by a gradual cooling last until the 19th century; coldest episodes occurred during the 13th, 15th, and 19th century; and the exceptionally high temperature after 1850 CE. Several sharp cooling events mark the temperature response to large explosive volcanic perturbations, for example, the 1453 Kuwae, 1810 Unknown and 1815 Tambora eruption. The largest volcanic perturbation was estimated to be the 1258 Unknown. Together with four other moderate to large sulfate injections during the century - 1228, 1268, 1275 and 1285 CE, this particularly large eruption caused a clear temperature decrease of several tenths of a degree Celsius for the entire 13th century. This suggests the possible role of these temporal-closely spaced eruptions may have in initiating the climate variation of that period. The model temperature appeared to be lie at the high end of the proxy reconstruction range during the17th and most of the 19th

century, probably because of the low long-term variations in the solar forcing time series we used.

The model produced more cooling than the reconstructions for the 1258 Unknown eruption. There could be multiple reasons for this. On the one hand, IVI2 may overestimate the forcing for large volcanic eruptions due to the linear assumption I made between the atmospheric sulfate mass loading and its radiative perturbation. The model may be too sensitive to volcanic forcing due to its simplicity. On the other hand, temperature reconstructions also contain significant uncertainties, especially for old periods like this. Beside, *Robock* [2005] showed that temperature reconstructions based on tree ring records tend to underestimate the cooling following volcanic eruptions because of compensating growth from the diffuse radiation caused by volcanic aerosols.

Chapter 8: Conclusions and Possible Future Work

The previous chapters describe my work in collecting and extracting the volcanic signals from ice core records, in identifying the year and magnitude of the great 15th century Kuwae eruption, in studying the spatial distribution of volcanic aerosol in Greenland and Antarctic ice sheets, in developing the time series of stratospheric volcanic sulfate aerosol loading as well as the monthly and spatially dependent volcanic forcing index for the past 1500 years, and in modeling the temperature response to volcanic forcing. In this chapter I summarize the results and implications of this work and outline some directions of future work on this topic.

Ice Core Collection and Signal Extraction Methods

53 ice core records from Arctic and Antarctica were collected in this study, including both electrical conductivity measurement and actual sulfate records. The extensive number of ice cores, more than double of that in any previous studies, reduced the errors inherent in reconstructions based on a single or small number of cores, which enables us to obtain much higher accuracy in both detection of events and quantification of the radiative effects.

I developed a volcanic signal extraction methodology that provides robust estimates for a wide range of population distributions.

The 15th Century Kuwae eruption

I combined 33 ice core records, 13 from the Northern Hemisphere and 20 from the Southern Hemisphere to determine the timing and magnitude of the Great Kuwae Eruption in the mid-15th century. By accounting for the dating uncertainties associated with each record, I found a large volcanogenic acid deposition event during 1453-1457

A.D., which pointed to late 1452 or early 1453 as the time when the Kuwae eruption took place. This result provides an important reference to evaluate and improve the dating of ice core records. I estimated the average total sulfate deposition from the Kuwae eruption using the ice core sulfate records. The result was 93 kg SO_4/km^2 in Antarctica and 45 kg SO_4/km^2 in Greenland after adjusting for the spatial variation, which made it the second largest stratospheric event during the past 1500 years, surpassing the Tambora eruption of 1815 which produced a year without summer.

The Spatial Variation of Volcanic Sulfate Aerosol in Greenland and Antarctic Ice Sheets

I have used 44 ice core sulfate records, 26 from our collection, six PARCA ice core records, and 12 from *Clausen and Hammer* [1988], to examine the spatial distribution of the volcanic sulfate aerosol in the polar ice sheets. The ice cores cover the major areas of both Greenland and Antarctic ice sheet, thus give a good spatial representation. I calculated the sulfate deposition of the largest eruptions during the past millennium for individual ice core record, and found spatial variation of about 35% for Laki and Katmai sulfate deposition among Greenland ice cores, and 50% for Tambora deposition among both Greenland and Antarctic ice sheet. This spatial variation could increase substantially for less significant or less well known events. This large spatial difference points to the importance of using as many ice core as available to reconstruct the past volcanic radiative forcing history.

I also examined the relative magnitude of sulfate deposition in each individual ice core with respect to the Greenland and Antarctic mean. I found most of the ice cores display a consistent pattern, and it resembles the general pattern of precipitation in the

area. This indicates the importance of precipitation in remove the volcanic sulfate aerosol in these high-latitude regions. The result provides a guideline to not only qualitatively evaluate but also quantitatively adjust the stratospheric volcanic sulfate aerosol loading based on single or a few ice core records.

I found a similar spatial distribution pattern between the volcanic sulfate deposition and the 1952-1954 and 1961-1962 bomb test fallout in the Greenland ice cores, which confirms the previous assumption that the transport and deposition of bomb test debris resemble those of the volcanic aerosol.

The Development of Stratospheric Volcanic Sulfate Aerosol Loading History and the Monthly and Spatially Dependent Forcing Index

Combining the 44 ice core sulfate records used in above chapter and nine ECM records, I build an event chronology and calculated the total ice core sulfate deposition for volcanic eruptions during the past 1500 years. The results were spatially adjusted to account for the reduction of ice core availability in early period. I then converted the ice core sulfate depositions to global stratospheric aerosol loadings by multiplying a set of calibration factors that were obtained from three technologies: radioactive deposition from nuclear bomb tests, Pinatubo sulfate deposition in eight Antarctic ice cores, and climate model simulations of volcanic sulfate transport and deposition following the 1783 Laki, 1815 Tambora, 1912 Katmai, and 1991 Pinatubo eruptions. Our estimations for 1815 Tambora, 1883 Krakatau, 1963 Agung, and 1991 Pinatubo eruption agree well with those based on radiation, pathology, and satellite observations.

For GCM simulations, I developed a monthly and spatially dependent volcanic forcing index by applying a stratospheric transport parameterization to calculate the

spread of aerosol within the stratosphere plus a latitude-time dependent function to describe the production and sedimentation of aerosols. The vertical distribution of volcanic sulfate aerosol was interpolated based on the information obtained from 11 Lidar observations of Pinatubo aerosols. The index is a function of month from 501 to 2000 A.D., latitude from 90°S to 90°N at 10° resolution, and height from 9 km to 31 km at 0.5 km resolution. It is the longest and the most-advanced volcanic forcing time series of this type, because it was based on the most comprehensive set of ice core records, plus an updated signal extraction method, ice-core-deposition to global stratospheric aerosol loading conversion factors, and a more advanced spatial-temporal transport parameterization scheme. This new volcanic forcing data set can be used in climate model simulations to better characterize the natural causes of climate change, which will lead to improved prediction of anthropogenic impacts on climate.

EBM Simulation of Temperature Response to Volcanic Eruptions

I applied the global stratospheric volcanic aerosol loading time series, together with solar and anthropogenic forcings, to an upwelling diffusion EBM to simulate the global temperature response for the period of 850-2000 A.D. With climate sensitivity of 3 °C for doubling CO_2 the model produced temperature change on the order of 0.2 °C for solar variation, and volcanic cooling ranges from 0.1°C for small events to almost 3 °C for the largest 1259 Unknown eruption. The series of eruptions during the 13th century probably set the stage for Little Ice Age, and both solar and volcanic cooling contributed to the over all LIA during 15th to 19th century. The warming in the 20th century was the combined effect of solar, volcanic, and GHG forcing, with the GHG played the dominant role.

Comparing the model simulation with instrumental observations for the past 150 years, I found that the model can accurately simulated the cooling of about 0.2-0.3°C for the three tropical eruptions, i.e., 1883 Krakatau, 1963 Agung, and 1991 Pinatubo eruption. The model simulated temperature responses for the largest eruptions during the period (i.e., 1259 Unknown, 1453 Kuwae, and 1815 Tambora) are larger than most of the proxy temperature reconstructions, probably due to the reduced accuracy in the temperature reconstruction for the early period, the linearity assumption of conversion from ice core sulfate deposition to atmospheric radiative forcing and the simplicity of EBM simulations, or the underestimation of cooling (based on tree ring records) after big eruptions due to the diffusion of solar radiation.

Sources of Error

In chapter 6 I described the areas of errors when using ice core records to reconstruct the volcanic forcing index and how this work has eliminated or minimized these errors. I also estimated the uncertainty (40-45%) in IVI2, which includes 5-10% uncertainty caused by different volcanic signal extraction criteria; 25% uncertainty due to the choice of calibration factor; and 10% uncertainty in high-latitude sulfate deposition when assuming different eruption seasons in the transport program simulations. However, there are other sources that can not be easily quantified. One major source of error is related to the conversion from stratospheric volcanic sulfate aerosol loading to radiative forcing in W m^{-2}. At first the optical property is not necessary proportional to the mass of sulfate aerosol in the atmosphere as I had assumed. Beyond a certain point (15 megatons based on *Pinto et al.* [1989]), further sulfur injection may only increase the size of sulfate particles rather than the number of small ones [*Pinto et al.*, 1989]. Since large particles

fall out of stratosphere sooner and they tend to produce warming instead of cooling effects, IVI2 may overestimate the radiative perturbation and thus the climate impact of large eruptions. Secondly, the conversion from optical depth to W m^{-2} is a simplification of complex radiative calculations, ignoring the effects of particle size distribution and altitude of aerosol particle.

Another major error comes from the calculation of Arctic and Antarctic mean volcanic sulfate deposition. Although I have included in this study an extensive body of ice cores that any study has ever used, the number of ice core records available for averaging changes one eruption to another and it decreases dramatically for the period before 1500 CE. Study of its spatial distribution pattern undercounted some of this uncertainty, and future studies with more ice core records will further reduce the error.

These uncertainties in IVI2 may have contributed to the over all discrepancy between the EBM simulated temperature and proxy reconstructions. Nevertheless, there are significant errors in the reconstruction of solar forcing and the temperature itself, probably larger than those in IVI2, as they are based on less physical evidence. Furthermore, the EBM is an extreme simplification of actual climate processes. It does not allow climate feedbacks such as change of clouds or ice cover. It also does not resolve latitudinal differences, or contain any dynamical or hydrological processes in the atmosphere.

Possible Future Research

GCM simulations with the new monthly and spatially dependent volcanic forcing index may result in better past temperature response to volcanic aerosols. In particular, one can study the cumulative effects of the temporal-closely spaced eruptions by

conducting GCM simulations for the 13th century. I found five large and moderate volcanic eruptions (1228, 1259, 1268, 1275 and 1285 CE) during the period. With my estimation of the 1259 Unknown eruption, the cumulative volcanic sulfate flux in 13th century was 2 to 10 times larger than that in any other century within the last millennium. Its coincidence with the period of transition (1300-~1400) from the Medieval Warm Period (MWP, ~800-1300) to the Little Ice Age (LIA, ~1400-1800) suggests the possible role of the frequent large volcanic eruptions within a few decades or a century may have in initiating, enhancing or reversing a climate change. Previous studies [*Lean et al.*, 1995; *Free and Robock*, 1999; *Crowley*, 2000] have derived somehow contradictory quantifications of the relative contribution to LIA cooling between solar and volcanic activities with large uncertainties. GCM simulations with this new index may allow a clearer conclusion about the causes of the LIA.

The index can also used in GCM simulations to test the climate sensitivity. Works have already to done to constrain the climate sensitivity [*Wigley et al.*, 2005; *Hegerl et al.*, 2006] using GCM and simple EBM simulations, respectively. The new volcanic forcing index may bring new perspective on the subject.

References

Ammann, C. M., G. A. Meehl, W. M. Washington, and C .S. Zender (2003), A monthly and latitudinally varying volcanic forcing dataset in simulations of 20th century climate, *Geophys. Res. Lett.*, *30* (12), doi:10.1029/2003GL016875.

Ammann, C., F. Joos, D.S. Schimel, B.L. Otto-Bliesner, and R.A. Tomas (2007), Solar influence on climate during the past millennium: Results from transient simulations with NCAR climate system model, *PNAS*, *104*, 3,713-3,718.

Angell, J., and J. Forshover (1985), Surface temperature changes following the six major volcanic episodes between 1780 and 1980, *J. Clim. Appl. Met.*, *24*, 937-951.

Ansmann, A., I. Mattis, U. Wandinger, F. Wagner, J. Reichardt, and T. Deshler (1997), Evolution of the Pinatubo aerosol: Raman lidar observations of particle optical depth, effective radius, mass, and surface area over Central Europe at 53.4 degrees N, *Journal of the Atmospheric Sciences*, *54* (22), 2,630-2,641.

Antuña, J. C., A. Robock, G. L. Stenchikov, L. W. Thomason, and J. E. Barnes (2002), Lidar validation of SAGE II aerosol measurements after the 1991 Mount Pinatubo eruption, *J. Geophys. Res., 107* (D14), 4194, doi:10.1029/2001JD001441.

Antuña, J. C., A. Robock, G. L. Stenchikov, J. Zhou, C. David, J. Barnes, and L. Thomason (2003): Spatial and temporal variability of the stratospheric aerosol cloud produced by the 1991 Mount Pinatubo eruption. *J. Geophys. Res.*, **108 (D20)**, 4624, doi:10.1029/2003JD003722.

Bard, E., G.M. Raisbeck, F. Yiou, and J. Jouzel (2000), Solar irradiance during the last 1200 years based on cosmogenic nuclides, *Tellus*, *52B*, 985-992.

Bennett, B., Worldwide dispersion and deposition of radionuclides produced in atmospheric tests (2002), *Health Physics*, *82* (5), 644-655.

Bertrand, C., M.F. Loutre, M. Crucifix, and A. Berger (2002), Climate of the last millennium: a sensitivity study, *Tellus Series a-Dynamic Meteorology and Oceanography*, *54* (3), 221-244.

Bigler, M., D. Wagenbach, H. Fischer, J. Kipfstuhl, H. Millar, S. Sommer, and B. Stauffer (2002), Sulphate record from a northeast Greenland ice core over the last 1200 years based on continuous flow analysis, *Ann. Glaciol., 35*, 250-256.

Box, J.E., D.H. Bromwich, and L.S. Bai, Greenland ice sheet surface mass balance 1991-2000 (2004): Application of Polar MM5 mesoscale model and in situ data, *J. Geophys. Res.*, *109* (D16), D16105, doi:10.1029/2003JD004451.

Bradley, R. S. (1988), The explosive volcanic-eruption signal in Northern Hemisphere continental temperature records, *Climatic Change*, *12* (3), 221-243.

Bradley, R.S., M.K. Hughes, and H.F. Diaz (2003), Climate in Medieval time, *Science*, *302* (5644), 404-405.

Briffa, K. R., P. D. Jones, F. H. Schweingruber, and T. J. Osborn (1998), Influence of volcanic eruptions on Northern Hemisphere summer temperature over the past 600 years, *Nature*, *393*, 450-455.

Briffa, K.R., T.J. Osborn, and F.H. Schweingruber (2004), Large-scale temperature inferences from tree rings: a review, *Global and Planetary Change*, *40* (1-2), 11-26.

Bromwich, D.H., Z.C. Guo, L.S. Bai, and Q.S. Chen (2004), Modeled antarctic precipitation. Part I: Spatial and temporal variability, *J. Clim.*, *17* (3), 427-447.

Bryson, R., and Goodman (1980), Volcanic activity and climatic changes, *Science*, *207*, 1,041-1,044.

Budner, D., and J. H. Cole-Dai (2003), The number and magnitude of large explosive volcanic eruptions between 904 and 1865 A.D.: quantitative evidence from a new south pole ice core, in *Volcanism and the Earth's Atmosphere*, edited by A. Robock, and C. Oppenheimer, pp. 165-176, AGU, Washington, D.C.

Castellano, E., S. Becagli, M. Hansson, M. Hutterli, J. R. Petit, M. R. Rampino, M. Severi, J. P. Steffensen, R. Traversi, and R. Udisti (2005), Holocene volcanic history as recorded in the sulfate stratigraphy of the European Project for Ice Coring in Antarctica Dome C (EDC96) ice core, *J. Geophys. Res.*, *110*, D06114, doi:10.1029/2004JD005259.

Clausen, H. B., and C. U. Hammer (1988), The Laki and Tambora eruptions as revealed in Greenland ice cores from 11 locations, *Ann. Glacio.*, *10*, 16-22.

Clausen, H.B., N.S. Gundestrup, S.J. Johnsen, R. Bindschadler, and J. Zwally (1988), Glaciological investigations in the Créte area, central Greenland: a research for a new deep-drilling site, *Ann. Glacio.*, *10*, 10-15.

Clausen, H.B., C.U. Hammer, C.S. Hvidberg, D. DahlJensen, J.P. Steffensen, J. Kipfstuhl, and M. Legrand (1997), A comparison of the volcanic records over the past 4000 years from the Greenland Ice Core Project and Dye 3 Greenland Ice Cores, *J. Geophys. Res*, *102* (C12), 26,707-26,723.

Cleveland, W. S. (1979), Robust locally weighted regression and smoothing scatterplots, *J. American Statistical Association*, *74*, 829-836.

Cleveland, W. S., and S. J. Devlin (1988), Locally weighted regression: An approach to regression analysis by local fitting, *J. Amer. Stat. Assoc.*, *83*, 596-610.

Cole-Dai, J. H., E. Mosley-Thompson, and L. Thomason (1997), Annually resolved southern hemisphere volcanic history from two Antarctic ice cores, *J. Geophys. Res.*, *102* (D14), 16,761-16,771.

Cole-Dai, J. H., and E. Mosley-Thompson (1999), The Pinatubo eruption in South Pole snow and its potential value to ice core paleovolcanic records, *Ann. Glaciol., 29*, 99-105.

Cole-Dai, J. H., E. Mosley-Thompson, S. P. Wight, and L. Thomason (2000), A 4100-year record of explosive volcanism from an East Antarctica ice core, *J. Geophys. Res.*, *105*, 24,431-24,441.

Cressman, G. (1959), An operational objective analysis scheme, *Mon. Weather Rev.*, *87*, 367-374.

Crowley, T. J. (2000), Causes of climate change over the past 1000 years, *Science*, *289* (5477), 270-277.

Crowley, T.J., and K.Y. Kim (1999), Modeling the temperature response to forced climate change over the last six centuries, *Geophys. Res. Lett., 26* (13), 1,901-1,904.

D'Arrigo, R., R. Wilson, B. Liepert, and P. Cherubini (2007), On the "divergence problem" in northern forests: A review of the tree-ring evidence and possible causes, *Glob. Planetary Change*, *42*, doi:10.1016/j.gloplacha.2007.03.004.

Delmas, R. J., S. Kirchner, J. M. Palais, and J. R. Petit (1992), 1000 years of explosive volcanism recorded at the South-Pole, *Tellus B*, *44* (4), 335-350.

Dixon, D., P. A. Mayewski, S. Kaspari, S. Sneed, and M. Handley (2004), A 200 year sub-annual record of sulfate in West Antarctica, from 16 ice cores, *Ann. Glaciol.*, *39*, 1-12.

Dyer, A.J., and B.B. Hicks (1968), Global spread of volcanic dust from the Bali eruption of 1963, *Quart. J. R. Met. Soc.*, *94*, 545-554.

Fiacco, R.J., T. Thordarson, M.S. Germani, S. Self, J.M. Palais, S. Whitlow, and P.M. Grootes (1994), Atmospheric aerosol loading and transport due to the 1783-84 Laki eruption in Iceland, interpreted from ash particles and acidity in the GISP2 ice core, *Quat. Res.*, *42* (3), 231-240.

Fisher, D., and R. Koerner (1994), Signal and noise in four ice core records from the Agassiz Ice Cap, Ellesmere Island, Canada: details of the last millennium for stable isotopes, melt and solid conductivity., *Holocene*, *4*, 113-120.

Fisher, D., N. Reeh, and H. Clausen (1985), Stratigraphic noise in time series derived from ice cores, *Ann. Glaciol.*, *7*, 76-83.

Fisher, D. A., R. M. Koerner, and N. Reeh (1995), Holocene climatic records from Agassiz Ice Cap, Ellesmere Island, Nwt, Canada, *Holocene*, *5* (1), 19-24.

Franklin, B. (1982 reprint), Meteorological imaginations and conjectures, w*eatherwise*, *35*, 262,.

Free, M., and A. Robock (1999), Global warming in the context of the Little Ice Age, *Journal of Geophysical Research*, *104* (D16), 19,057-19,070.

Fröhlich, C., and J. Lean (2004), Solar radiative output and its variability: evidence and mechanisms, *The Astron Astrophys Rev*, *12*, 273-320.

Gao, C., L. Oman, A. Robock, and G. L. Stenchikov (2007), Atmospheric volcanic loading derived from bipolar ice cores accounting for the spatial distribution of volcanic deposition, *J. Geophys. Res.*, 112, D09109, doi:10.1029/2006JD007461.

Gao, C., A. Robock, S. Self, J. B. Witter, J. P. Steffenson, H. B. Clausen, M. L. Siggaard-Andersen, S. Johnsen, P. A. Mayewski, and C. Ammann (2006), The 1452 or 1453 AD Kuwae eruption signal derived from multiple ice core records: Greatest volcanic sulfate event of the past 700 years, *J. Geophys. Res.*, *111* (D12), doi:10.1029/2005JD006710.

Gilliland, R., and S. Schneider (1984), Volcanic, CO_2 and solar forcings of Northern and Southern Hemisphere surface air temperatures, *Nature*, *310*, 38-41.

Graf, H.F., Q. Li, and M.A. Giorgetta (2007), Volcanic effects on climate: revisiting the mechanisms, *Atmos. Chem. Phys., 7 (17)*, 4,503-4,511.

Grieser, J., and C. D. Schönwiese (1999), Parameterization of spatio-temporal patterns of volcanic aerosol induced stratospheric optical depth and its climate radiative forcing, *Atmosfera*, *12* (2), 111-133.

Hammer, C. U. (1977), Past volcanism revealed by Greenland ice sheet impurities, *Nature*, *270* (5637), 482-486.

Hammer, C. U. (1980), Acidity of polar ice cores in relation to absolute dating, past volcanism, and radio echoes, *J. Glaciol.*, *25* (93), 359-372.

Hansen, J. E., A. Lacis, R. Ruedy, and M. Sato (1992), Potential climate impact of Mount Pinatubo eruption, *Geophys. Res. Lett.*, *19*, 215-218.

Hansen, J.E., M. Sato, and R. Ruedy (1997), Radiative forcing and climate response, *J. Geophys. Res.*, *102*, 6,831-6,864.

Haynes, P., and E. Shuckburgh (2000), Effective diffusivity as a diagnostic of atmospheric transport 1. Stratosphere, *J. Geophys. Res. 105* (18), 22,777-22,794.

Hegerl, G., T.J. Crowley, W.T. Hyde, and D. Frame (2006), Climate sensitivity constrained by temperature reconstructions of the last seven centuries, *Nature*, *440*, doi:10.1038/nature04679.

Hegerl, G.C., T.J. Crowley, W.T. Hyde, and D.J. Frame (2007), Climate modelling - Uncertainty in climate-sensitivity estimates - Reply, *Nature*, *446* (7131), E2-E2.

Hegerl, G.C., F.W. Zwiers, P.A. Stott, and V.V. Kharin (2004), Detectability of anthropogenic changes in annual temperature and precipitation extremes, *J.Climate*, *17* (19), 3,683-3,700.

Hegerl, G.C., K. Hasselmann, U. Cubasch, J.F.B. Mitchell, E. Roeckner, R. Voss, and J. Waszkewitz (1997), Multi-fingerprint detection and attribution analysis of greenhouse gas, greenhouse gas-plus-aerosol and solar forced climate change, *Climate Dynamics*, *13* (9), 613-634.

Hitchman, M.H., M. McKay, and C.R. Trepte (1994), A climatology of stratospheric aerosol, *J. Geophys. Res.*, *99*, 20,689-20,700.

Holton, J. R., P. H. Haynes, M. E. Mcintyre, A. R. Douglass, R. B. Rood, and L. Pfister (1995), Stratosphere-troposphere exchange, *Rev. Geophys.*, *33*, 403-439.

Humphreys, W. (1913), Volcanic dust and other factors in the production of climatic changes, and their possible relation to ice gases, *J. Franklin Inst.* (Aug.), 131-172.

Humphreys, W. (1940), *Physics of the Air*, 676 pp., Dover, Mineola, N.Y.

IPCC, 2007: *Climate Change 2007: The Physical Science Basis. Contribution of Working Group I to the Fourth Assessment Report of the Intergovernmental Panel on Climate Change*, Solomon, S., D. Qin, M. Manning, Z. Chen, M. Marquis, K. B. Averyt, M. Tignor and H. L. Miller (eds.), Cambridge University Press, Cambridge, United Kingdom and New York, NY, USA, 996 pp.

Jones, P. D., and M. E. Mann (2004), Climate over past millemnia, *Rev. Geophys.*, *42*, doi:10.1029/2003RG000143.

Kent, G.S., and M.P. McCormick (1988), Remote sensing of stratospheric aerosol following the eruption of El Chichon, *Opt. News*, *14*, 11-19.

Koch, D., G.A. Schmidt, and C.V. Field (2006), Sulfur, sea salt, and radionulide aerosols in GISS ModelE, *J. Geophys. Res.*, *111* (D06206), doi:10.1029/2004JD005550.

Krueger, A.J., L.S. Walter, P.K. Bhartia, C.C. Schnetzler, N.A. Krotkov, I. Sprod, and G.J.S. Bluth (1995), Volcanic sulfur dioxide measurements from the total ozone mapping spectrometer instruments, *J. Geophys. Res.*, *100* (D7), 14,057-14,076.

Kurbatov, A.V., G.A. Zielinski, N.W. Dunbar, P.A. Mayewski, E.A. Meyerson, S.B. Sneed, and K.C. Taylor (2006), A 12,000 year record of explosive volcanism in the Siple Dome Ice Core, West Antarctica, *J. Geophys. Res.*, *111* (D12), D12307, doi:10.1029/2005JD006072.

La Marche, V. C., and K. K. Hirschboeck (1984), Frost rings in trees as records of major volcanic eruptions, *Nature*, *307*, 121-126.

Lamb, H. H. (1970), Volcanic dust in the atmosphere, with a chronology and assessment of its meteorological significace, *Philos. Trans. R. Soc. London*, *266* (A), 425-533.

Lamb, H.H. (1977), Supplementary volcanic dust veil index assessments, *Clim. Monit.*, *6*, 57-67.

Lamb, H.H. (1983), Update of the chronology of assessments of the volcanic dust veil index, *Climate Monitor*, *12*, 79-90.

Langway, C.C., H.B. Clausen, and C.U. Hammer (1988), An inter-hemispheric volcanic time-marker in ice cores from Greenland and Antarctica, *Ann. Glaciol.*, *10*, 102-108.

Langway, C.C., K. Osada, H.B. Clausen, C.U. Hammer, and H. Shoji (1995), A 10-century comparison of prominent bipolar volcanic events in ice cores, *J. Geophys. Res*, *100* (D8), 16,241-16,247.

Lean, J., J. Beer, and R. Bradley (1995), Reconstruction of solar irradiance since 1610 - implications for climate-change, *Geophys. Res. Let.*, *22* (23), 3,195-3,198.

Legrand, M., and R. Delmas (1987), A 220 year continuous record of volcanic H_2SO_4 in the Antarctic ice sheet, *Nature*, *327*, 671-676.

Legrand, M., and D. Wagenbach (1999), Impact of Cerro Hudson and Pinatubo volcanic eruptions on the Antarctic air and snow chemistry, *J. Geophys. Res.*, *104*, 1,581-1,596.

Mao, J.P., and A. Robock (1998), Surface air temperature simulations by AMIP general circulation models: Volcanic and ENSO sisals and systematic errors, *J.Clim.*, *11* (7), 1,538-1,552.

Mayewski, P. A., W. B. Lyons, M. J. Spencer, M. S. Twickler, C. F. Buck, and S. Whitlow (1990), An ice-core record of atmospheric response to anthropogenic sulfate and nitrate, *Nature*, *346* (6284), 554-556.

Mayewski, P. A., L. D. Meeker, M. C. Morrison, M. S. Twickler, S. I. Whitlow, K. K. Ferland, D. A. Meese, M. R. Legrand, and J. P. Steffensen (1993), Greenland ice core signal characteristics: An expanded view of climate change, *J. Geophys. Res.*, *98* (D7), 12,839-12,847.

McCormick, M. P. (1994), SAM II Aerosol data. NASA Langley Research Center. Mail Stop 157B. Hampton, Virginia 23681-0001. USA.

McCormick, M. P., and P. H. Wang (1987), Satellite measurements of stratospheric aerosols, in Transport Processes in the Middle Atmosphere, edited by G. Visconti and R. Garcia, pp. 103-120.

McCormick, M.P., and R.E. Veiga (1992), SAGE II measurements of early Pinatubo aerosols, *Geophys. Res. Lett.*, *19*, 155-158.

McPeters, R.D. (1995), Reply to the comment on the paper "The atmospheric SO2 budget for Pinatubo derived from NOAA-11 SBUV/2 spectral data", *Geophys. Res. Lett.*, *22*, 317-320.

Miles, M., and P. Gildersleeves (1978), Volcanic dust and changes in Northern Hemisphere temperature, *Nature*, *271*, 735-736.

Mitchell, J. (1961), Recent secular changes of the global temperature, *Ann. N.Y, Acad. Sci.,*, *95*, 235-250.

Mitchell, J. (1970) A preliminary evaluation of atmospheric pollution as a cause of the global temperature fluctuation of the past century, in *Global Effects of Environmental Pollution*, edited by S.F. Singer, 139-155.

Monzier, M., C. Robin, and J.-P. Eissen (1994), Kuwae (~1425 A.D.): the forgotten caldera, *J. Volcanol. Geotherm. Res.*, *59*, 207-218.

Moore, J. C., H. Narita, and N. Maeno (1991), A continuous 770-year record of volcanic activity from East Antarctica, *J. Geophys. Res.*, *96* (D9), 17,353-17,359.

Mosley-Thompson, E., T. A. Mashiotta, and L. Thompson (2003), High resolution ice core records of late Holocene volcanism: Current and future contributions from the Greenland PARCA cores, in *Volcanism and the Earth's Atmosphere*, edited by A. Robock, and C. Oppenheimer, pp. 153-164, AGU, Washington, D.C.

Mosley-Thompson, E., L. G. Thompson, J. Dai, M. Davis, and P. N. Lin (1993), Climate of the last 500 years: High-resolution ice core records, *Quaternary Sci. Rev.*, *12* (6), 419-430.

Naveau, P., C. Ammann, H.-S. Oh, and W. Guo (2003), An automatic statistical methodology to extract pulse-like forcing factors in climate time series: Application to volcanic events, in *Volcanism and the Earth's Atmosphere*, edited by A. Robock, and C. Oppenheimer, pp. 177-186, AGU, Washington, D. C.

Newhall, C. G., and S. Self (1982), The volcanic explosivity index (VEI): an estimate of explosive magnitude for historical volcanism, *J. Geophys. Res.*, *87*, 1231-1238.

Oman, L., A. Robock, G. Stenchikov, G.A. Schmidt, and R. Ruedy (2005), Climate response to high latitude volcanic eruptions, *Journal of Geophysical Research*, *110* (D13), D13103, dio:10.1029/2004JD005487.

Oman, L., A. Robock, G.L. Stenchikov, T. Thordarson, D. Koch, D.T. Shindell, and C.C. Gao (2006), Modeling the distribution of the volcanic aerosol cloud from the 1783-1784 Laki eruption, *J. Geophys. Res*, *111* (D12), D12209, doi:10.1029/2005JD006899.

Palmer, A. S., V. I. Morgan, A. J. Curran, T. D. Van Ommen, and P. A. Mayewski (2002), Antarctic volcanic flux ratios from Law Dome ice cores, *Ann. Glaciol.*, *35*, 329-332.

Pang, K. D. (1993), Climatic impact of the mid-fifteenth century Kuwae caldera formation, as reconstructed from historical and proxy data, *Eos Trans.*, *74*, 106.

Pinto, J.P., R.P. Turco, and O.B. Toon (1989), Self-limiting physical and chemical effects in volcanic eruption clouds, *J. Geophys. Res.*, *94*, 11,165-11,174.

Rampino, M.R., and S. Self (1982), Historic eruptions of Tambora (1815), Krakatau (1883), and Agung (1963), their stratospheric aerosols, and climatic impact, *Quaternary Res.*, *18* (2), 127-143.

Reusch, D.B., P.A. Mayewski, S.I. Whitlow, I.I. Pittalwala, and M.S. Twickler (1999), Spatial variability of climate and past atmospheric circulation patterns from central west Antarctic Glaciochemistry, *J. Geophys. Res.*, *104* (D6), 5,985-6,001.

Robertson, A., J. Overpeck, D. Rind, E. Mosley-Thompson, G. Zielinski, J. Lean, D. Koch, J. Penner, I. Tegen, and R. Healy (2001), Hypothesized climate forcing time series for the last 500 years, *J. Geophys. Res.*, *106* (D14), 14,783-14,803.

Robock, A. (1978), Internally and externally caused climate change, *J. Archaeological Science*, *35*, 1111-1122.

Robock, A. (1979), The "Little Ice Age": Northern hemisphere average observations and model simulations, *Science*, *206*, 1402-1404.

Robock, A. (1989), Volcanoes and climate, in *A Challenge for Science amd Society in the 21st Century*, edited by N.A. Ser., pp. 309-314.

Robock, A. (1991), The volcanic contribution to climate change of the past 100 years, in *Greenland-Gas-Induced Climatic Change: A Critical Appraisal of Simulations and Observations*, edited by M.E. Schlesinger, pp. 429-444, Elsevier Sci., New York.

Robock, A. (2000), Volcanic eruptions and climate, *Rev. Geophys.*, *38*, 191-219.

Robock, A (2005), Cooling following large volcanic eruptions corrected for the effect of diffuse radiation on tree rings. *Geophys. Res. Lett.*, 32, L06702, doi:10.1029/2004GL022116.

Robock, A., and M. P. Free (1995), Ice cores as an Index of global volcanism from 1850 to the present, *J. Geophys. Res*., *100* (D6), 11,549-11,567.

Robock, A., and M. Free (1996), The volcanic record in ice cores for the past 2000 years, in *Climatic Variations and Forcing Mechanisms of the Last 2000 Years*, edited by P. Jones, R. Bradley, and J. Jouzel, pp. 533-546, Springer-Verlag, Berlin.

Robock, A. and J. Mao (1992), Winter warming from large volcanic eruptions, *Geophys. Res. Lett.*, *19*, 2405-2408.

Robock, A., and J. Mao (1995), The volcanic signal in surface-temperature observations, *J. Clim. 8* (5), 1,086-1,103.

Robertson, A., J. Overpeck, D. Rind, E. Mosley-Thompson, G. Zielinski, J. Lean, D. Koch, J. Penner, I. Tegen, and R. Healy (2001), Hypothesized climate forcing time series for the last 500 years, *J. Geophys. Res.*, *106* (D14), 14,783-14,803.

Sato, M. (1995), Update of Stratospheric Aerosol Optical Depths. On: http://www.giss.nasa.gov./data/strataer/STRATAER.table.txt.

Sato, M., J. E. Hansen, M. P. McCormick, and J. B. Pollack (1993), Stratospheric aerosol optical depths, 1850-1990, *J. Geophys. Res*., *98* (D12), 22,987-22,994.

Self, S., and A.J. King, Petrology and sulfur and chlorine emissions of the 1963 eruption of Gunung Agung, Bali, Indonesia (1996), *Bull. Volcanol*, *58* (4), 263-285.

Self, S., R. Gertisser, T. Thordarson, M.R. Rampino, and J.A. Wolff (2004), Magma volume, volatile emissions, and stratospheric aerosols from the 1815 eruption of Tambora, *Geophys. Res. Lett.*, *31* (20), L20608, doi:10.1029/2004GL020925.

Siebert, L., and T. Simkin (2002), *Volcanoes of the World: an Illustrated Catalog of Holocene Volcanoes and their Eruptions*. Smithsonian Institution, Global Volcanism Program Digital Information Series, GVP-3, (http://www.volcano.si.edu/world/).

Simarski, L. T. (1996), Constantinople's volcanic twilight, *Saudi Aramco World*, *47*, 8-13.

Simkin, T., and L. Siebert (1994), *Volcanoes of the World*, 349 pp., Geoscience Press, Tucson, Az.

Solomon, S. (1999), Stratospheric ozone depletion: A review of concepts and history, *Reviews of Geophysics*, *37*, 275-316.

Solomon, S., R.W. Portmann, R.R. Garcia, L.W. Thomason, P. L.R., and M.P. McCormick (1996), The roles of aerosol variations inn anthropogenic ozone depletion at northern midlatitudes, *J. Geophys. Res.*, *101*, 6713-6727.

Sommer, S., C. Appenzeller, R. Rothlisberger, M. Hutterli, B. Stauffer, D. Wagenbach, H. Oerter, F. Wilhelms, D. J. Miller, and R. Mulvaney (2000a), Glacio-chemical study spanning the past 2 kyr on three ice cores from Dronning Maud Land, Antarctica 1. Annually resolved accumulation rates, *J. Geophys. Res*., *105* (D24), 29,411-29,421.

Sommer, S., D. Wagenbach, R. Mulvaney, and H. Fischer (2000b), Glacio-chemical study spanning the past 2 kyr on three ice cores from Dronning Maud Land, Antarctica 2. Seasonally resolved chemical records, *J. Geophys. Res.*, *105*, 29,423-29,433.

Stenchikov, G. L., I. Kirchner, A. Robock, H.-F. Graf, J. C. Antuña, R. G. Grainger, A. Lambert, and L. Thomason (1998), Radiative forcing from the 1991 Mount Pinatubo volcanic eruption. *J. Geophys. Res*., *103*, 13,837-13,857.

Stenchikov, G., A. Robock, V. Ramaswamy, M. D. Schwarzkopf, K. Hamilton, and S. Ramachandran (2002), Arctic Oscillation response to the 1991 Mount Pinatubo eruption: Effects of volcanic aerosols and ozone depletion, *J. Geophys. Res.*, *107 (D24)*, 4803, doi:10.1029/2002JD002090.

Stenchikov, G., K. Hamilton, A. Robock, V. Ramaswamy, and M. D. Schwarzkopf (2004), Arctic Oscillation response to the 1991 Pinatubo eruption in the SKYHI GCM with a realistic Quasi-Biennial Oscillation, *J. Geophys. Res.*, *109*, D03112, doi: 10.1029/2003JD003699.

Stenchikov, G., K. Hamilton, R. J. Stouffer, A. Robock, V. Ramaswamy, B. Santer, and H.-F. Graf (2006), Arctic Oscillation response to volcanic eruptions in the IPCC AR4 climate models, *J. Geophys. Res.*, *111*, D07107, doi:10.1029/ 2005JD006286.

Stenni, B., R. Caprioli, L. Cimino, C. Cremisini, O. Flora, R. Gragnani, A. Longinelli, V. Maggi, and C. Torcini (1999), 200 years of isotope and chemical records in a firn

core from Hercules Neve, northern Victoria Land, Antarctica, *Ann. Glaciol.*, *29*, 106-112.

Stenni, B., M. Proposito, R. Gragnani, O. Flora, J. Jouzel, S. Falourd, and M. Frezzotti (2002), Eight centuries of volcanic signal and climate change at Talos Dome (East Antarctica), *J. Geophys. Res.*, *107* (D9), doi:10.1029/2000JD000317.

Stevenson, D.S., C.E. Johnson, E.J. Highwood, V. Gauci, W.J. Collins, and R.G. Derwent (2003), Atmospheric impact of the 1783-1784 Laki eruption: Part I Chemistry modelling, *Atmos. Chem. Phys.*, *3*, 487-507.

Stothers, R.B. (1984), The great Tambora eruption in 1815 and its aftermath, *Science*, *224* (4654), 1,191-1,198.

Stothers, R.B. (1996), Major optical depth perturbations to the stratosphere from volcanic eruptions: Pyrheliometric period, 1881-1960, *J.Geophys. Res.*, *101* (D2), 3,901-3,920.

Thordarson, T., and S. Self (2003), Atmospheric and environmental effects of the 1783-1784 Laki eruption: A review and reassessment, *J.Geophys. Res., 108* (D1), 4011, doi:10.1029/2001JD002042.

Thordarson, T., S. Self, and S. Steinthorsson (1993), Aerosol loading of the Laki fissure eruption and its impact on climate, *Eos Trans*, AGU, *74*, 106.

Timmreck, C., H.F. Graf, and J. Feichter (1999), Simulation of Mt. Pinatubo volcanic aerosol with the Hamburg climate model ECHAM4, *Theoretical and applied climatology*, *62* (3-4), 85-108.

Toon, O. B., and J. B. Pollack (1980), Atmospheric aerosols and climate, *Am. Sci.*, *68*, 268-278.

Traufetter, F., H. Oerter, H. Fischer, R. Weller, and H. Miller (2004), Spatio-temporal variability in volcanic sulphate deposition over the past 2kyr in snow pits and firn cores from Amundsenisen, Antarctica, *J. Glaciol.*, *50*, 137-146.

United Nations Scientific Committee on the Effects of Atomic Radiation (UNSCEAR) (1982), Ionizing radiation: Sources and biological effects, report to the General Assembly, with annexes, *U.N. Publ. E.82.IX.8*, 773 pp., New York.

United Nations Scientific Committee on the Effects of Atomic Radiation (UNSCEAR) (2000), Sources and effects of ionizing radiation, report to the General Assembly, with scientific annexes, vol. 1, Sources, *U.N. Publ. E.00.IX.3*, 647 pp., New York.

Usoskin, I.G., S.K. Solanki, M. Schussler, M. K., and K. Alanko (2003), A millennium scale sunspot number reconstruction: evidence for an unusually active sun since the 1940s, *Phys. Rev. Let.*, *91*, 211101-1-4.

Witter, J. B., and S. Self (2007), The Kuwae (Vanuatu) eruption of AD 1452: potential magnitude and volatile release, *Bull. Volcano, 69*, 301-308.

Wigley, T.M.L., C.M. Ammann, B.D. Santer, and S.C.B. Raper (2005), Effect of climate sensitivity on the response to volcanic forcing, *J. Geophys. Res., 110* (D09107).

Wigley, T. M. L., and S. C. B. Raper (1987), Thermal-expansion of sea-water associated with global warming, *Nature, 330* (6144), 127-131.

Wigley, T. M. L., and S. C. B. Raper (1992), Implications for climate and sea-level of revised IPCC emissions scenarios, *Nature, 357* (6376), 293-300.

Wigley, T. M. L., and S. C. B. Raper (2001), Interpretation of high projections for global-mean warming, *Science, 293* (5529), 451-454.

Zielinski, G. A. (1995), Stratospheric loading and optical depth estimates of explosive volcanism over the last 2100 years derived from the Greenland-Ice-Sheet-Project-2 ice core, *J. Geophys. Res., 100* (D10), 20,937-20,955.

Zielinski, G.A. (2000), Use of paleo-records in determining variability within the volcanism-climate system, *Quat. Sci. Rev. 19* (1-5), 417-438.

Zielinski, G., J. Dibb, Q. Yang, P. Mayewski, S. Whitlow, and M. S. Twickler (1997), Assessment of the record of the 1982 El Chichón eruption as preserved in Greenland snow, *J. Geophys. Res., 102*, 30,031-30,045.

Zielinski, G. A., M. S. Germani, G. Larsen, M. G. L. Baillie, S. Whitlow, M. S. Twickler, and K. Taylor (1995), Evidence of the Eldgja (Iceland) eruption in the GISP2 Greenland ice core - relationship to eruption processes and climatic conditions in the 10th-century, *Holocene, 5* (2), 129-140.

Zielinski, G.A., P.A. Mayewski, L.D. Meeker, S. Whitlow, M.S. Twickler, M. Morrison, D.A. Meese, A.J. Gow, and R.B. Alley (1994), Record of volcanism since 7000-bc from the GISP2 Greenland ice core and implications for the volcano-climate system, *Science, 264* (5161), 948-952.

Appendix A

Procedure to calculate sulfate fluxes for ice cores with sulfate concentration records

A1. Cores With Sulfate Contents in μequiv./l:

- Assume the density of the sample solution is similar to that of water, i.e., 1 μequiv.SO_4/l ≈ 1 μequiv. SO_4/kg.
- Use 1 kg/l as the density if the accumulation is in water equivalent, and 0.85 kg/l as the density if the accumulation is in ice equivalent.
- Multiply the sulfate content (in μequiv./kg) with the factor [L = 48 (g/equiv. SO_4^{2-})× annual accumulation (m/yr in either water or ice equivalents) × water or ice density (in kg/l)] or [L = 48 (g/equiv. SO_4^{2-}) × annual accumulation in (g cm^{-2} yr^{-1}) or (kg/km^2 yr)] to convert them to fluxes (kg/km^2 yr).

A2. NorthGRIP1:

Since the NorthGRIP1 record we used only contains the sulfate content (in μequiv./kg) corresponding to annual depth intervals and the 55-cm average ice or snow density for the first 100 m of ice-core, we used the following procedure to calculate the sulfate fluxes:

- Linearly interpolate the 55-cm averaged densities for the first 100 m of ice core to the depth intervals that corresponding to the annual depositions.
- Assume the ice density as 0.85 kg/l for the data after the first 100 meters.
- Multiply the sulfate content (in μequiv./kg) with the factor [L = 48 (g/equiv. SO_4^{2-})× annual deposition (in m) × ice density for each annual depth interval (in kg/l)] to convert them to fluxes (kg/km^2 yr).

A3. Cores With Sulfate Contents in μg/l, ng/g, or ppb:

- Assume the density of the sample solution is the same as that of water, i.e., 1 μg/l ≈ 1 μg/kg = 1 ng/g = 1 ppb.
- Use 1 kg/l as the density if the accumulation is in water equivalent, and 0.85 kg/l as the density if the accumulation is in ice equivalent.
- Multiply the sulfate content with the factor [L = annual accumulation (m/yr in either water or ice equivalents) × water or ice density (in kg/l)] or just with the annual accumulation if it is in (g cm^{-2} $yr^{-}1$) or (kg/km^2 yr) to convert them to fluxes (in kg/km^2 yr).

Table 2-1. Ice core time series used in the study. Ice cores marked with * are ones used by [*Robock and Free*, 1995]. ECM = electrical conductivity measurement, DEP=dielectric profiling, NSS SO4=non-sea-salt sulfate, CFA=continuous flow analysis, NSS-conductivity=non-sea-salt conductivity, EXS=excess sulfate.

Name	Location	Period	Resolution	Measure Type	Units	Reference
A84*	80.7ºN, 73.1ºW	1223-1961	1/yr	ECM	µA	*Fisher et al.* [1995]
A77*	80.7ºN, 73.1ºW	453-1853	1/yr	ECM	µA	*Fisher et al.* [1995]
NGT_B20	79ºN, 36.5ºW	830-1993	12/yr	CFA	ng/g (ppb)	*Bigler et al.* [2002]
NorthGRIP1.ECM	75.1ºN, 42.3ºW	190-1969	2/yr	ECM		*Gao et al.* [2006]
NorthGRIP1.SO_4	75.1ºN, 42.3ºW	190-1969	1/yr	Total SO_4	µequiv/kg	*Gao et al.* [2006]
GISP2*	72.6ºN, 38.5ºW	1-1984	0.5/yr	NSS SO_4	ppb	*Zielinski* [1995]
Dye3 deep	72.6ºN, 37.6ºW	1-1768	4/yr	ECM		*Gao et al.* [2006]
Greenland Site T	72.6ºN,38.5 W	1731-1989	1/yr	EXS	kg/km^2	*Mosley-Thompson et al.* [1993]
GRIP main	71.3ºN, 26.7ºW	1-1642	4/yr	ECM		*Gao et al.* [2006]
Crête	71.1ºN, 37.3ºW	553-1778	4/yr	ECM		*Gao et al.* [2006]
Greenland Site A	70.8ºN, 36°W	1715-1985	1/yr	EXS	kg/km^2	*Mosley-Thompson et al.* [1993]
Renland	70.6ºN, 35.8ºW	1000-1984	1/yr	ECM		*Gao et al.* [2006]
20D*	65ºN, 45ºW	1767-1983	1/yr	NSS SO_4	ng/g	*Mayewski et al.* [1990]
Mt. Logan*	60.6ºN, 141ºW	1689-1979	1/yr	total SO_4	µequiv/l	*Mayewski et al.* [1990]
Law Dome	66.7ºS 112.8ºE	1301-1995	12/yr	NSS SO_4	µequiv/l	*Palmer et al.* [2002]
Dyer	70.7ºS, 65ºW	1505-1989	1/yr	total SO_4 flux	kg/km^2	*Cole-Dai et al.* [1997]
G15*	71.2ºS, 46ºE	1210-1983	varies	DEP	µS/m	*Moore et al.* [1991]
Talos Dome	72.8ºS, 159.1ºE	1217-1996	varies	NSS SO_4	µequiv/l	*Stenni et al.* [2002]
Hercules Névé	73.1ºS, 165.5ºE	1774-1992	1/yr	NSS SO_4	µequiv/l	*Stenni et al.* [2002]
Dome C*	74.7ºS, 124.2ºE	1763 - 1973	1/yr	NSS SO_4	µequiv./l	*Legrand and Delmas* [1987]
DML_B32.SO_4	75ºS, 0ºW	159-1997	varies	NSS SO_4	ng/g	*Traufetter et al.* [2004]
DML_B32.ECM	75ºS, 0ºW	159-1997	12/yr	NSS-conductivity	µS/cm	*Sommer et al.* [2000]
DML_B33	75.2ºS, 6.5ºW	1-1996	12/yr	NSS-conductivity	µS/cm	*Sommer et al.* [2000]
DML_B31	75.6ºS, 3.5ºW	463-1994	12/yr	NSS-conductivity	µS/cm	*Sommer et al.* [2000]
Siple Station	76ºS, 84.3ºW	1417-1983	1/yr	Total SO_4 flux	kg/km^2	*Cole-Dai et al.* [1997]
ITASE 01-5	77ºS, 89ºW	1781-2002	varies	SO_4	µg/l	*Dixon et al.* [2004]
ITASE 00-5	77.7ºS, 124ºW	1708-2001	varies	SO_4	µg/l	*Dixon et al.* [2004]
ITASE 00-4	78ºS, 120ºW	1799-2001	varies	SO_4	µg/l	*Dixon et al.* [2004]
ITASE 01-3	78.1ºS, 95.6ºW	1859-2002	varies	SO_4	µg/l	*Dixon et al.* [2004]
ITASE 00-1	79.4ºS, 111ºW	1651-2001	varies	SO_4	µg/l	*Dixon et al.* [2004]
ITASE 99-1	80.6ºS,122.6ºW	1713-2000	varies	SO_4	µg/l	*Dixon et al.* [2004]
Plateau Remote*	84ºS, 43ºE	1-1986	1/yr	SO_4	ppb	*Cole-Dai et al.* [2000]
PS1*	90ºS	1010-1984	1/yr	NSS SO_4	ng/g	*Delmas et al.* [1992]
PS14*	90ºS	1800 - 1984	1/yr	NSS SO_4	ng/g	*Delmas et al.* [1992]
SP2001c1	90ºS	905-1999	1/yr	Total SO_4 flux	kg/km^2	*Budner and Cole-Dai* [2003]
SP95	90ºS	1487-1992	varies	SO_4	µg/l	*Dixon et al.* [2004]

Table 2-2. Sulfate depositions (kg/km^2) for the Laki and Tambora eruptions in 12 Greenland ice cores. All values obtained from Table 4 in *Clausen and Hammer* [1988].

Ice core sites	Latitude (°N)	Longiude(°W)	Laki Deposition	Tambora Deposition
Camp Century	77.18	61.11	294	63
North Central	74.62	39.60	100	48
Créte	71.12	37.32	138	53
Site A	70.63	35.82	96	58.41
Site B	70.65	37.48	167	71
Site D	70.64	39.62	291	129
Site E	71.76	35.85	62	13
Site G	71.15	35.84	145	94
Dye 3	65.18	43.83	173	54
4 B	65.17	43.93	168	98
18 C	65.03	44.39	190	25
Dye 2	66.48	46.33	231	N/A

Table 2-3. Sulfate depositions (kg/km^2) for the Laki, 1809 Unknown, and Tambora eruptions in six PARCA ice cores. All values obtained from Table 2 in in *Mosley-Thompon et al.* [2003].

Ice core sites	Latitude (°N)	Longiude(°W)	Laki Deposition	1809 Unknown Deposition	Tambora Deposition
GITS				33.2	48.4
D2	71.8	46.3	222.0	38.0	52.3
D3	69.8	44.0	323.5	46.7	85.4
Site T	72.5	38.5	114.6	33.2	40.6
Raven	65.9	46.3	142.6	25.8	55.3
Humboldt	78.5	56.8	79.7		
NASA-U	73.8	49.5	167.3		

Table 3-1. Average total sulfate depositions (kg/km^2) and the corresponding standard deviations based on different groups of ice cores for the Laki, 1809 Unknown, Tambora, and Krakatau eruptions. All values are calculated in the same way. Seven Southern Hemisphere (SH) cores: SP2001, PS1, Plateau Remote, Talos Dome, Law Dome, Siple Station, and B32. 17 SH cores: the above six cores plus SP95, ITASE015, ITASE005, ITASE004, ITASE013, TASE001, ITASE991, Dyer, Dome C, and PS14. Two Northern Hemisphere (NH) cores: B20 and NorthGRIP1. Seven NH cores: the above two cores plus Greenland Site A and T, GISP2, 20D, Mt. Logan. See Table 1 for details on these cores. PARCA data from four cores (GITS, D2, D3, and Raven) for Unknown and Tambora and five cores (D2, D3, Raven, Humboldt, and NASA-U) for Laki from Table 2-3. CH1988 data obtained by averaging the sulfate depositions of 12 and 11 NH cores from Table 2-2 .

Volcano	Latitude	Year	7 SH	17 SH	2 NH	7 NH	PARCA	CH1988
Kuwae	17°S	1452	93.0 ± 35.5	97.7**	24.8 ± 3.2	44.6**	N/A	N/A
Laki	64°N	1783	N/A	N/A	87.6 ± 4.2	103.2 ± 35.1	187.0 ± 91.8	171.3 ± 72.5
Unknown	tropical?	1809	25.1 ± 13.3	27.2 ± 12.3	17.7 ± 19.2	25.9 ± 15.2	35.9 ± 8.8	N/A
Tambora	8°S	1815	56.7 ± 32.8	59.4 ± 26.4	31.3 ± 8.5	49.5 ± 24.8	60.4 ± 16.9	64.2 ± 33.1
Krakatau	6°S	1883	12.4 ± 5.6	12.1 ± 5.9	4.6 ± 0.6	14.0 ± 7.4*	N/A	N/A

* The Krakatau signal does not show in the Mt. Logan ice core record. Therefore, the total deposition for the Krakatau eruption is averaged over six NH ice core records instead of seven.

** These are estimated values by multiplying the Kuwae deposition in column 4 and 6 with the average ratios of 7 vs. 17 SH and 2 vs. 7 NH ice core mean depositions, respectively. Thus, these two values roughly represent the average Kuwae depositions if all of the 17 SH and 7 NH ice cores Ire available.

Table 4-1. Estimates of stratospheric sulfate loading from large explosive volcanic eruptions. Shown in black are the tropical eruptions and in red are NH high-latitude eruptions.

Eruption	Year	Number of cores used in average	Ice core average sulfate deposition (kg/km^2)	Calibration factor (×10^9 km^2)	Hemispheric stratospheric sulfate aerosol loading (Tg)	Global stratospheric sulfate aerosol loading (Tg)	Other estimates (Tg)[a]
Unknown	1259	NH (3) SH (5)	146* 112*	1 1	146 112	258	N/A
Kuwae	1452	NH (2) SH (7)	45** 93**	1 1	45 93	138	235-414
Laki	1783	NH (24)	164	0.57	93	93	200
Unknown	1809	NH (11) SH (17)	28 26	1 1	28 26	54	N/A
Tambora	1815	NH (22) SH (17)	59 51	1 1	59 51	108	93-118
Krakatau	1883	NH (7) SH (18)	11 11	1 1	11 11	22	30-50
Katmai	1912	NH (6)	19	0.57	11	11	11
Agung	1963	SH (17)	11	1	11	17***	15-25
Pinatubo	1991	SH (10)	15	1	15	30	20-40

*The original deposition in Greenland and Antarctic ice sheet was multiplied by 1.13 and 1.27, respectively to account for the spatial variation. The multipliers were calculated by comparing the average deposition of the total 7 Northern Hemisphere and 17 Southern Hemisphere ice cores to those of the 3 Northern Hemisphere and 7 Southern Hemisphere cores that have 1259 Unknown signal.

**The original deposition in Greenland and Antarctic ice sheet was multiplied by 1.81 and 1.02, respectively. See *Gao et al*. [2006] for details.

***We found a large signal (about 7 kg/km^2) in the Greenland ice cores during 1963-1964, but this is probably due to the aerosol input from a high latitude NH eruption (Surtsey in Iceland). Since observations show that 2/3 of the aerosols were dispersed into the SH, we can calculate the global mass loading by multiply the SH loading by 1.5 to get the total 20 Tg of aerosols.

[a] Please see the text for the references.

Table 5-1. Deposition rates of Total β activities (mCi/km^2) for the 1953-1955 LNL and 1962-1966 HNL bomb tests in 13 Greenland ice core sites. All values obtained by averaging the local Total β activities records from Table 2 in *Clausen and Hammer* [1988].

Ice core sites	**Latitude (°N)**	**Longiude (°W)**	**Deposition 1953-1955**	**Deposition 1962-1966**
Hans Tavsen	82.4	38.15	1.63	11.1
Camp Century	77.18	61.11	2.78	17.1
NorthSite	75.8	42.4	2.51	11.3
North Central	74.62	39.60	1.28	12.6
Summit	72.3	38.0	3.81	13.8
Créte	71.12	37.32	3.36	15.7
Milcent	70.3	44.6	4.79	24.6
A1-S2	67.9	43.1	N/A	16.2
Dye 2	66.5	46.3	5.66	12.7
SNS 1	66.5	44.8	N/A	15.7
Dye3	65.2	43.8	3.02	14.7
SouthDome	63.6	44.6	2.38	20.2
DS 2	63.6	44.9	N/A	13.0

Table 5-2. Calculation of stratospheric partitioning of total β activity and the calibration factors. LNL is Low Northern Hemisphere Latitude and HNL is High Northern Hemisphere Latitude.

Years of β deposition	Stratospheric partitioning of total fission yield (Mt)[a]	Total β activity injected in the stratosphere (MCi)[b]	Average total β activity in Greenland ice cores (mCi/km^2)[c]	Calibration factor (L_B) for Greenland ice core records ($\times 10^9$ km^2)
1952-54 (LNL)	18.11	4.78	3.17	1.51
1961-62 (HNL)	69.64	18.39	15.08	1.22

[a]From Table 1 of *UNSCEAR* [2000].
[b]By applying the production rate of ^{90}Sr and ^{137}Cs of 0.105 MCi/Mt and 0.159 MCi/Mt.
[c]From Table 5-1.

Table 5-3. Calibration factors derived from three different methods ($\times 10^9$ km^2).

Method		For tropical eruptions based on NH ice cores			For tropical eruptions based on SH ice cores			For NH high latitude eruptions based on NH ice cores
		2:1 NH vs. SH	1:1 NH vs. SH	1:2 NH vs. SH	2:1 SH vs. NH	1:1 SH vs. NH	1:2 SH vs. NH	
Bomb test calculation (L_B)		1.1 – 1.5	1.5 – 2.0	2.0 – 3.0	N/A	N/A	N/A	1.6
Pinatubo observations(L_P)		N/A	N/A	N/A	1.5 – 2.0	2.0 – 2.7	2.7 – 3.6	N/A
Climate model simulations (L_{GISS})	Tambora	N/A	N/A	1.36	0.94	N/A	N/A	N/A
	Pinatubo	0.85	N/A	N/A	N/A	N/A	0.94	N/A
	Laki	N/A	N/A	N/A	N/A	N/A	N/A	0.58
	Katmai	N/A	N/A	N/A	N/A	N/A	N/A	0.55

Table 6-1. Exchange coefficients for different regions in percentage (%) per month. Original values from *Grieser and Schönwiese* [1999].

Regions	Original Values	Values in this paper
tropics → tropics	91	91
tropics → extratropics	30	50
extratropics → tropics	7	7
extratropics ↔ extratropics (winter-spring)	90	90
extratropics ↔ extratropics (summer-fall)	45	70
extratropics → winter polar vortex	10	10
extratropics → summer polar region	45	70
extratropics → polar region in spring and fall	28	40
polar region→ extratropics	10/45/28	4

Table 6-2. Total sulfate deposition from different volcanic signal extraction criteria.

Eruption	31pts+2MAD (Tg)	31pts+1.5MAD (Tg)	31pts+3MAD (Tg)	11pts+2MAD (Tg)	51pts+2MAD (Tg)	101pts+2MAD (Tg)	s.d.* (Tg)	Cvar * (%)
1809 Unknown	58.7	62.4	55.6	57.3	61.7	65.2	3.36	5.6
1815 Tambora	120	121	117	101	125	129	4.53	3.7
1831 Unknown	17.0	17.2	18.7	13.1	16.7	14.8	1.42	8.4
1835 Cosigüina	40.2	39.4	37.7	25.2	37.1	36.8	1.48	3.9
1883 Krakatau	26.9	27.8	22.5	21.1	26.2	22.1	2.63	10.5
1912 Katmai	22.0	22.3	21.1	19.3	22.9	25.4	1.61	7.1
1991 Pinatubo	30.1	30.3	20.0	7.2	27.6	30.2	4.40	15.9

* Standard deviation (s.d.) and coefficient of variance (Cvar) were calculated using the five sets of extraction criteria, leaving out the 11pts+2MAD criterion (see text).

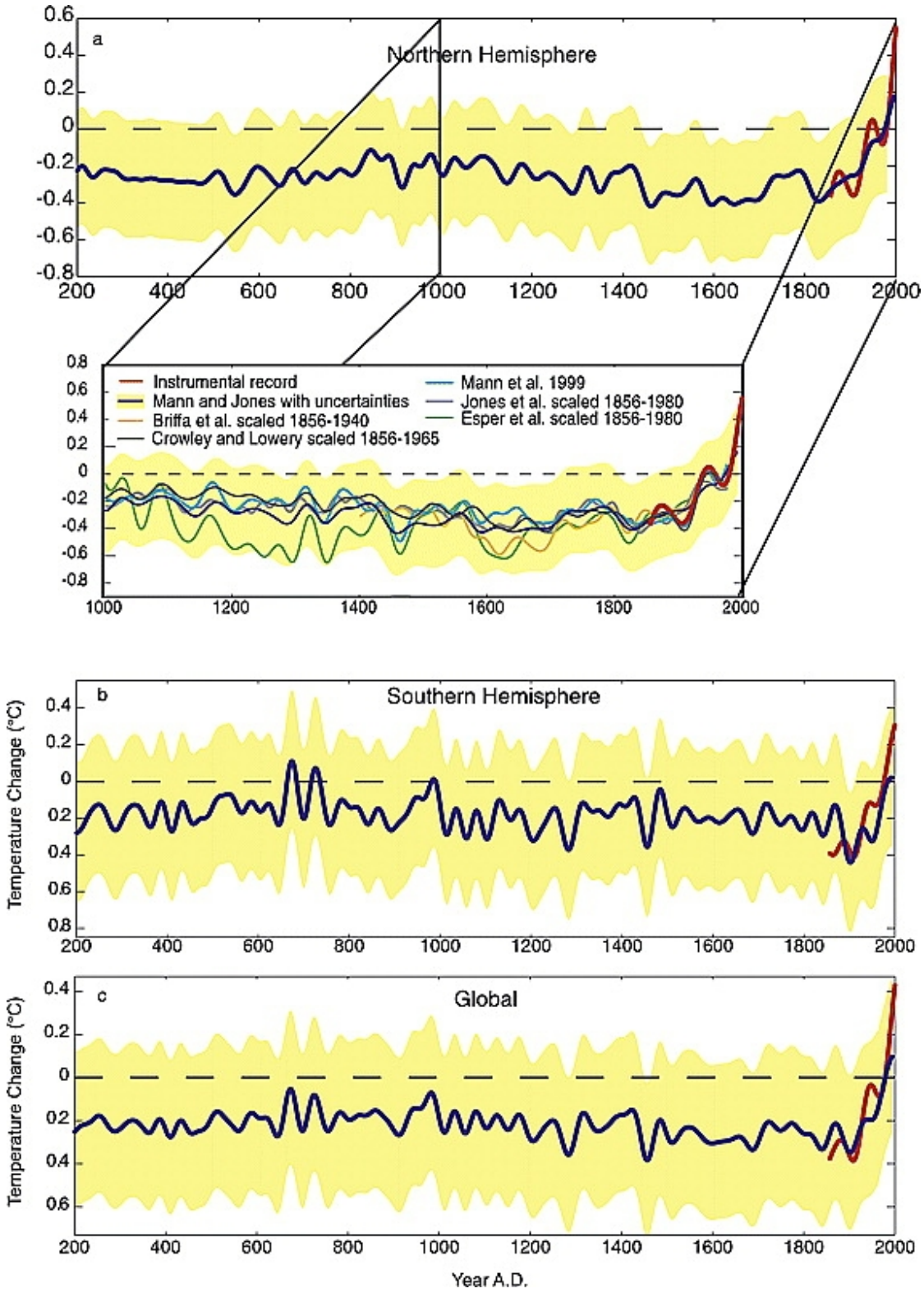

Figure 1-1. Reconstructions of (a) NH, (b) SH, and (c) global mean annual temperatures over the past two millennia. Smoothed (40-year low-passed) versions of these series are shown to highlight the low-frequency variations. Source: Jones and Mann [2004].

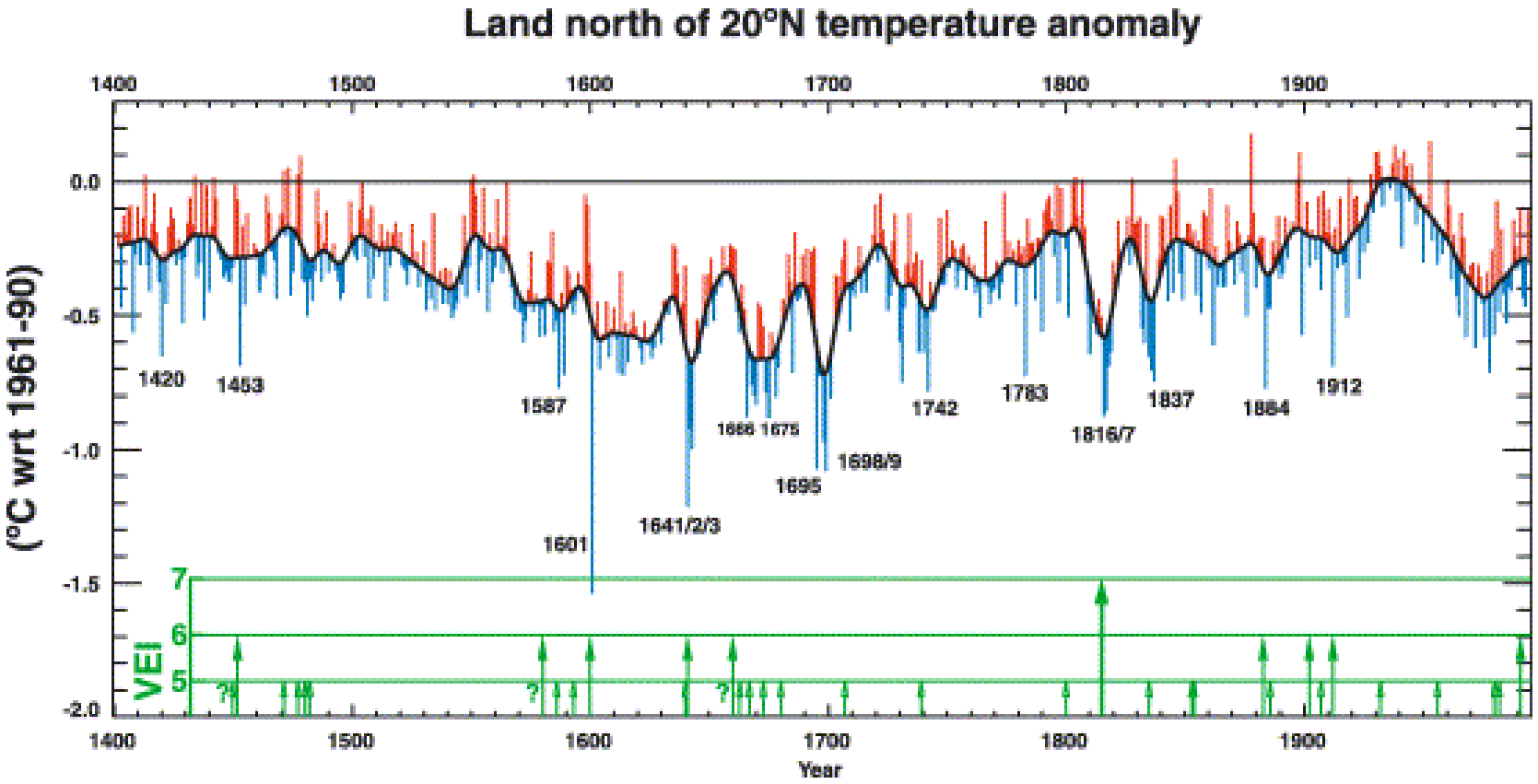

Figure 1-2. Estimates of warm-season temperature (anomalies from the 1961-1990 mean) for land areas north of 20°N. The smoothed curve is the 25-year low-pass filtered reconstruction. The Volcanic Explosivity Index (VEI) is indicated by the arrows at the bottom; ?marks those eruptions whose date is uncertain. Source: *Briffa et al*.[2004]

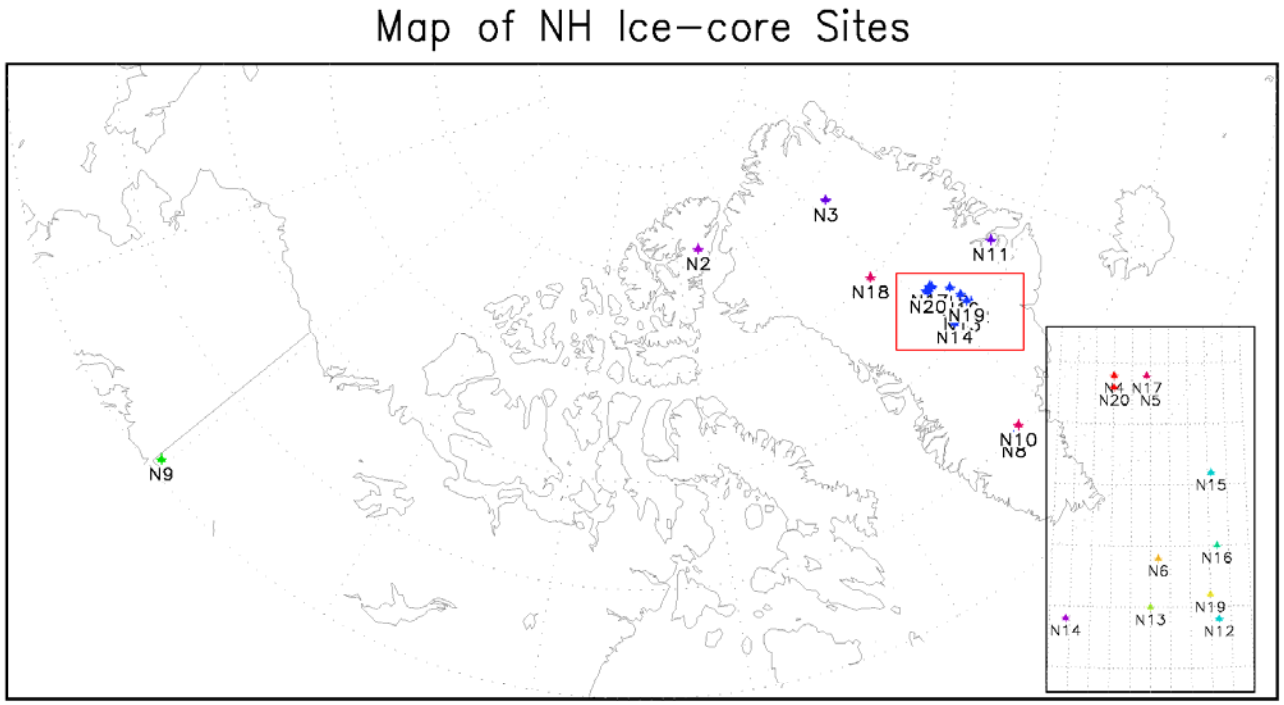

N1–A84 N2–A77 N3–NGT B20 N4–GISP2 N5–Summit N6–Crete
N7–Dye3 N8–20D N9–MtLogan N11–Renland N12–site A N13–site B
N14–site D N15–site E N16–site G N17–GRIP N18–NorthGRIP N19–GL siteA
N20–GL siteT

Note: sites 1&2, 7&8, 12&19 and 5&20 are at similar locations
The panel on the right is an expanded map of the sites in the red rectangle.

Figure 2-1. Distribution of ice core sites in Arctic. Please see Table 1 for the detail information of individual ice core.

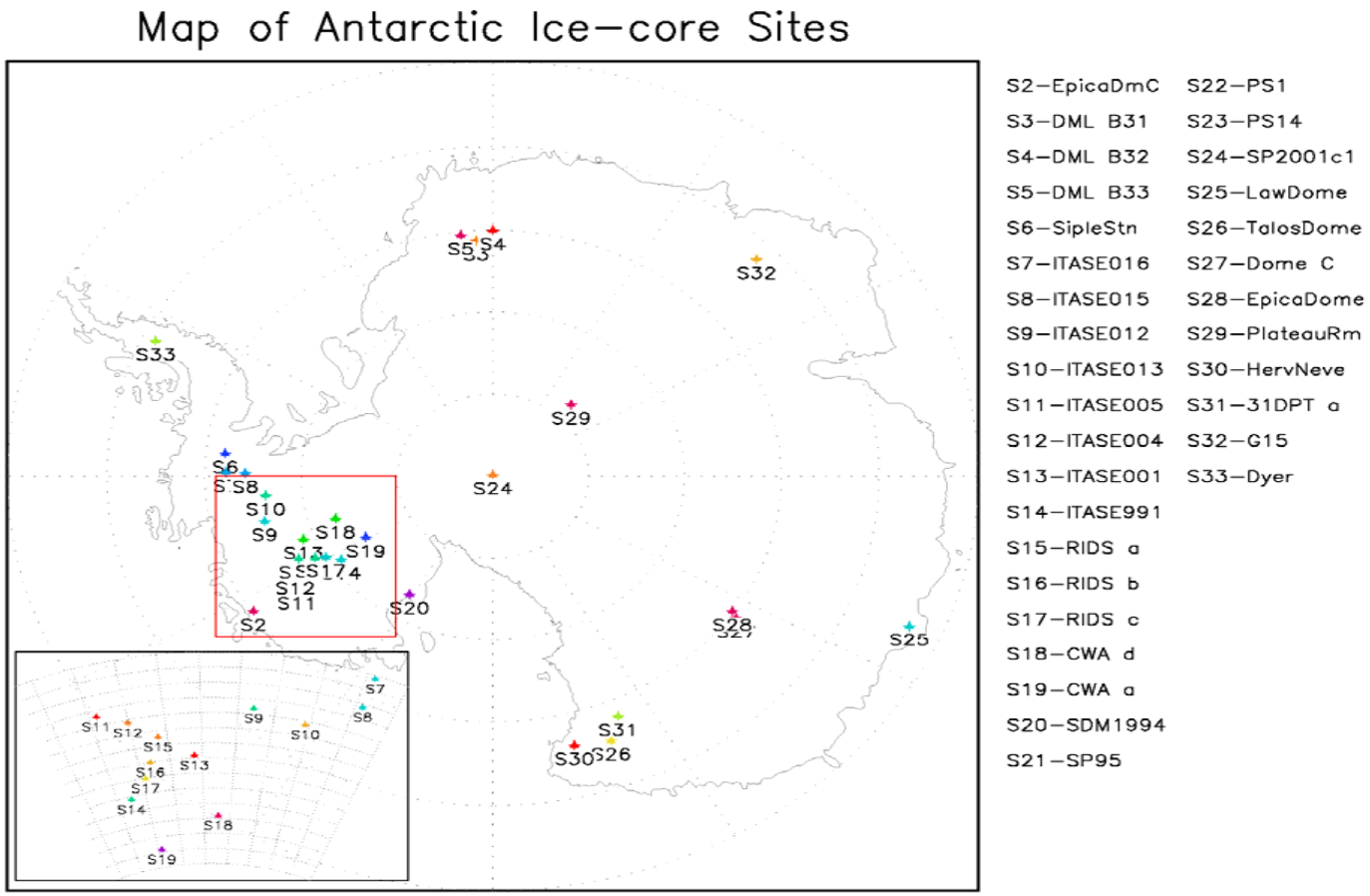

Sites S21,S22,S23 and S24 are at the same location.

The panel on the left is an expanded map of the sites in the red rectangle.

Figure 2-2. Distribution of ice core sites in Antarctica. Please see Table 1 for the detail information of individual ice core.

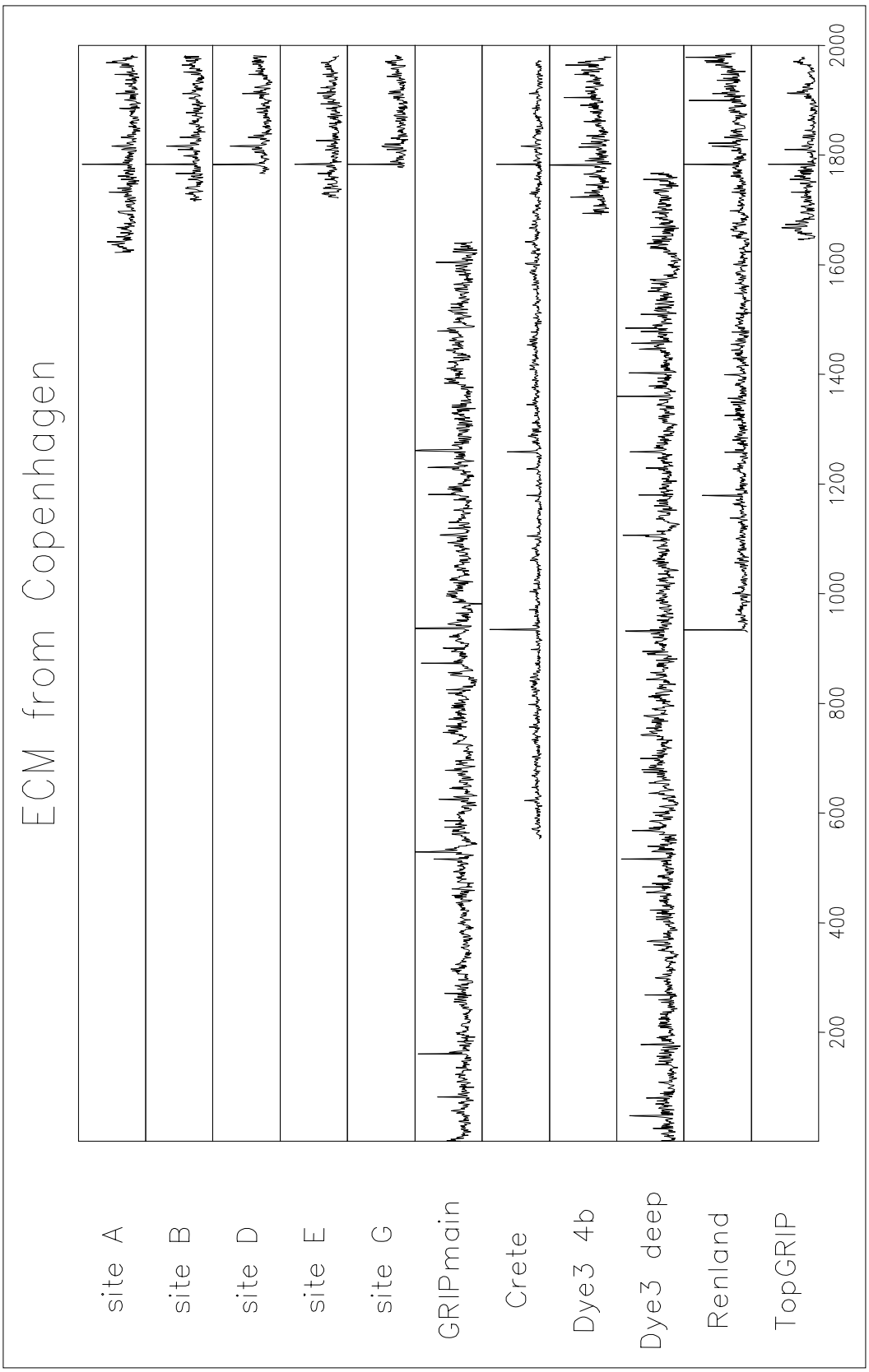
ECM from Copenhagen
site A
site B
site D
site E
site G
GRIPmain
Crete
Dye3 4b
Dye3 deep
Renland
TopGRIP
200
400
600
800
1000
1200
1400
1600
1800
2000

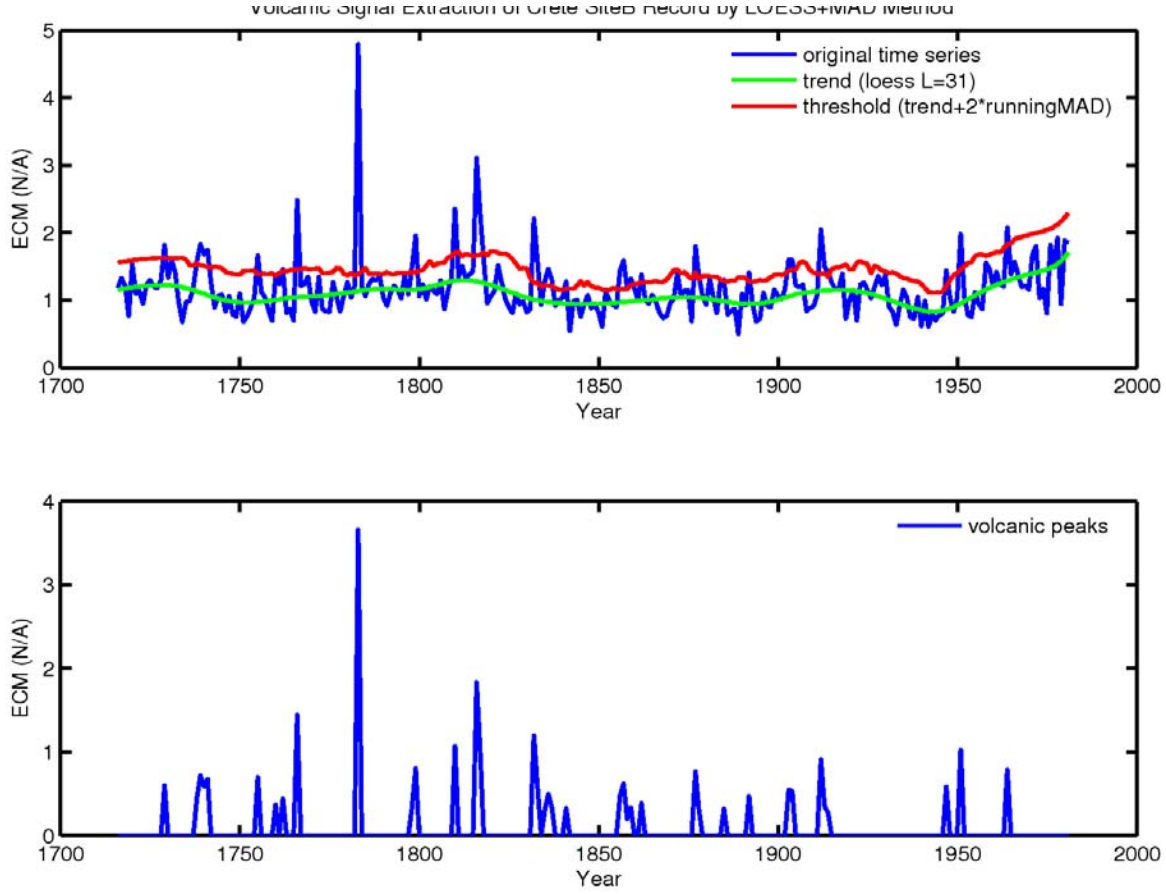

Figure 2-4. Example of volcanic signal extraction method.

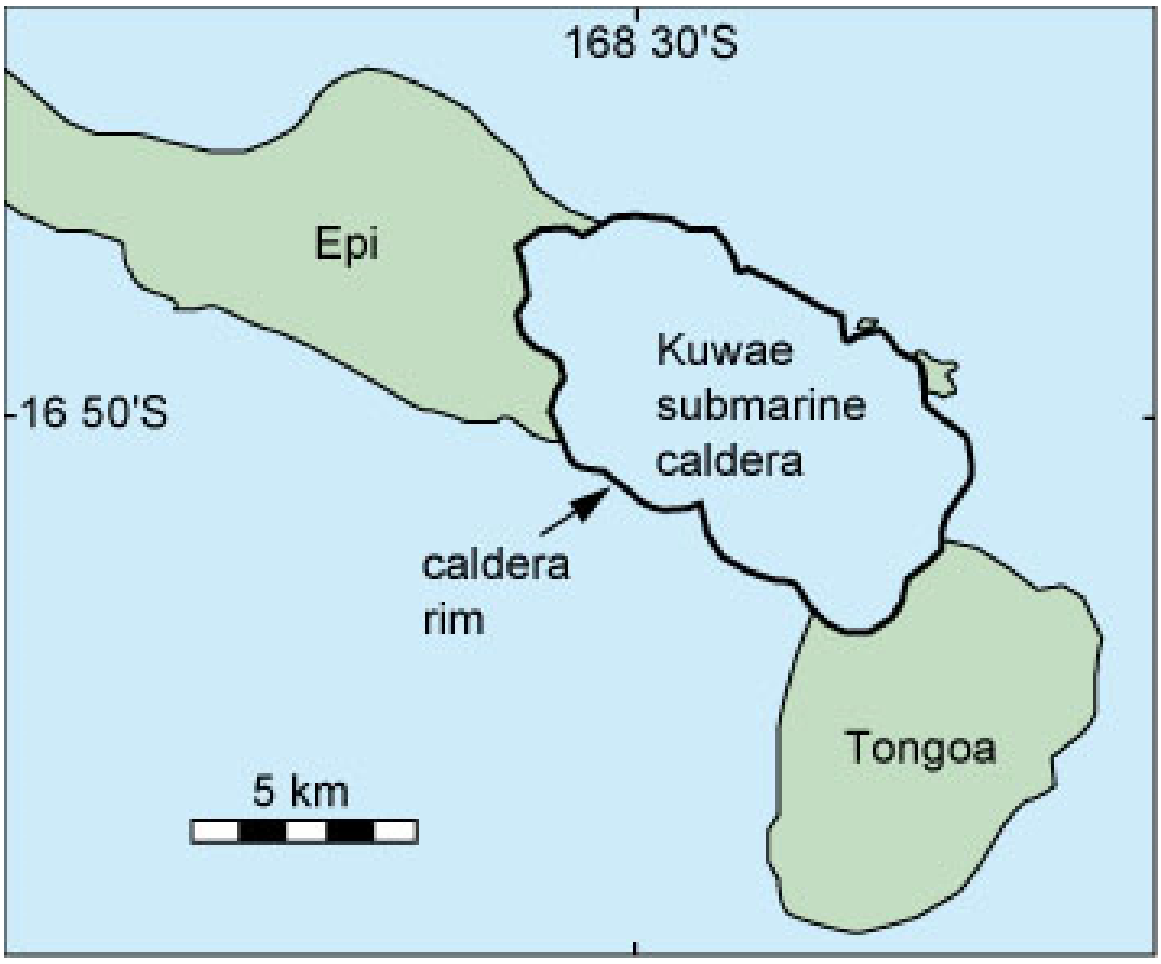

Figure 3-1. Map of Kuwae submarine caldera.

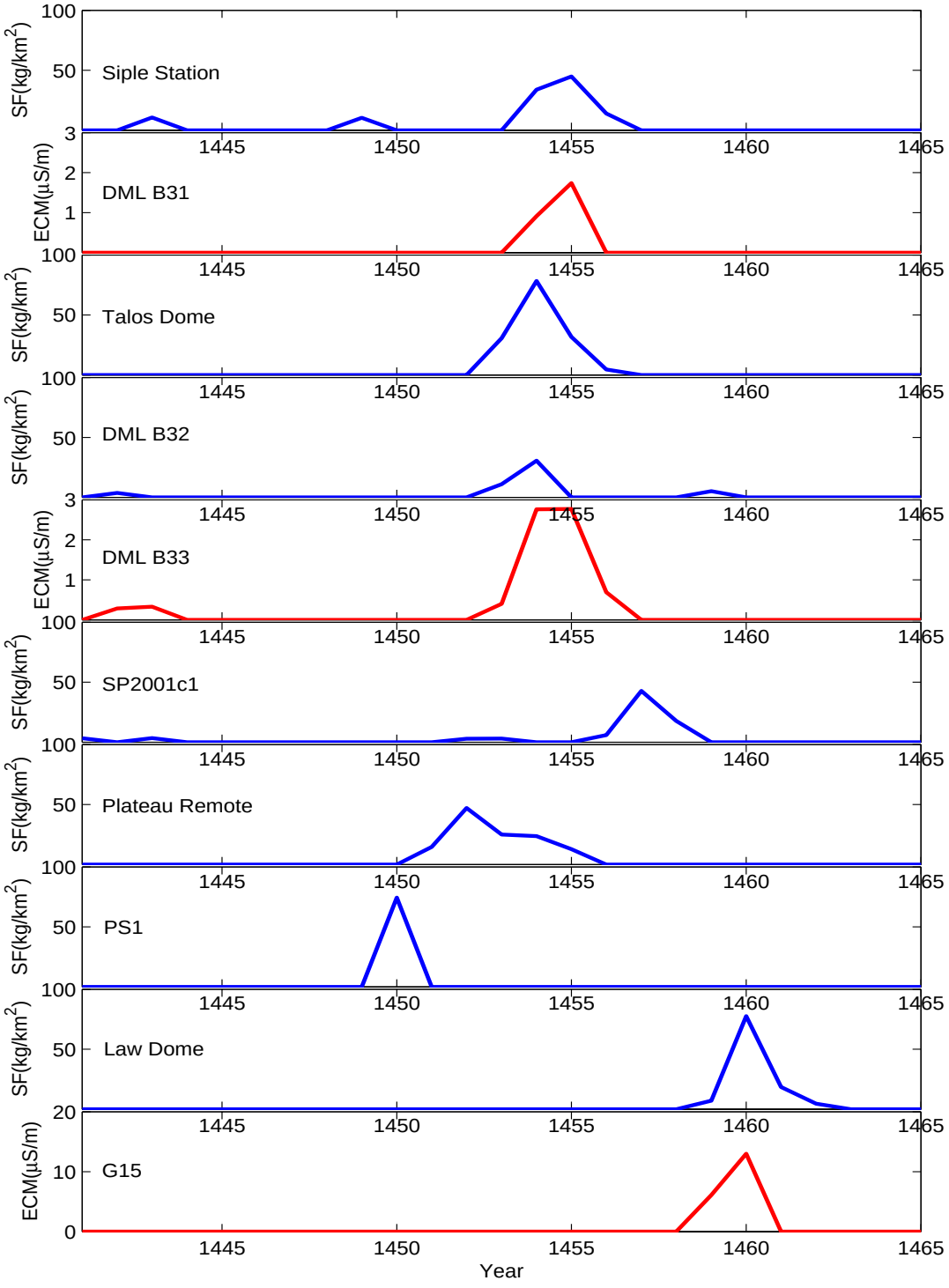

Figure 3-2. Kuwae signals extracted from the annual time series of the 10 Southern Hemisphere ice core records (see Table 2-1, Fig. 2-2). SF (in blue) is sulfate flux and ECM (in red) is electrical conductivity measurement.

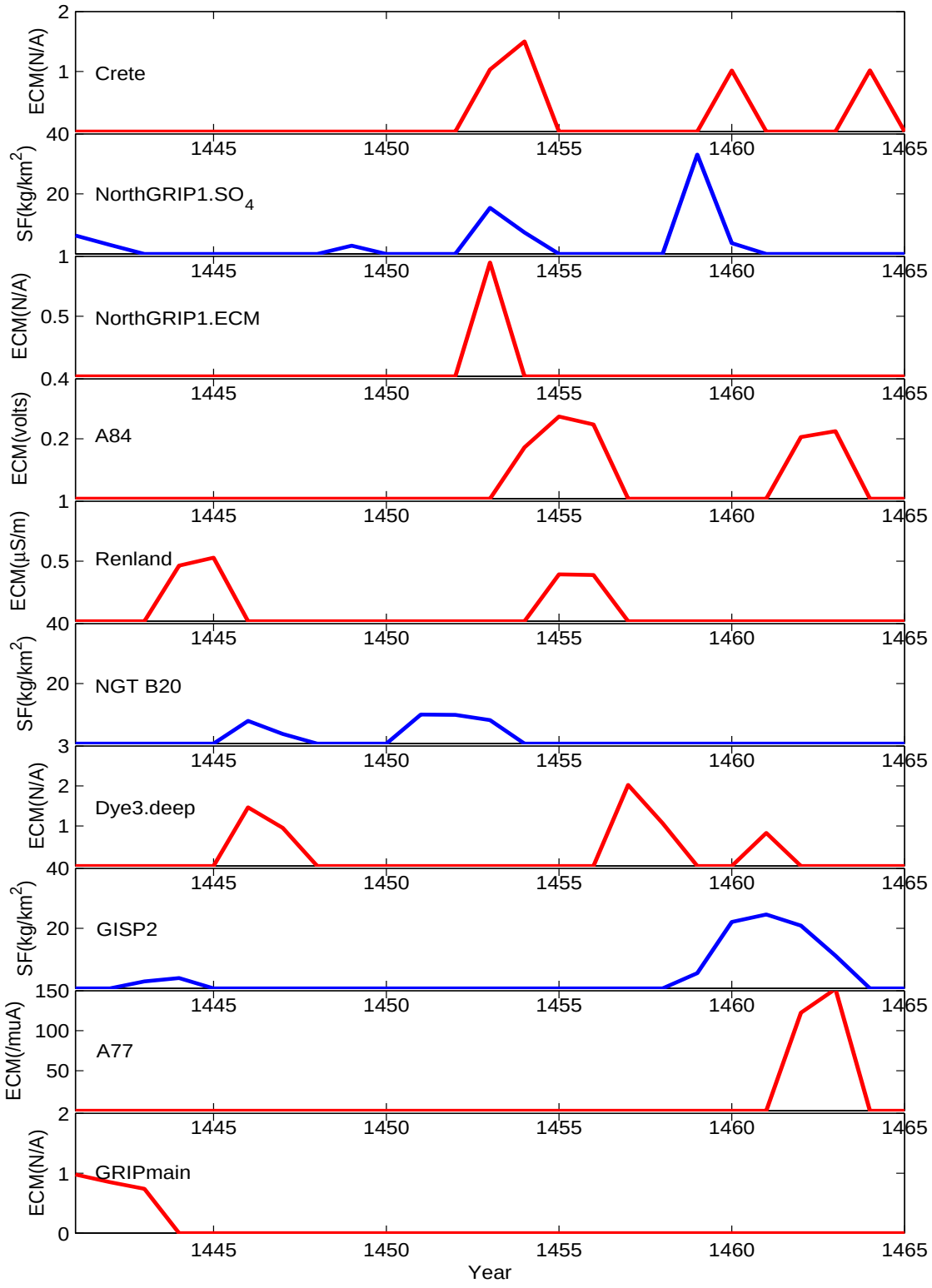

Figure 3-3. Kuwae signals extracted from the annual time series of the ten Northern Hemisphere ice core records (see Table 2-1, Fig. 2-1). SF (in blue) is sulfate flux and ECM (in red) is electrical conductivity measurement.

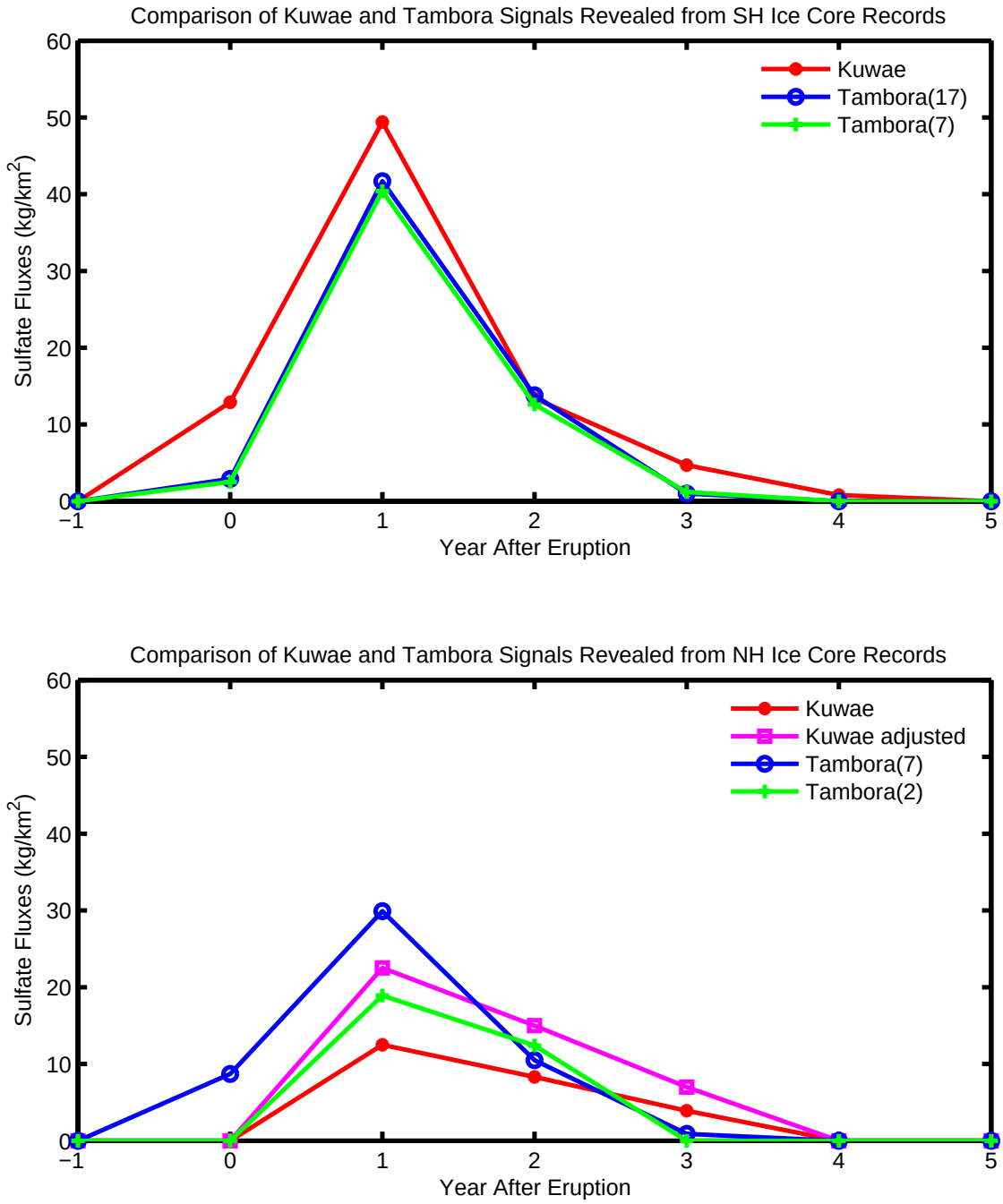

Figure 3-4. Comparison of the Kuwae and Tambora signals revealed from the ice core records. The eruption year was set to be 1452 and 1815 for Kuwae and Tambora, respectively; and the signals Ire adjusted to have the peak values line up in the year after eruption. Two sets of Tambora results Ire plotted for each hemisphere, one averaged over all the cores available and the other averaged over the same cores as Kuwae. The adjusted estimation (see the article for details) of Kuwae deposition is also plotted.

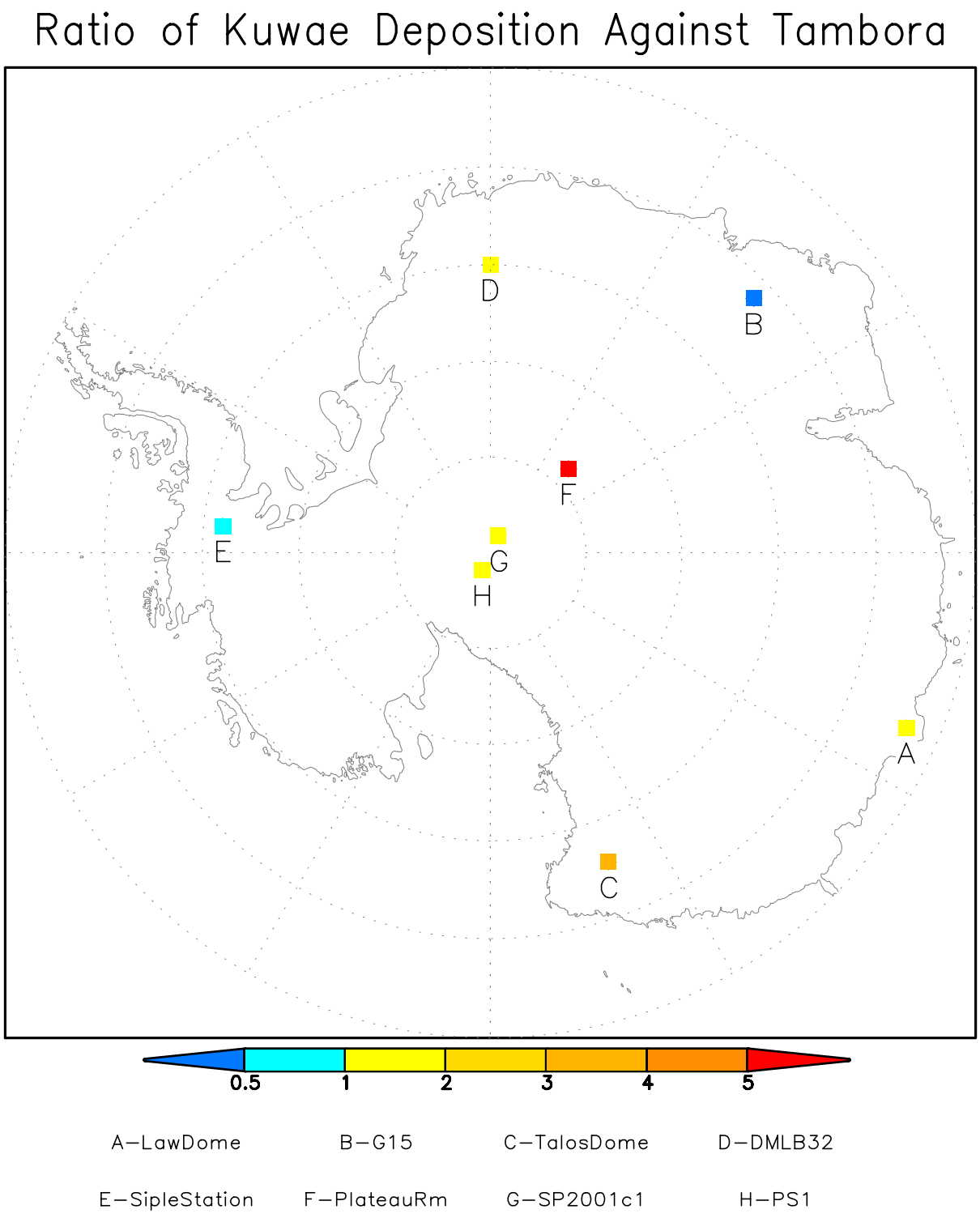

Figure 3-5: Spatial distribution of the ratio between the net deposition for Kuwae and Tambora eruption in eight Antarctic ice cores.

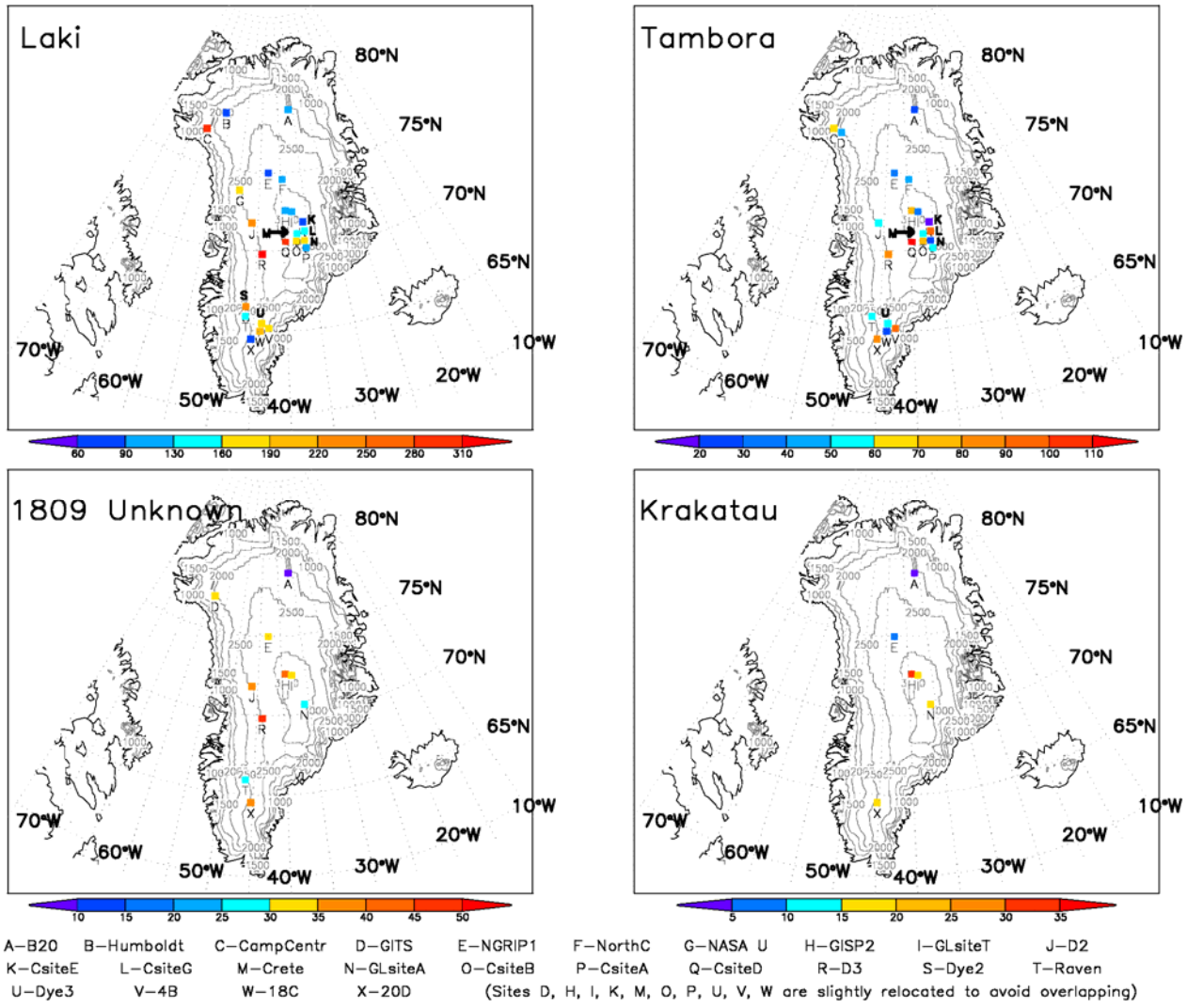

Figure 4-1. Spatial distribution of Laki, 1809 Unknown, Tambora, and Krakatau sulfate deposition (kg/km^2) in Greenland ice cores. The colors are defined so that the ones in blue indicate smaller than average deposition and the ones in yellow, orange, and red indicate larger than average.

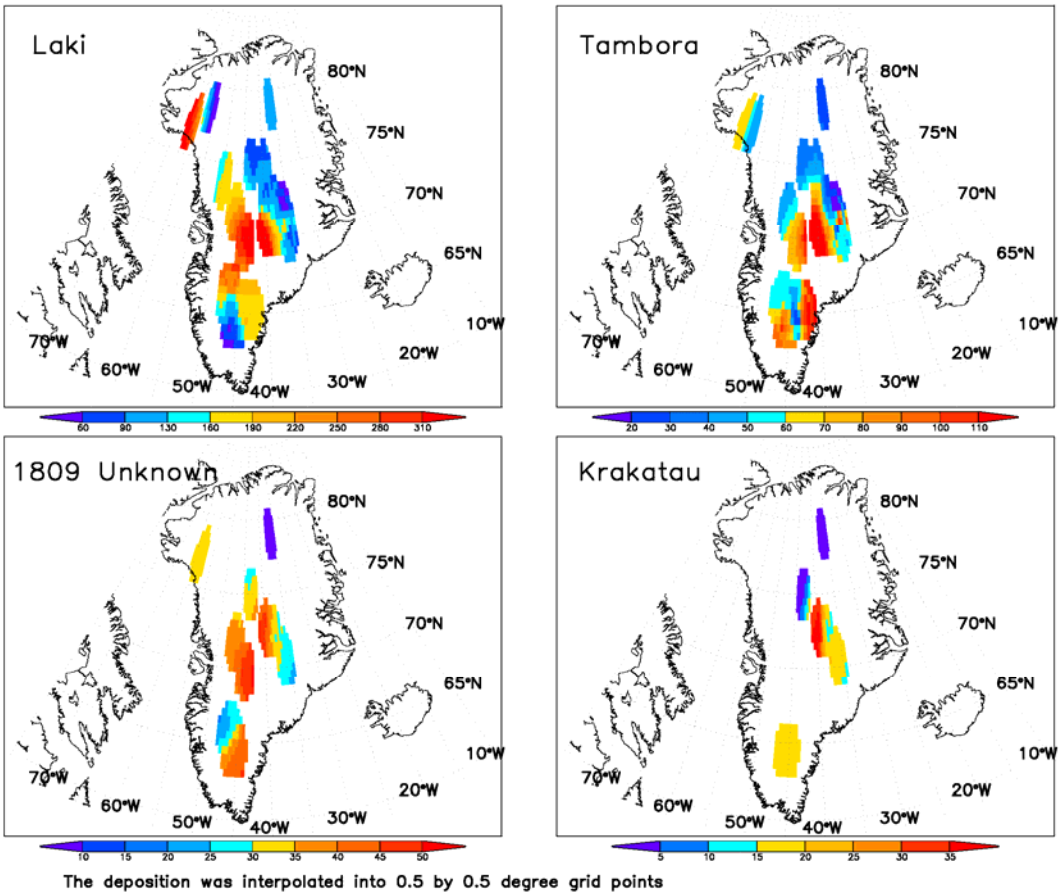

Figure 4-2. Same as Fig. 4.1 with the deposition was interpolated into 0.5°x0.5° grid points.

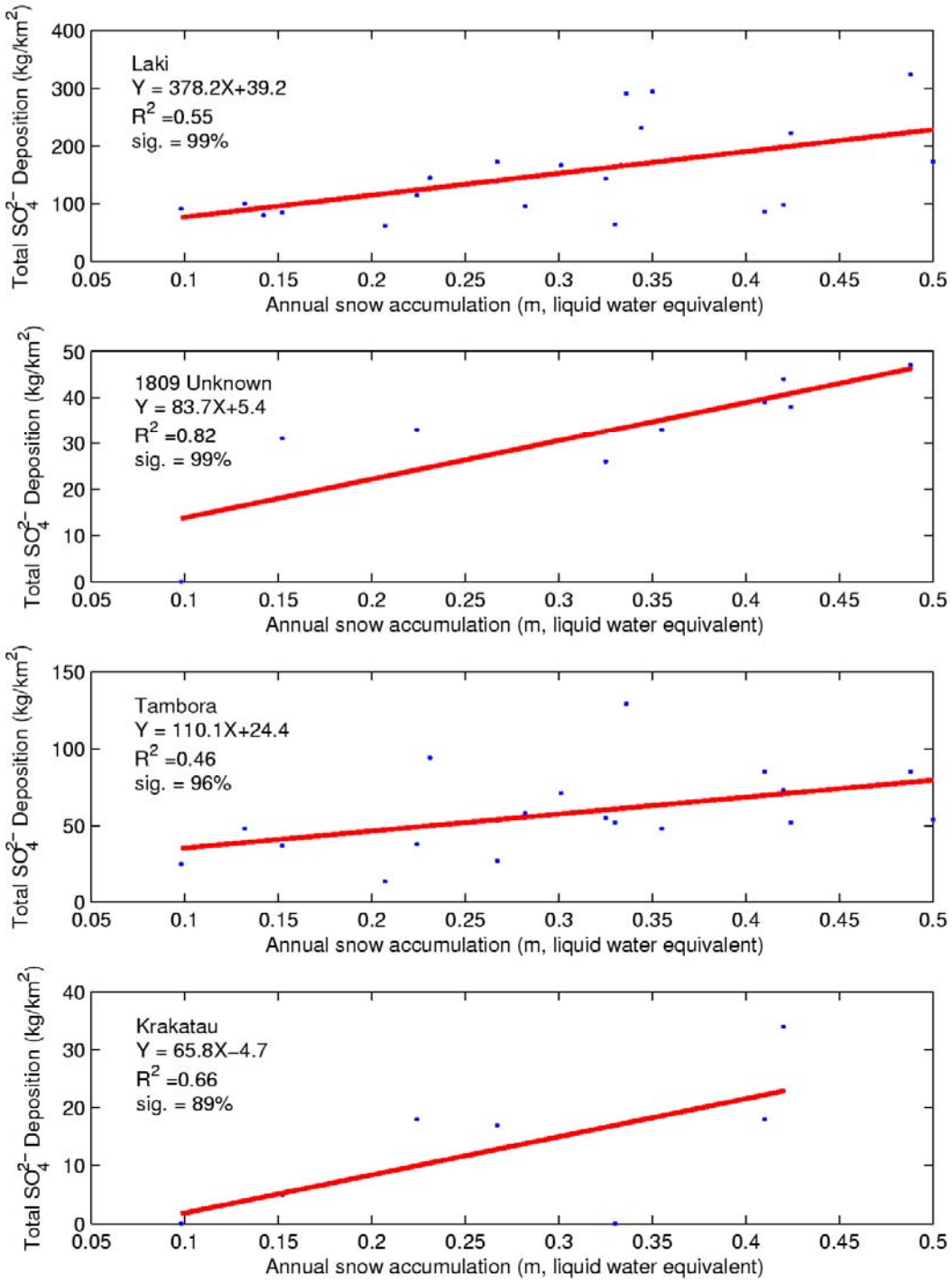

Figure 4-3. Relationship between the annual snow accumulation rates and the total sulfate fluxes in Greenland ice cores.

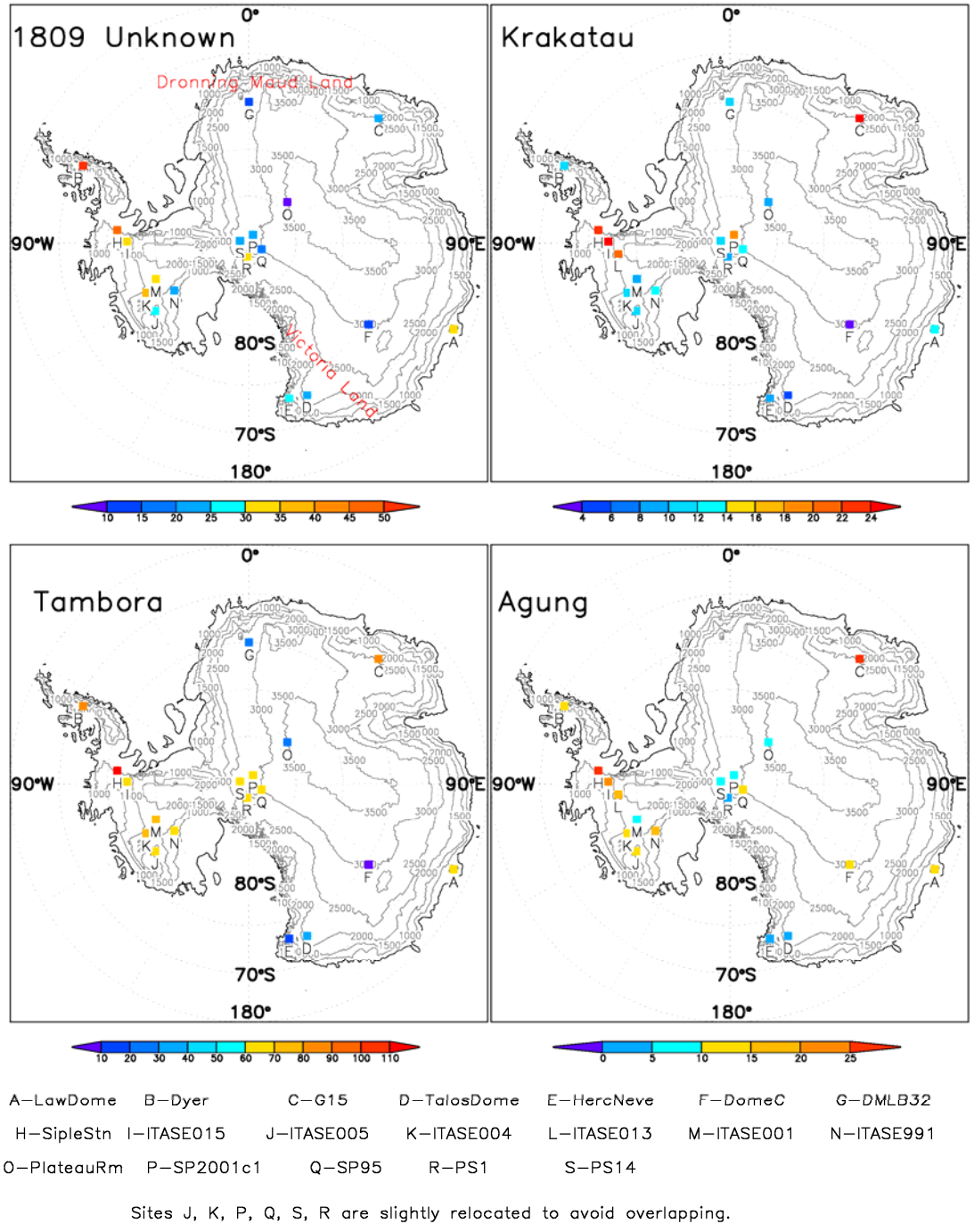

Figure 4-4. Spatial distribution of 1809 Unknown, Tambora, Krakatau and Agung sulfate deposition (kg/km^2) in Antarctic ice cores. The colors are defined so that the ones in blue indicate smaller than average deposition and the ones in yellow, orange, and red indicate larger than average.

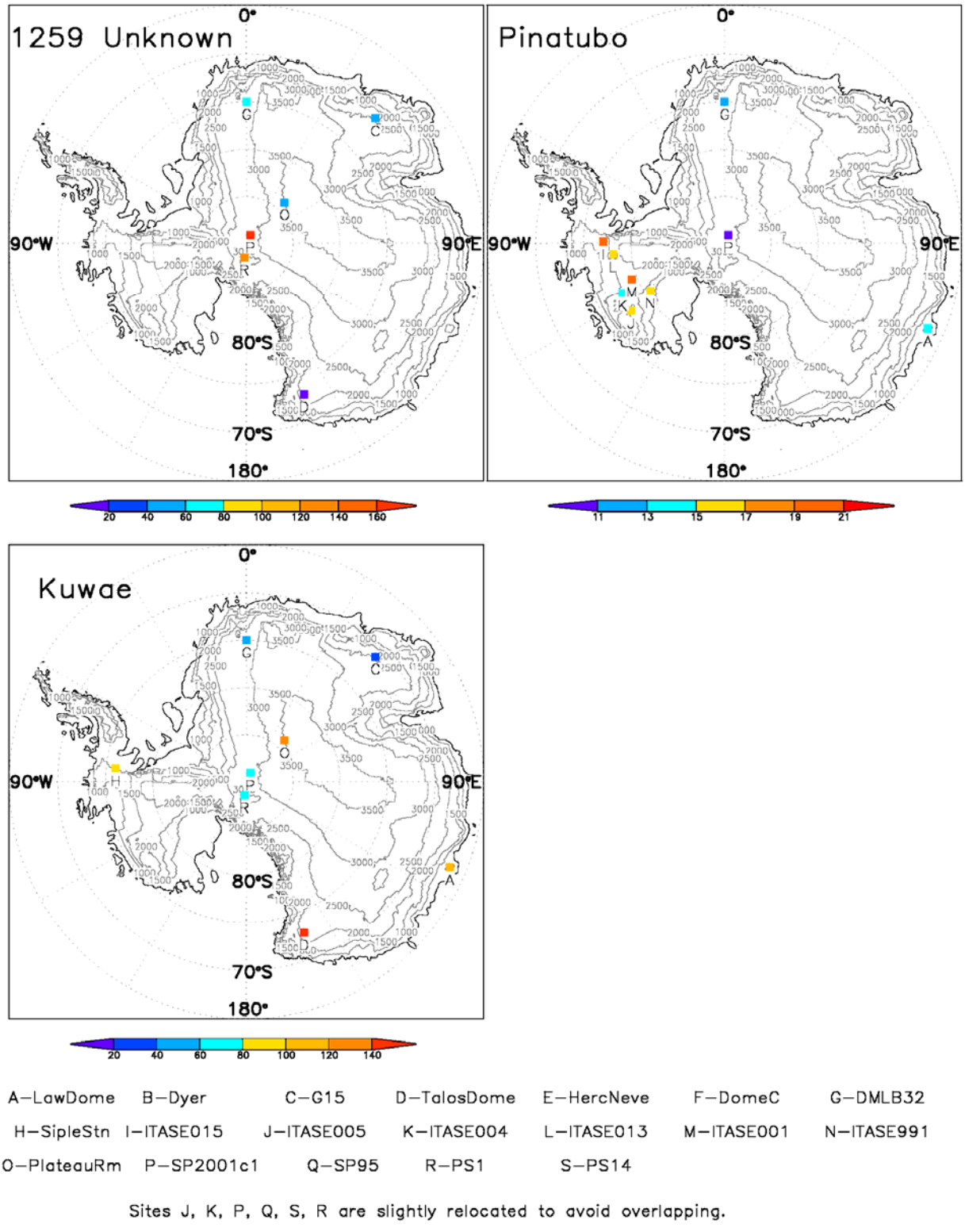

Figure 4-5. Same as Fig. 4 but for the 1259 Unknown, Kuwae, and Pinatubo eruption.

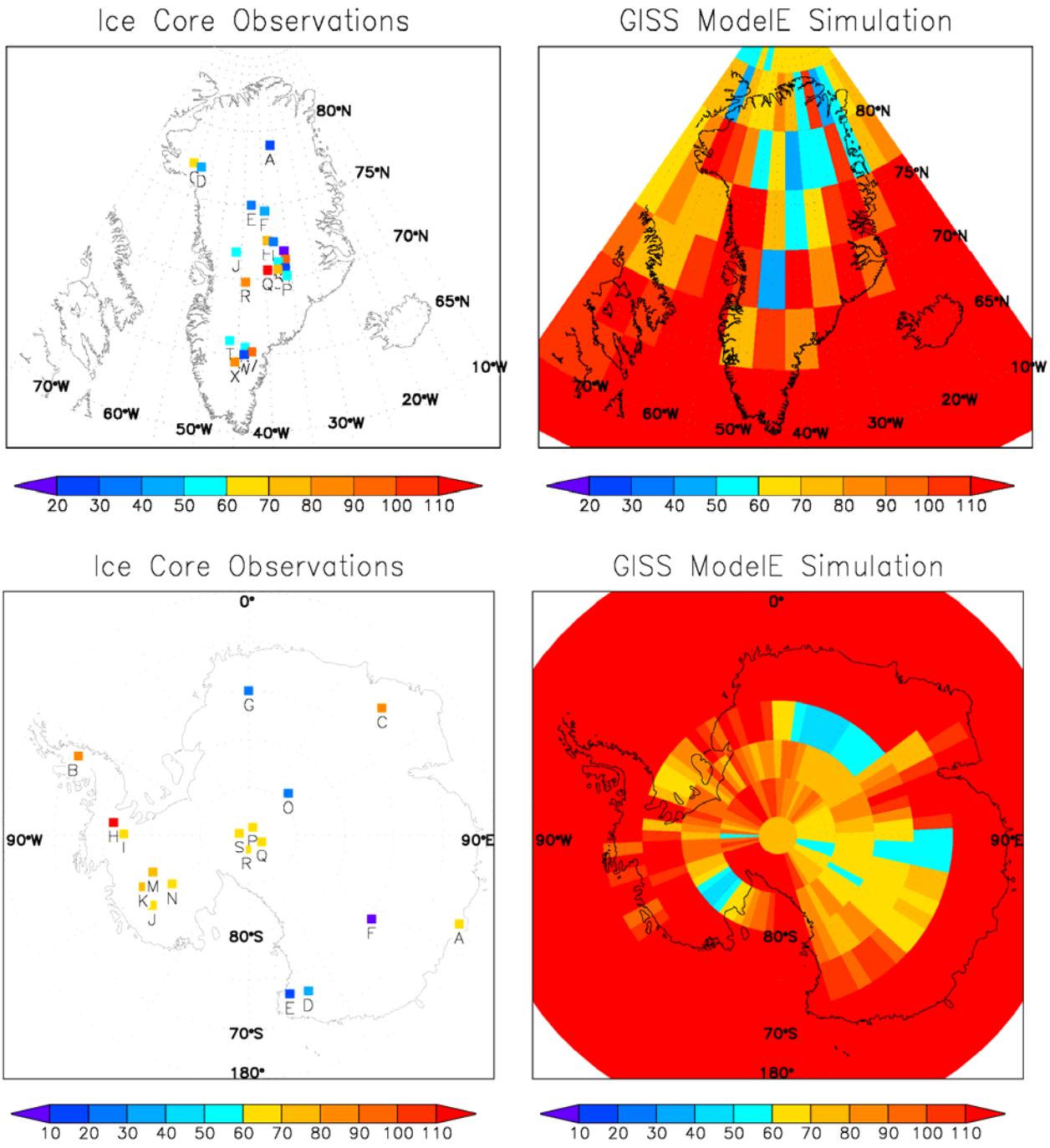

Figure 4-6. Comparison between the total Tambora sulfate deposition (kg/km^2) in Greenland (top panel) and Antarctic (bottom panel) ice core observations and in the GISS simulations.

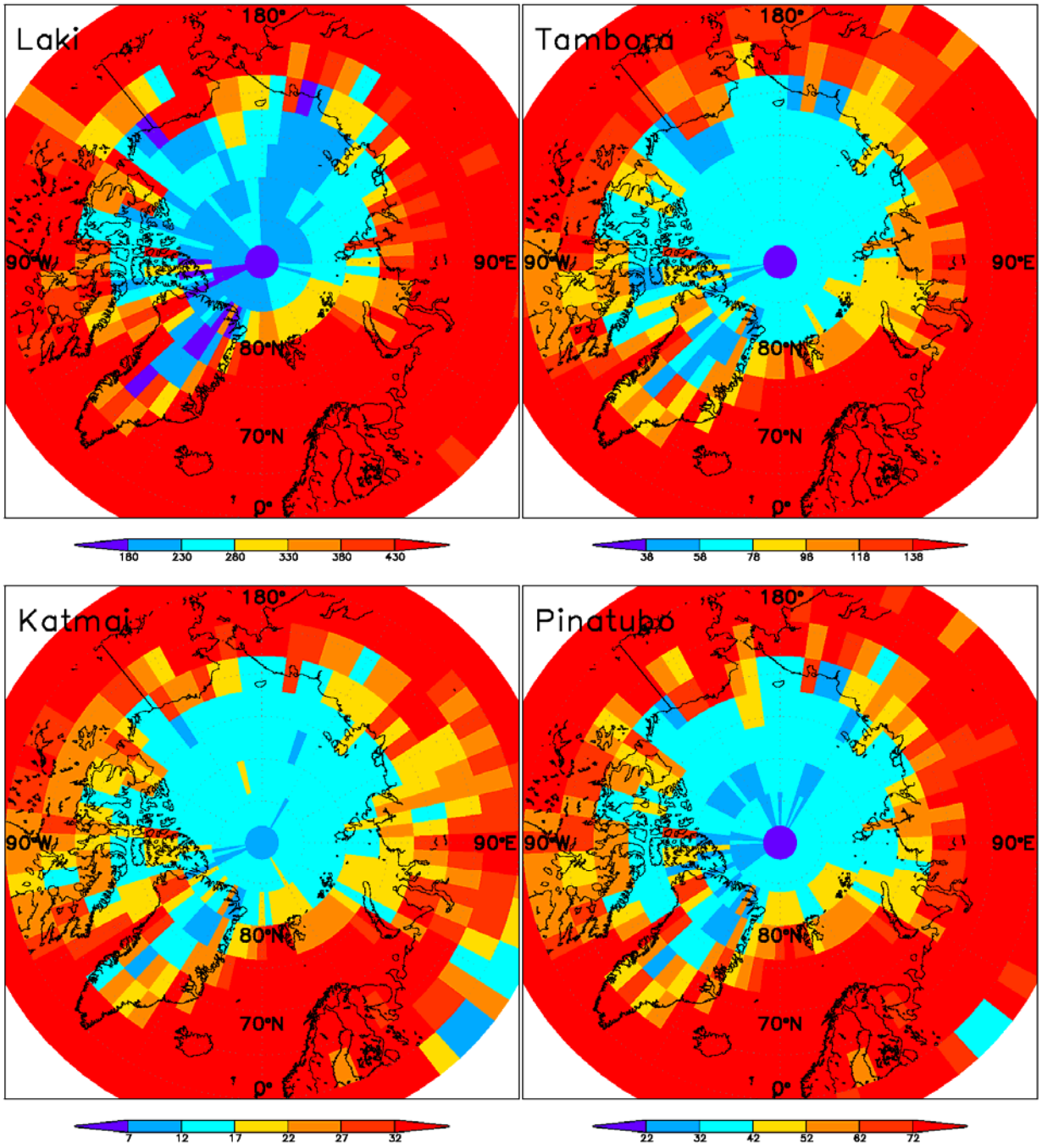

Figure 4-7. GISS simulated Laki, Tambora, Katmai, and Pinatubo deposition (kg/km^2) in the Arctic region. The colors are defined so that the ones in blue indicate smaller than average deposition for 66°N-82°N, 50°W-35°W and the ones in yellow, orange, and red indicate larger than average.

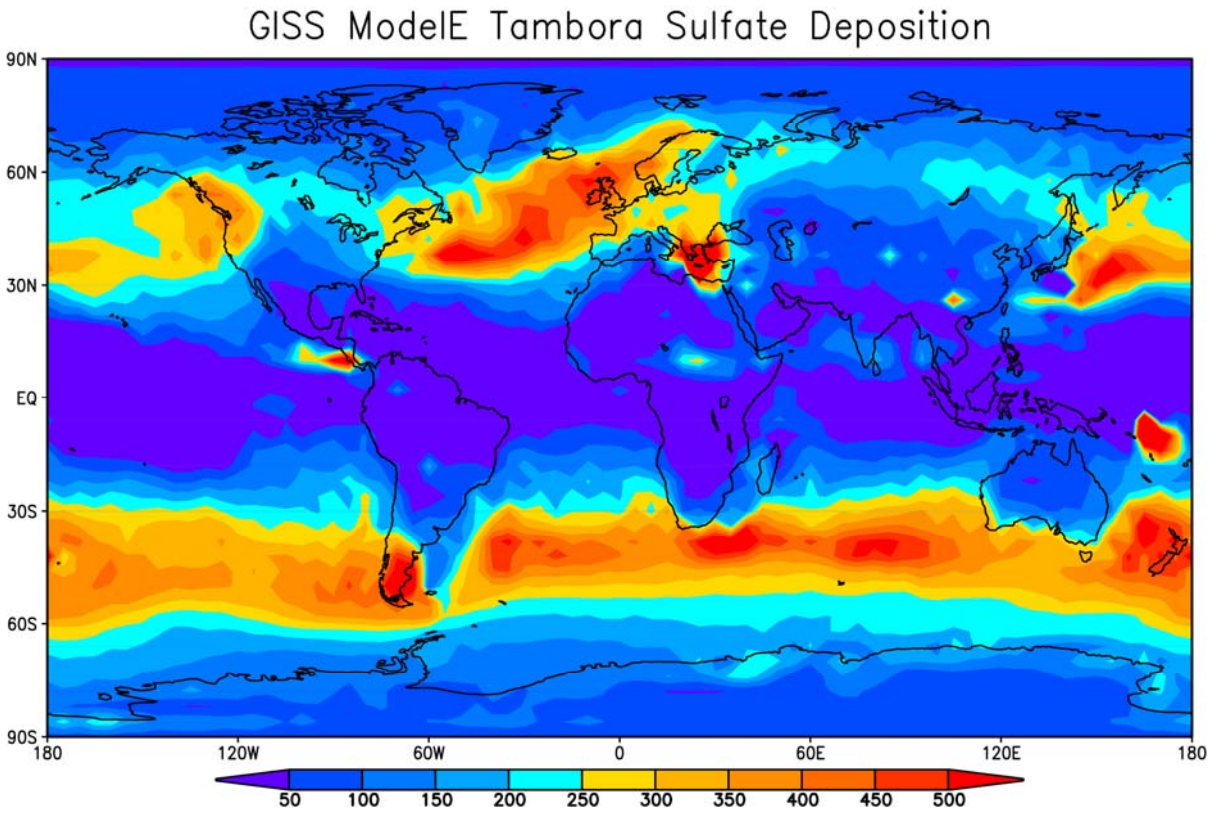

Figure 5-1. Global spatial distribution of the volcanic sulfate deposition (kg/km^2) after the 1815 Tambora eruption, simulated by the GISS ModelE. 55 Mt of SO_2 gas was put into the 24-32 km layer, which converted into 107 Mt of sulfate aerosols assuming a 75%:25% H_2SO_4:H_2O weight composition.

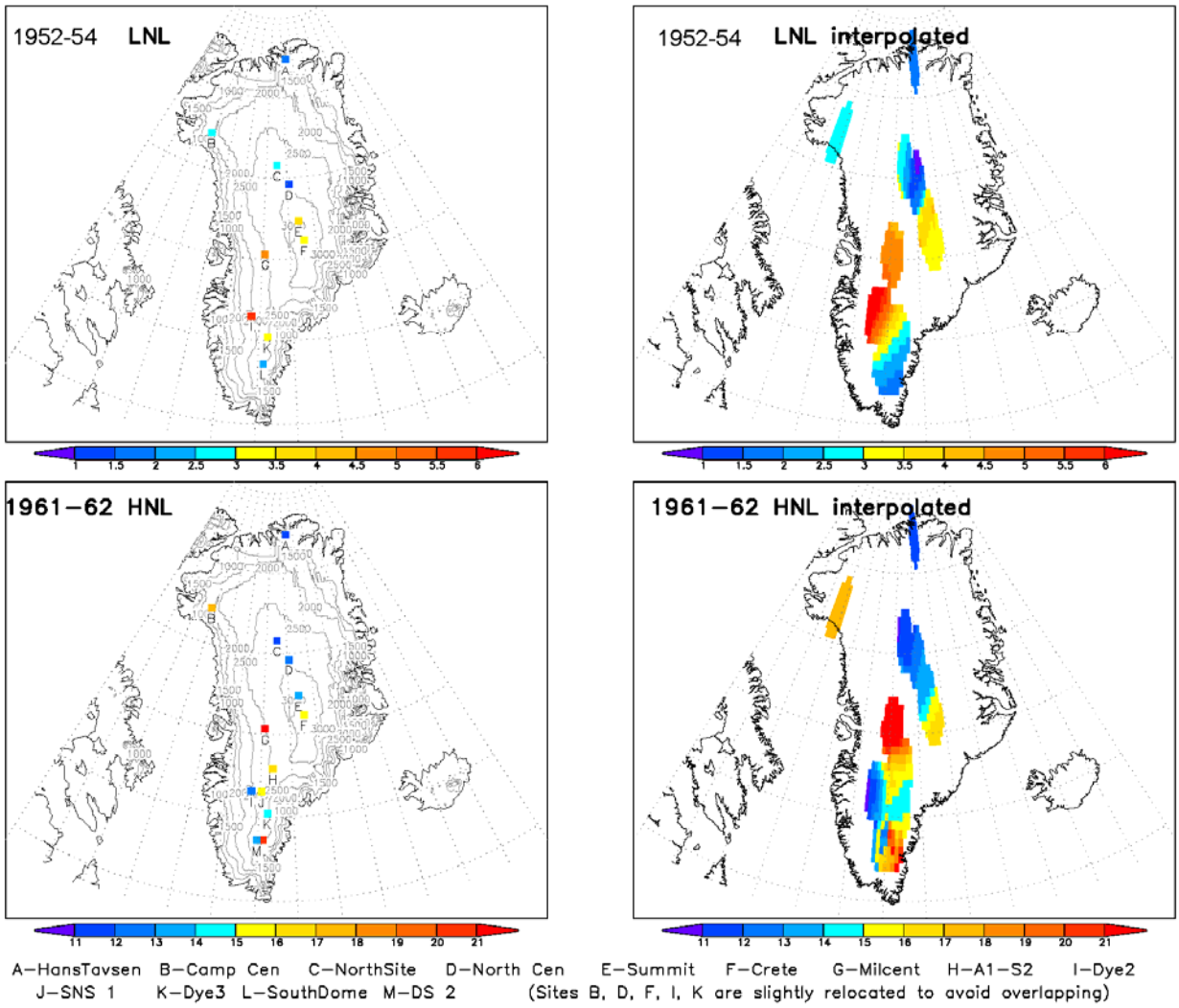

Figure 5-2. Spatial distribution of the total β activities from the 1952-54 LNL and 1961-62 HNL bomb tests.

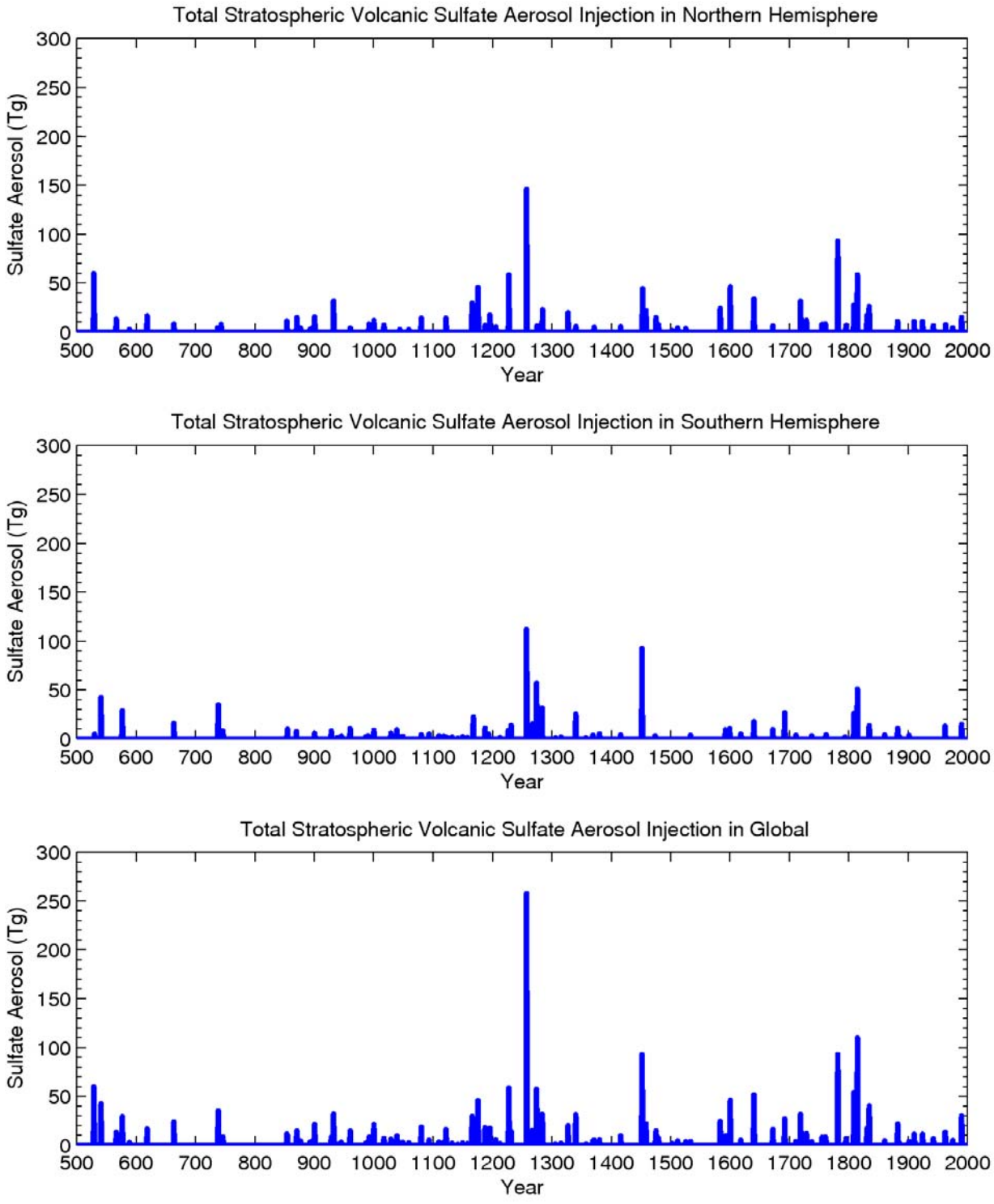

Figure 5-3. Total stratospheric volcanic sulfate aerosol injection for the past 1500 years in NH (up), SH (middle), and global (bottom).

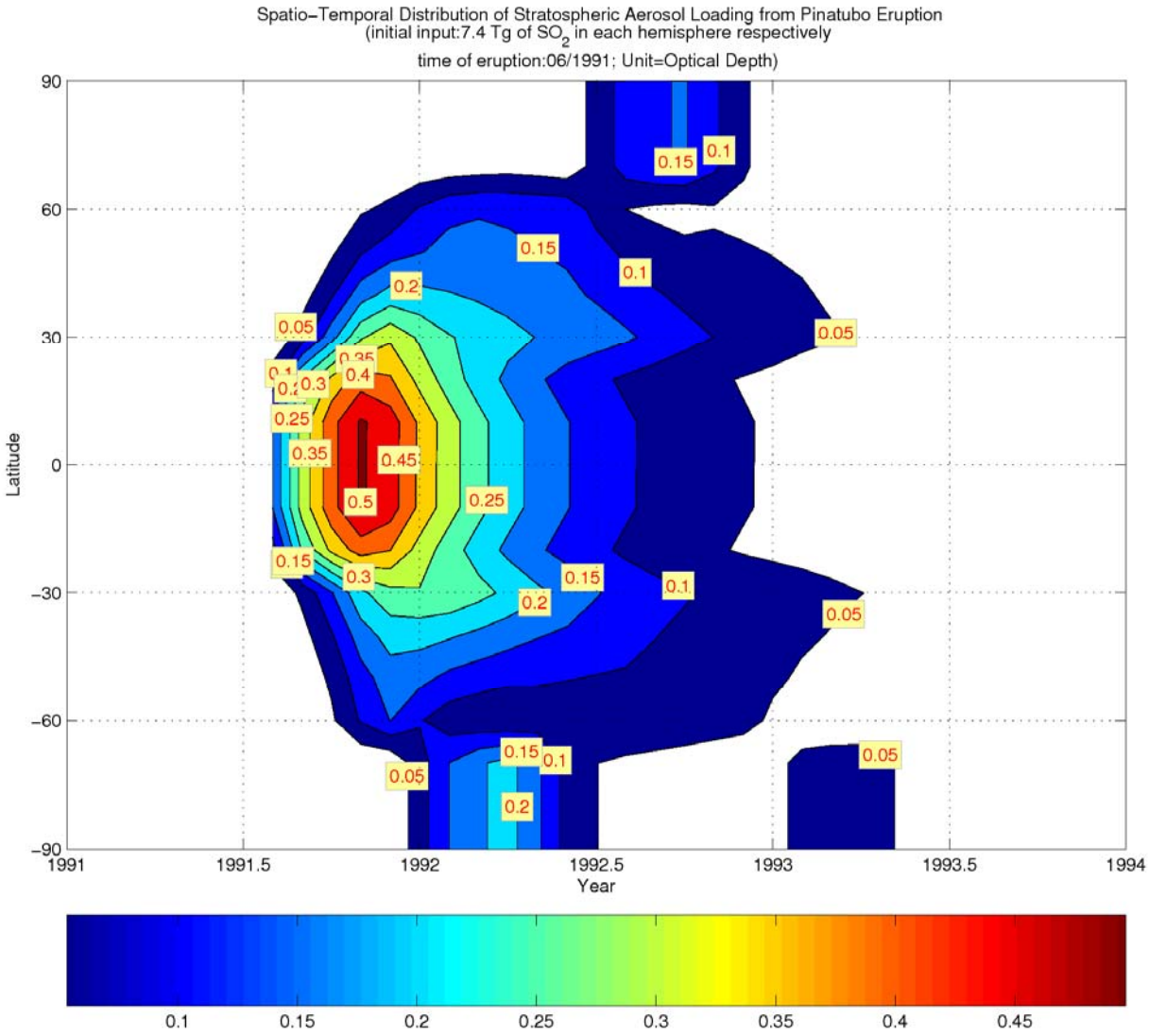

Figure 6-1. Distribution of total aerosol optical depth for the 1991 Pinatubo eruption from this study.

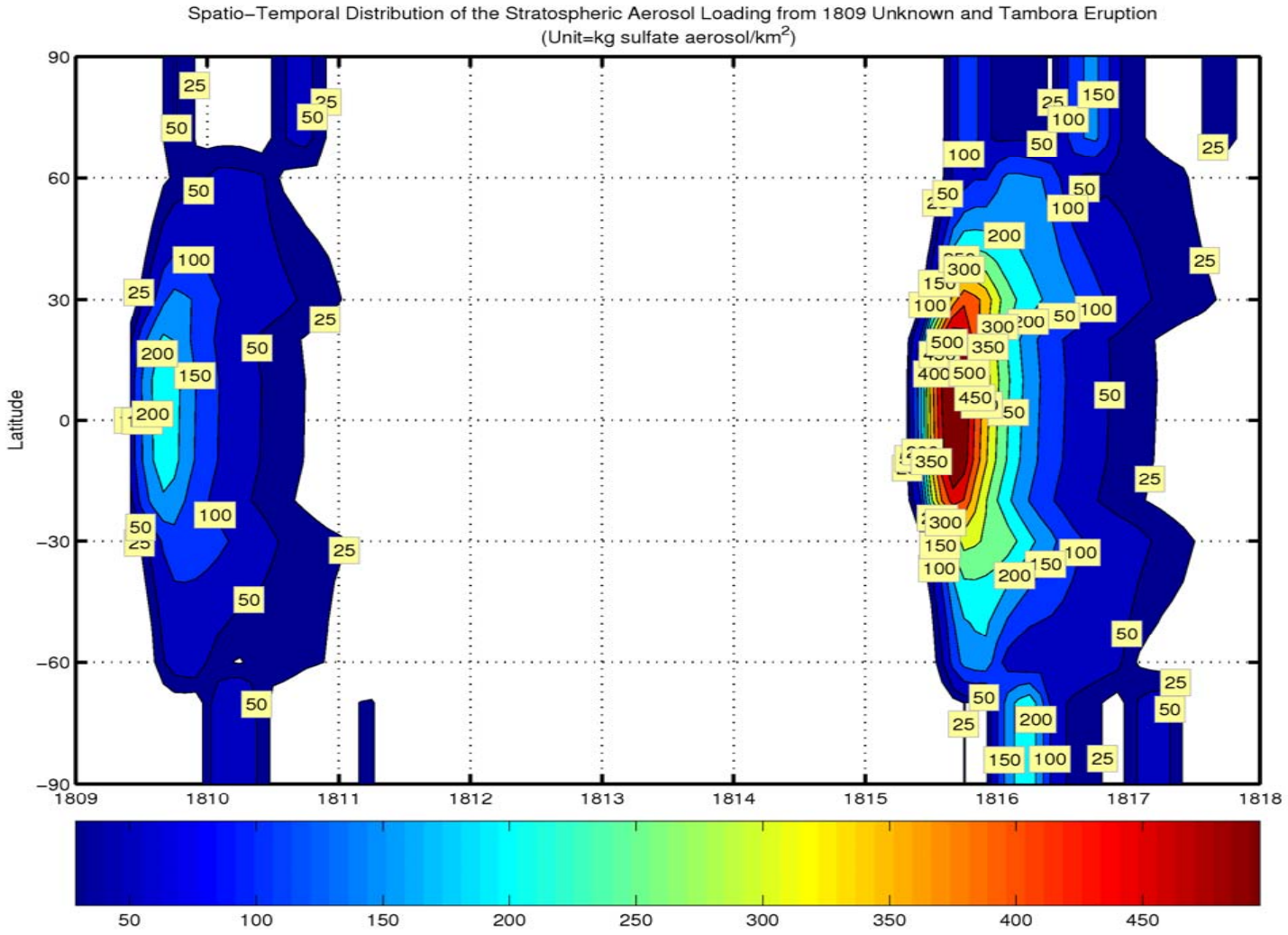

Figure 6-2. Distribution of sulfate aerosol loading from 1809 Unknown and 1815 Tambora eruptions.

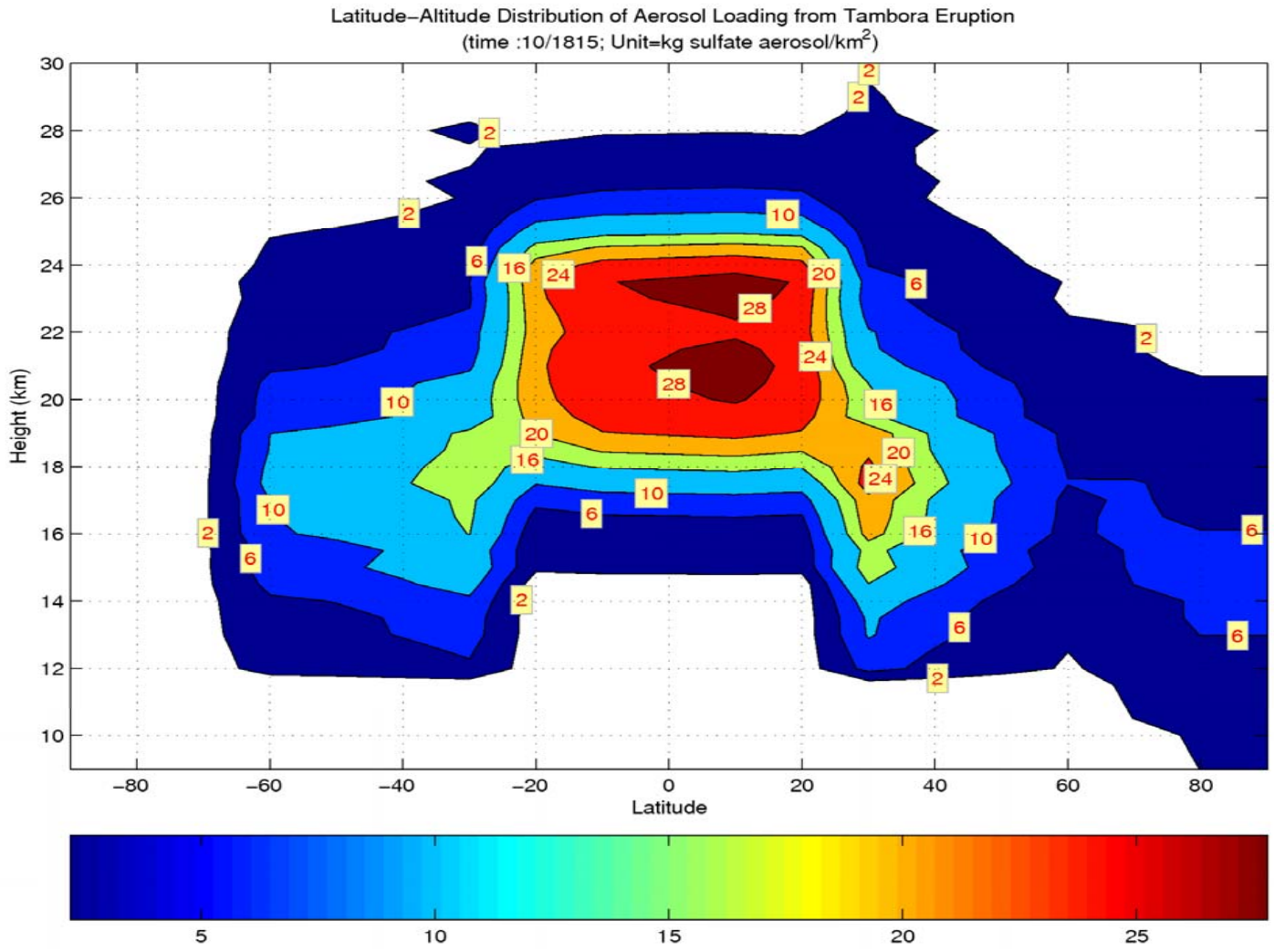

Figure 6-3. Latitude-altitude distribution of sulfate aerosol loading at Oct. 1815, six months after the Tambora eruption.

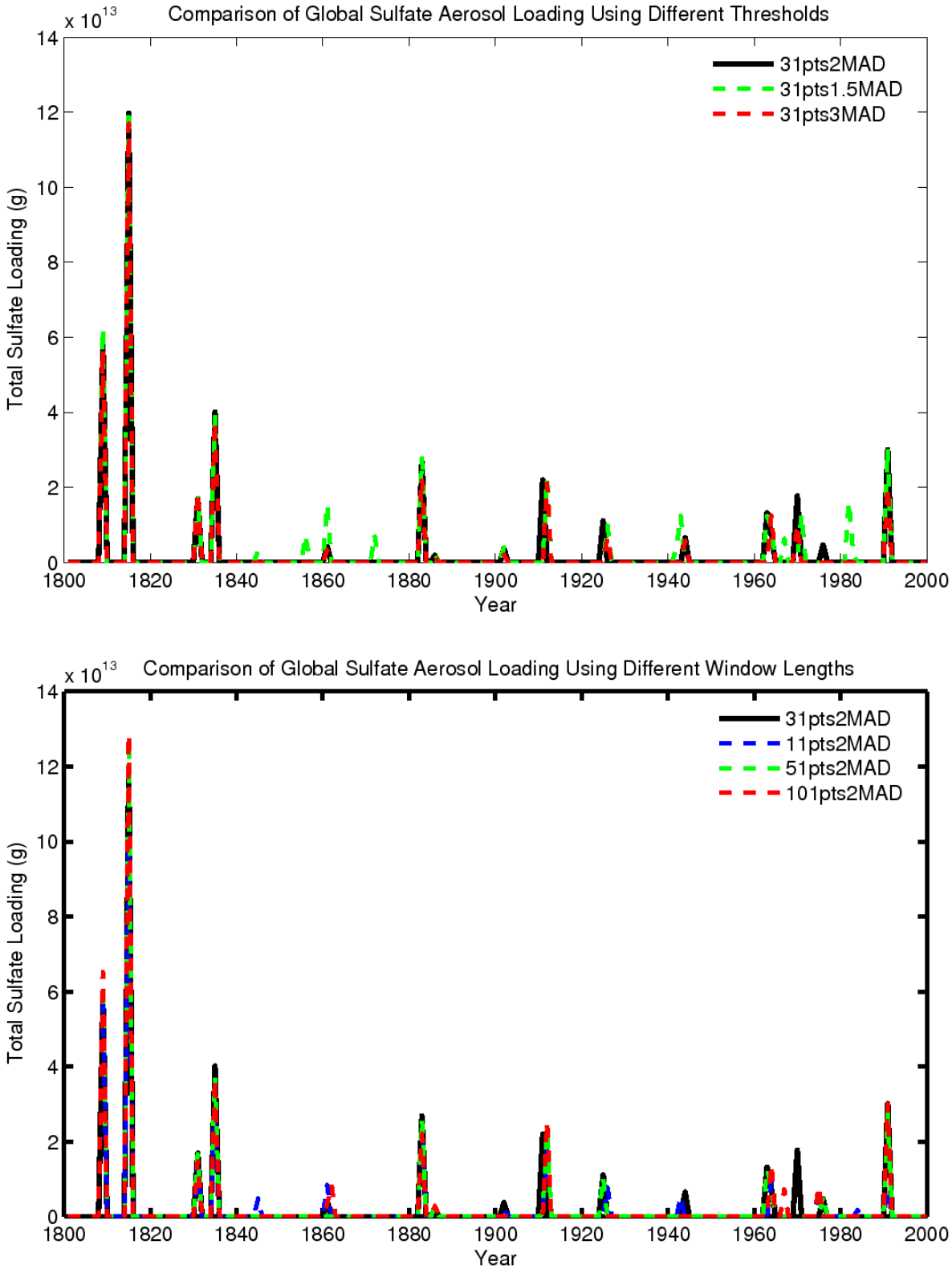

Figure 6-4. Comparison of global sulfate aerosol loading calculated using different signal extraction criteria for the period of 1801-2000 AD.

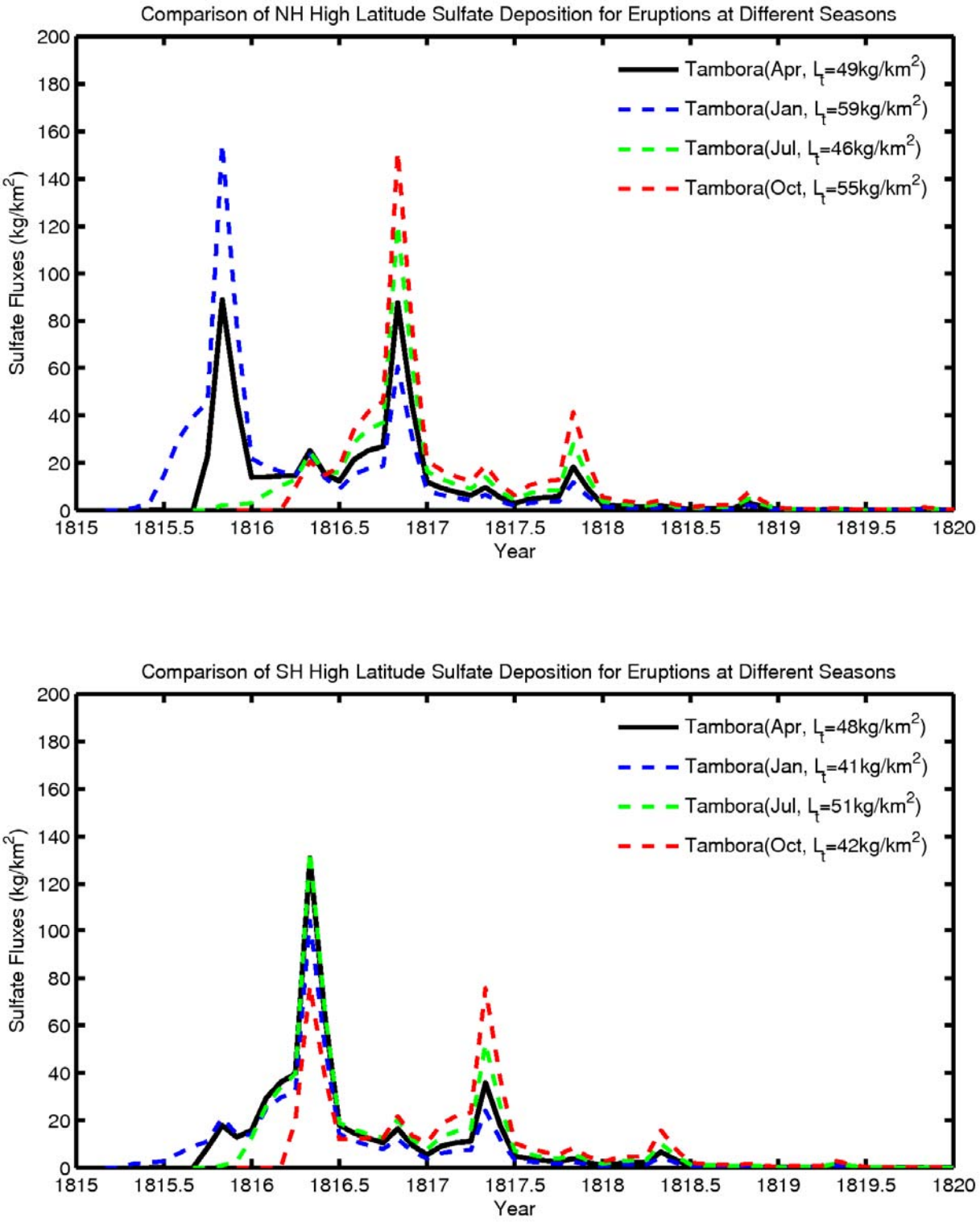

Figure 6-5. High latitude sulfate deposition for the Tambora eruption, assuming eruptions at different times of the year.

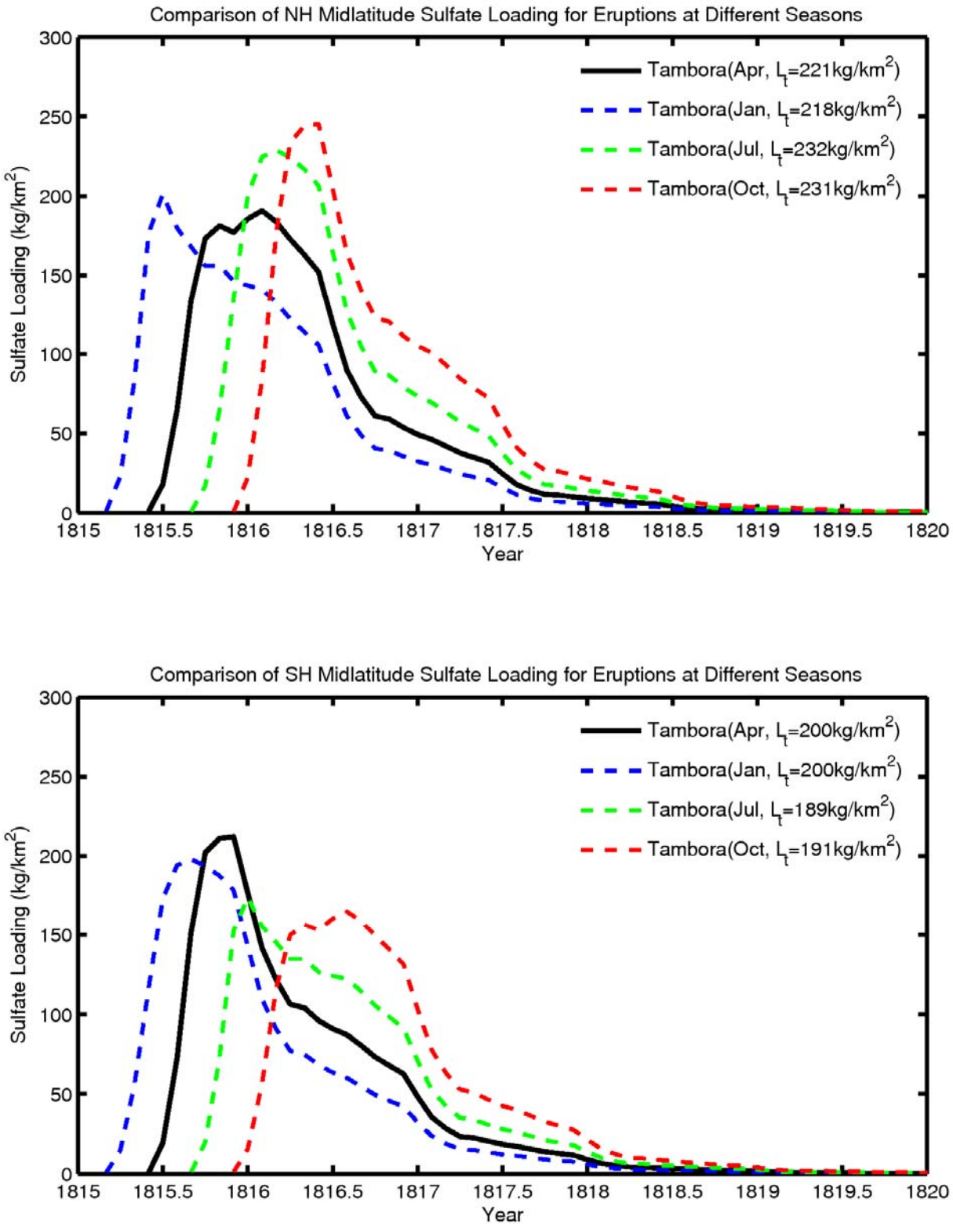

Figure 6-6. Midlatitude sulfate loading for the Tambora eruption, assuming eruptions at different times of the year.

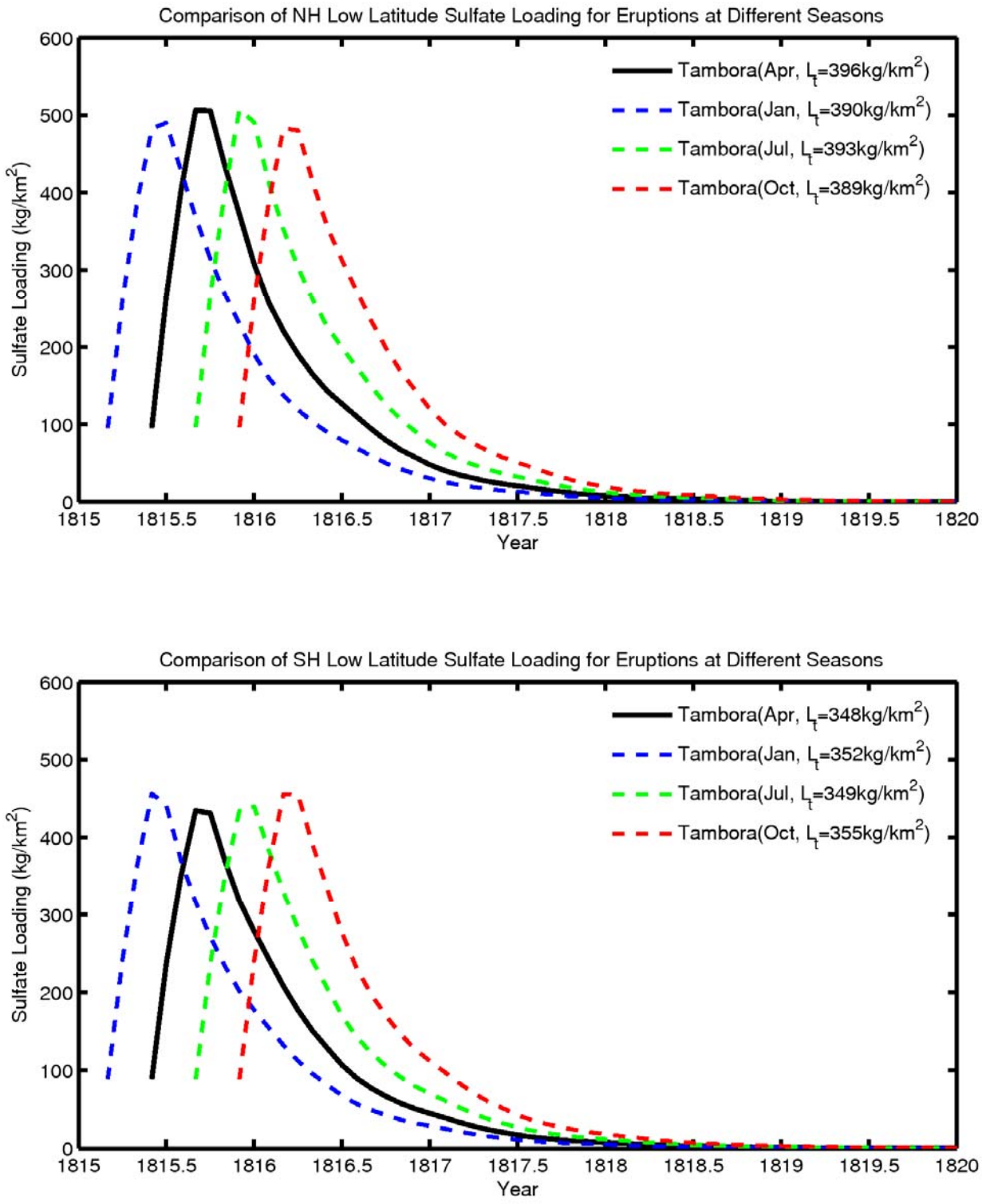

Figure 6-7. Low latitude sulfate loading for the Tambora eruption, assuming eruptions at different times of the year.

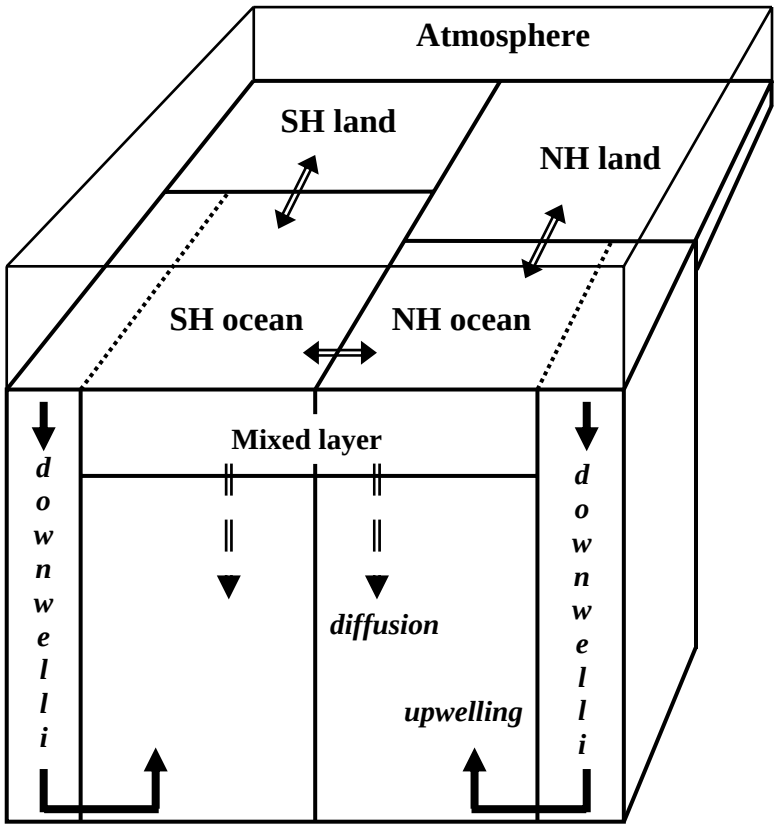

Figure 7-1 Geometry of the MAGICC model [Wigley and Raper, 1987, 1992]

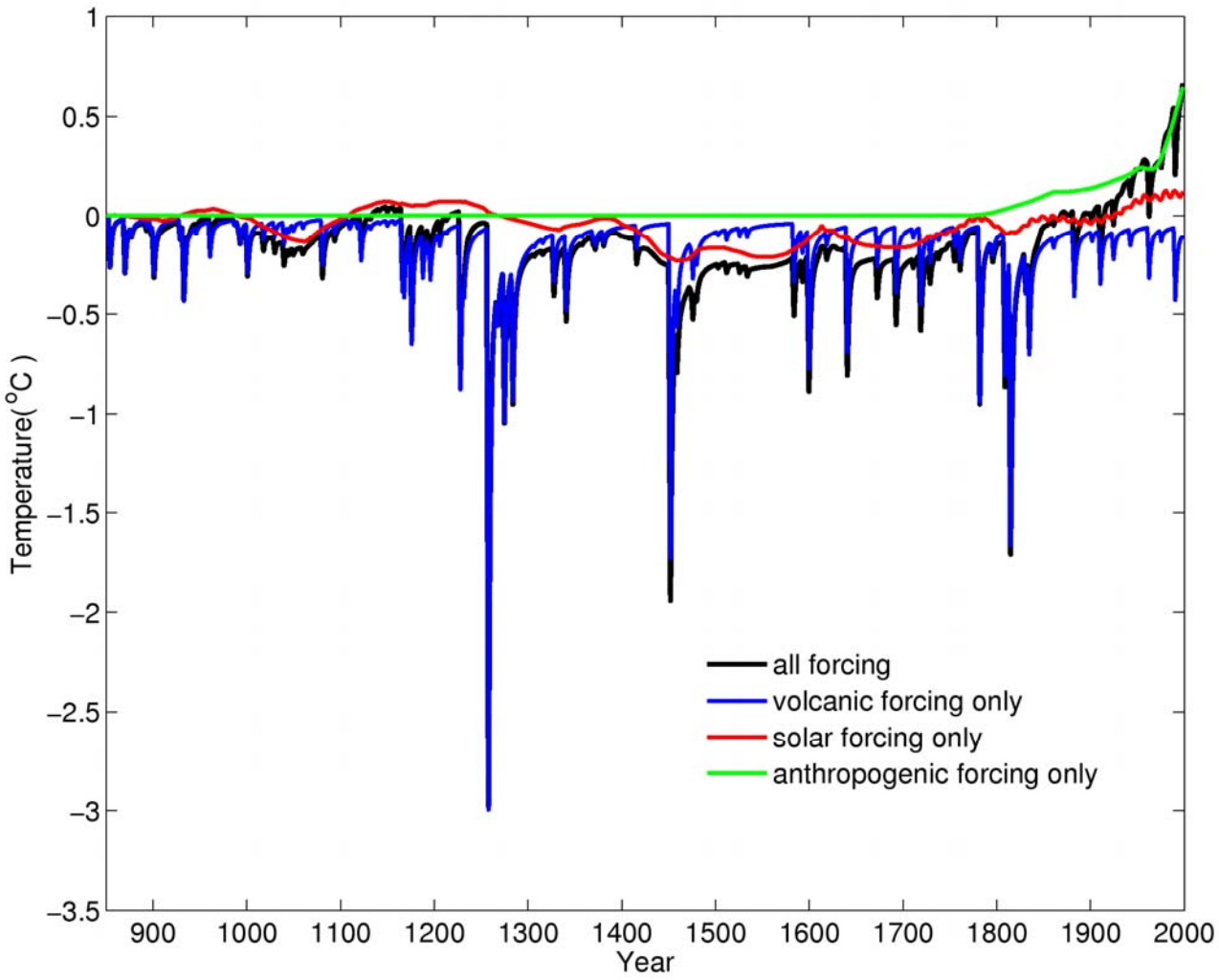

Figure 7-2 MAGICC simulate temperature response for individual climate forcing and the total radiative forcing.

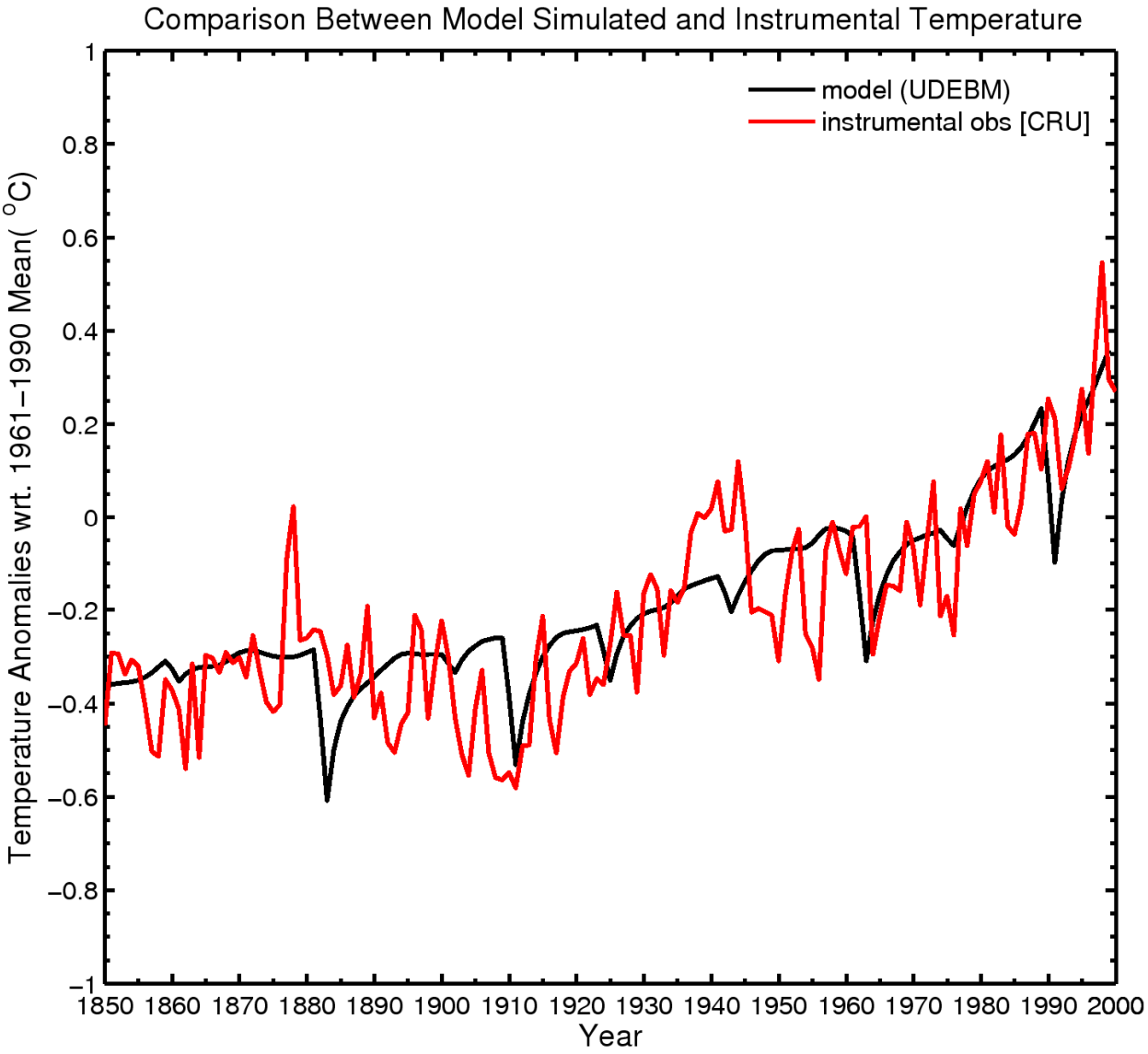

Figure 7-1. Global average surface air temperature anomalies, with respect to the 1961-1990 mean, simulated with the *Wigley and Raper* [1987, 1992] upwelling-diffusion energy balance model and observed (data from the Climatic Research Unit http://www.cru.uea.ac.uk/cru/data/temperature/).

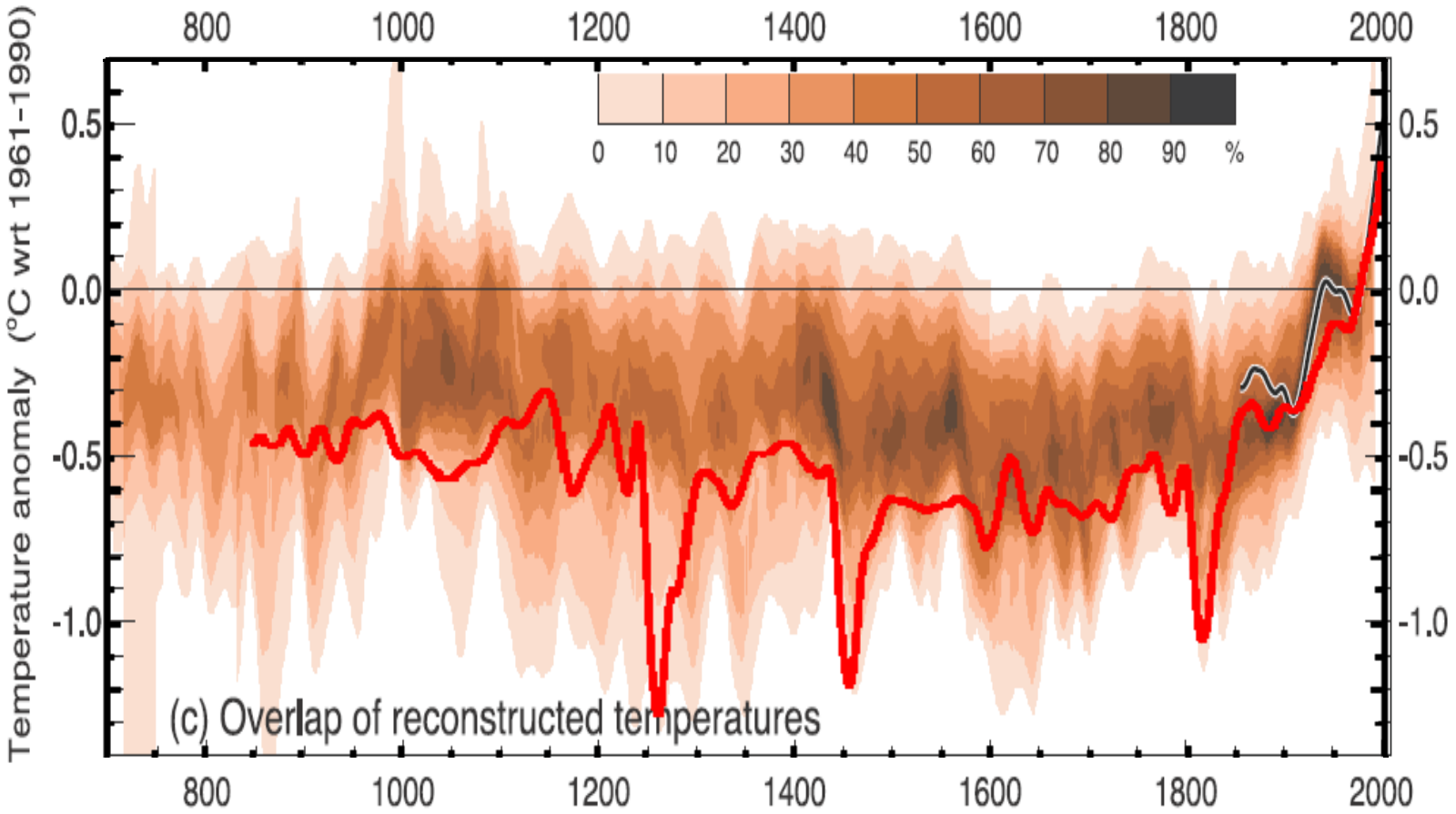

Figure 7-4. Comparison of EBM simulated NH temperature response (red curve) with temperature reconstructions (shaded, [*IPCC*, 2007, Fig. 6.10]) and instrumental observations (black curve). Plotted are the smoothed (31-yr weighted mean) temperature anomalies with respect to the 1961-1990 mean.

Curriculum Vita

Chaochao Gao

1996. 9 – 2000. 6	Zhejiang University	B.S. in Environmental Sciences Minor in Communication Science
2002. 9 – 2005. 6	Rutgers University	M.S. in Environmental Sciences
2005. 6 – 2008. 10	Rutgers University	Ph.D. in Environmental Sciences

2002. 9 – 2008. 7 Graduate Assistant, Rutgers University

Gao, C., A. Robock,. S. Self, J. Witter, J.P. Steffenson, H.B. Clausen, M-L. Siggaard-Andersen, S. Johnsen, P.A. Mayewski, and C. Ammann (2006), The 1452 or 1453 A.D. Kuwae eruption signal derived from multiple ice core records: Greatest volcanic sulfate event of the past 700 years, J. Geophys. Res., 111, D12107, doi:10.1029/2005JD006710. **Featured as Research Highlight in Nature, July 6, 2006**.

Oman, L., A. Robock, G.L. Stenchikov, T. Thordarson, D. Koch, D.T. Shindell, and **C. Gao** (2006), Modeling the sulfate deposition to the Greenland ice sheet from the Laki eruption, J. Geophys. Res., 111, D12209, doi:10.1029/2005JD006899.

Gao, C., L. Oman, A, Robock, and G. L, Stenchikov (2007), Atmospheric volcanic loading derived from bipolar ice cores accounting for the spatial distribution of volcanic deposition, doi:10.1029/2006JD007461, J. Geophys. Res., D09109, doi:10.1029/2006JD007461.

Gao, C., A. Robock, and C. Ammann (2008), Volcanic forcing of climate over the past 1500 years: an improved ice-core-based index for climate models, J. Geophys. Res., in press.